AD-A098 545 MOTOROLA INC SCOTTSDALE AZ GOVERNMENT ELECTRONICS DIV F/G 20/2
DOUBLY ROTATED CUT SAW DEVICES.(U)
APR 81 D F WILLIAMS, F Y CHO DAAK20-79-C-0275
UNCLASSIFIED DELET-TR-79-0275-2 NL

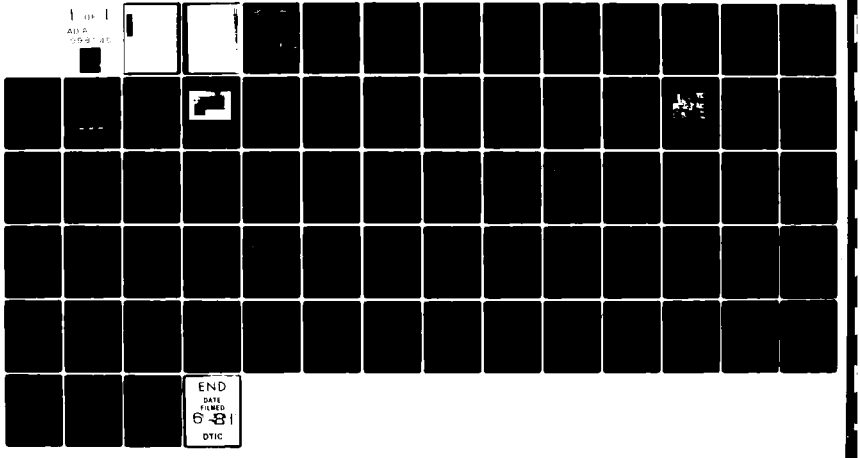

END
DATE FILMED
6-81
DTIC

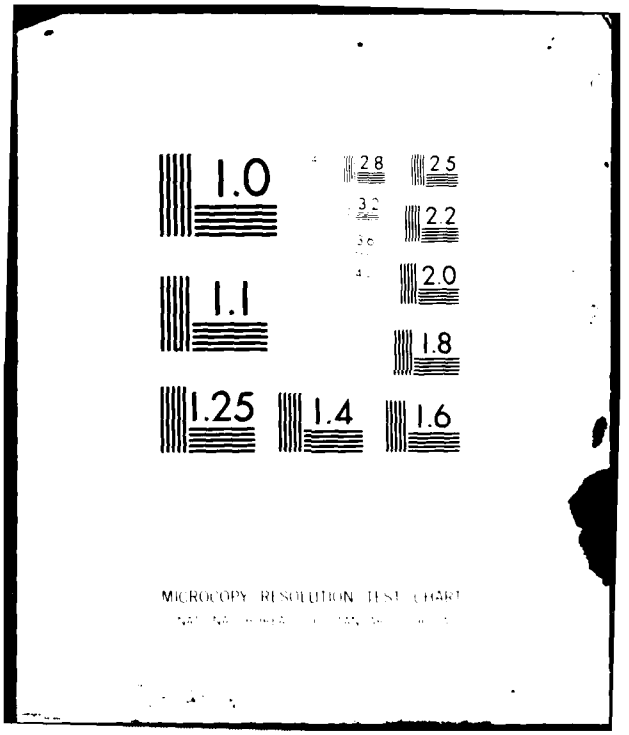
1.0
2.8
2.5
3.2
2.2
3.6
4.0
2.0
1.1
1.8
1.25
1.4
1.6
MICROCOPY RESOLUTION TEST CHART

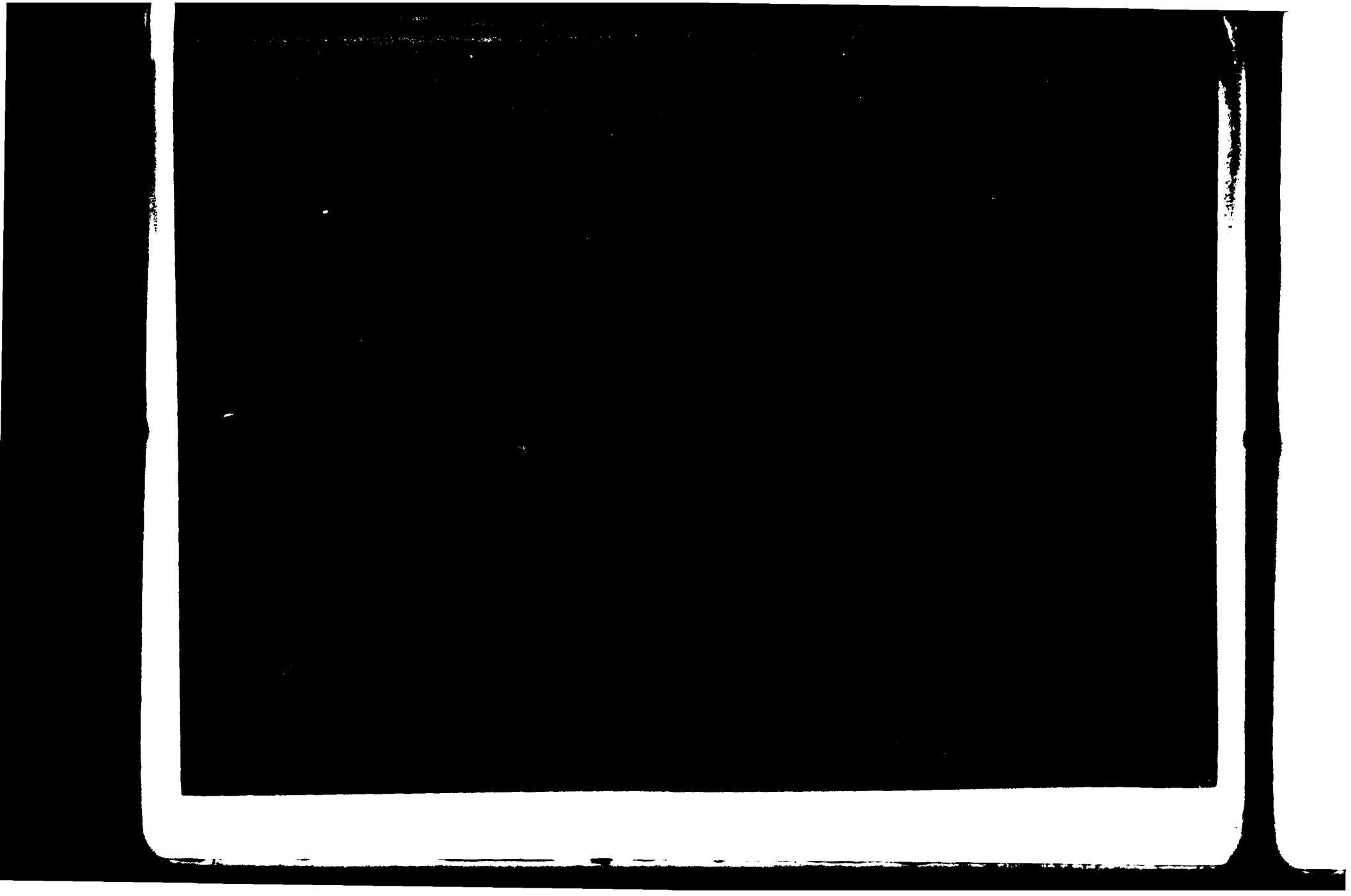

UNCLASSIFIED

SECURITY CLASSIFICATION OF THIS PAGE (When Data Entered)

| (19) REPORT DOCUMENTATION PAGE | READ INSTRUCTIONS BEFORE COMPLETING FORM |
|---|---|
| (18) DELET TR-79-0275-2 ✓ AD-A098 545 | 2. RECIPIENT'S CATALOG NUMBER |
| 4. TITLE (and Subtitle) (6) Doubly Rotated Cut SAW Devices, | 5. TYPE OF REPORT & PERIOD COVERED Interim Report March 1980 thru 1 September 1980 |
| | 6. PERFORMING ORG. REPORT NUMBER |
| 7. AUTHOR(s) (10) D.F. Williams, F.Y. Cho | 8. CONTRACT OR GRANT NUMBER(s) (15) DAAK20-79-C-0275 |
| 9. PERFORMING ORGANIZATION NAME AND ADDRESS Motorola, GED 8201 E. McDowell Rd. Scottsdale, AZ 85252 | 10. PROGRAM ELEMENT, PROJECT, TASK AREA & WORK UNIT NUMBERS 612705.H94.09.11.01 |
| 11. CONTROLLING OFFICE NAME AND ADDRESS Director, US Army Electronics Tech & Devices Lab ATTN: DELET-MM Fort Monmouth, NJ 07703 (11) | 12. REPORT DATE Apr[illegible]81 (12) 76 |
| | 13. NUMBER OF PAGES 64 |
| 14. MONITORING AGENCY NAME & ADDRESS(if different from Controlling Office) (7) | 15. SECURITY CLASS. (of this report) UNCLASSIFIED |
| | 15a. DECLASSIFICATION/DOWNGRADING SCHEDULE |

16. DISTRIBUTION STATEMENT (of this Report)

Approved for Public Release; Distribution Unlimited.

17. DISTRIBUTION STATEMENT (of the abstract entered in Block 20, if different from Report)

DTIC ELECTE MAY 6 1981 S D A

18. SUPPLEMENTARY NOTES

19. KEY WORDS (Continue on reverse side if necessary and identify by block number)

Surface Acoustic Waves, Quartz, Temperature Coefficient of Frequency, X-Ray Orientation

20. ABSTRACT (Continue on reverse side if necessary and identify by block number)

The objective of this program is the exploratory development of doubly rotated cuts of quartz possessing superior Surface Acoustic Wave (SAW) properties for applications involving environmentally hardened devices. The key properties examined and optimized both th[illegible]retically and experimentally are: first, second and third order Temperature Coefficients of Delay (TCD), piezoelectric coupling factor, power flow angle, Bulk Acoustic Wave (BAW) inverse velocity surfaces, degeneracies and leaky waves, and sensitivities of the above quantities to misorientations and manufacturing tolerances.

DD FORM 1 JAN 73 1473 EDITION OF 1 NOV 65 IS OBSOLETE

UNCLASSIFIED

SECURITY CLASSIFICATION OF THIS PAGE (When Data Entered)

The program consists of two major task areas comprising an interactive numerical/experimental approach. Task I involves the numerical computation of the key SAW properties for doubly rotated quartz substrates for the purpose of locating promising angular ranges with properties superior to the singly rotated cuts now in existence. More detailed calculations follow to refine the angular coordinates in order to specify cuts for experimental verification in Task II. In Task II, sets of substrates with promising orientations identified in Task I will be prepared and SAW device patterns will be fabricated for evaluation of the key SAW properties. The experimental results of this task will be correlated with the theoretical predictions and an iterative process developed for refinement of both theoretical and experimental parameters. As the program proceeds, working SAW device models will be delivered as a demonstration of progress and an indication of the future potential of the doubly rotated cuts. Depending upon the progress made and time and budget limitations, additional properties in the area of nonlinear elasticity will be investigated. This report contains the results of Task II.

# TABLE OF CONTENTS



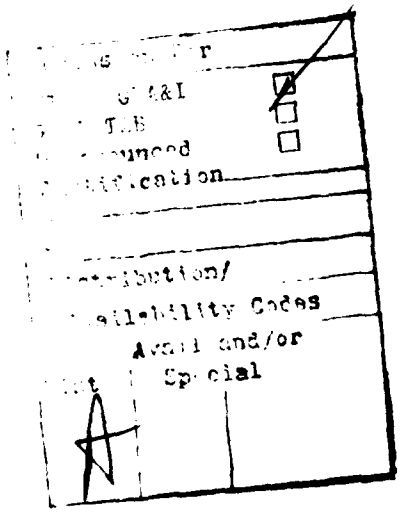

# LIST OF ILLUSTRATIONS

# SECTION I

# INTRODUCTION

## 1. PROGRAM OBJECTIVE

The objective of this program is the exploratory development of doubly rotated cuts of quartz possessing superior Surface Acoustic Wave (SAW) properties for applications involving environmentally hardened devices. The key properties examined and optimized both theoretically and experimentally are: first, second and third order Temperature Coefficients of Frequency (TCF), piezoelectric coupling factor, power flow angle, Bulk Acoustic Wave (BAW) inverse velocity surfaces, and sensitivities of the above quantities to misorientations and manufacturing tolerances.

## 2. PROGRAM SCOPE

The program consists of two major task areas comprising an interactive numerical/experimental approach. Task I involves the numerical computation of the key SAW properties for doubly rotated quartz substrates for the purpose of locating angular ranges with properties superior to the singly rotated cuts now in existence. More detailed calculations followed to refine the angular coordinates in order to specify cuts for experimental verification in Task II. In Task II, sets of substrates with promising orientations identified in Task I are prepared and SAW device patterns fabricated for evaluation of the key SAW properties. The experimental results of this task are correlated with the theoretical predictions, and an iterative process develops for refinement of both theoretical and experimental parameters. As the program proceeds, working SAW device models will be delivered as a demonstration of progress and an indication of the future potential of the doubly rotated cuts. Depending upon the progress made and time and budget limitations, additional properties in the area of nonlinear elasticity will be investigated.

## 3. TECHNICAL APPROACH SUMMARY

During this period the first iteration theoretical calculations performed to characterize doubly rotated cuts of quartz were completed. Theoretically temperature-stable cuts with zero $TCF^{(1)}$ and $TCF^{(2)}$ as small as $-1.0 \times 10^{-8}$ were located. This represents a better than three-fold improvement over the ST cut. Experimental measurements of the TCF's have been performed on some doubly rotated cuts. Zero $TCF^{(1)}$ SAW devices for

---

[1]"Numerical Computation of Acoustic Surface Waves in Layered Piezoelectric Media-Computer Program Descriptions", William Jones, William Smith, Donald Perry, Final Report F19628-70-C-0027, prepared for Air Force Cambridge Research Laboratories by Hughes Aircraft Company.

[2]"On The Temperature Dependence of the Velocity of Surface Waves in Quartz", B.K. Sinha and H.F. Tiersten, Proceedings of the 32nd Annual Symposium of Frequency Control, 1978, pp. 150-153.

which the second order temperature term is the dominant term have been fabricated. Measured values of $TCF^{(2)}$ of these devices as low as $-1.5 \times 10^{-8}$ have been obtained. The agreement between the experimental and the calculated results was excellent. Measured first order TCF's and those calculated by Sinha and Tiersten's perturbation program were found to differ by less than 3 ppm/C°, and second order TCF's calculated by the finite difference method were found to differ by less than 0.005 ppm/C°$^2$. Both the measured and calculated third order TCF's were found to be too small to be a significant factor in device performance.

To accurately characterize the properties of doubly rotated quartz, this program has utilized two basic theoretical approaches for the identification of zero TCF's. Two computer programs available at Motorola are used. The first program calculates the first, second and third order TCF's of rotated cuts using a finite difference method.[1] This technique is simple, well established, and has been used for analytically determining the temperature coefficient curves for singly and doubly rotated cuts of quartz. To more accurately determine the first order temperature coefficient of frequency, a second program which encompasses lattice skewing effects is used. This more complete theoretical approach is based on the work of Sinha and Tiersten.[2] Its utility has been verified. The characterization of the other key parameters is achieved with standard SAW programs used routinely for material characterization and device development.

Accurately oriented quartz bars, supplied by Motorola Carlisle, are cut and oriented at Motorola and polished at Crystal Technology. During this program, many substrates are fabricated from a single bar with incremental angular deviations about selected angular positions. The angular orientation of the doubly rotated substrates is defined to an accuracy of within ±5 minutes using X-ray diffractometry and precision wafer saw's with doubly rotating mounts.

A complete SAW test area and optical laboratory form the basis for the experimental evaluation of the key SAW parameters of the doubly rotated quartz delay lines, oscillators and resonators. The equipment is set up for rapid display, measurement and recording of propagation directions, TCF's, velocities, beam steering angles and diffraction.

The excellent agreement between the experimental and theoretical results, and the success with which low TCF cuts have been located, confirmed the utility and accuracy of the techniques used in the program. The second theoretical and experimental iterations promise to yield orientations and devices with even greater temperature stability than those already obtained.

# SECTION II

# TECHNICAL DISCUSSION

## 1. INTRODUCTION

The search for a temperature stable cut of quartz for application to SAW devices has lead to the investigation of the doubly rotated cuts. Theoretical studies have indicated that doubly rotated cuts of quartz promise much better temperature stability than the commonly used ST cut. Task I of this program, which encompassed the first iteration calculations of the doubly rotated cuts of quartz, has been successfully completed. Task II, with major emphasis on experimental work, is currently being performed.

In Task I theoretical analyses have been performed and angular rotations promising very low $TCF^{(1)}$ and $TCF^{(2)}$ have been plotted. Important SAW device design parameters, such as coupling coefficient, velocity and power flow angle, have also been computed to characterize each area. As part of Task II, experimental results establishing the degree of correlation with theory have been obtained.

Theoretical propagation characteristics, as discussed in paragraph 2 below, impose strict fabrication tolerances on the SAW cuts and mask alignment due to large values of $\partial TCF1/\partial\psi$. Thus a mask had to be designed to compensate for fabrication errors. This design work is presented in paragraph 3. Since experimental technique is an important criteria in the determination of correlation between theory and experiment, all procedures followed as well as equipment used are discussed in paragraph 4. Paragraph 5 presents experimental determination of propagation characteristics which illustrate an excellent agreement between theoretical calculation and experimental results. Paragraph 6 contains the results of the doubly rotated cut TCF measurements made to date.

Theoretical calculations have been in good agreement with experimental results. Doubly rotated cuts of quartz with an improvement of $TCF^{(2)}$ by at least a factor of two over the ST cut have been obtained. A further improvement is expected after a second iteration has been performed and promising areas examined.

## 2. THEORETICAL PROPAGATION CHARACTERISTICS

In cutting quartz and aligning masks on it, there is always some maximum achievable accuracy. It is also useful to know how all of the acoustic quantities considered vary with angle. Quantities such as TCF, phase velocity, power flow angle, $\Delta V/V$, and bulk wave velocity surfaces are of interest to this program. These quantities can be accurately determined by directly calculating the quantities at $\phi = (\phi_0+\Delta\phi)$, $\theta = (\theta_0+\Delta\theta)$, and $\psi = (\psi_0+\Delta\psi)$. Calculation of the angular dependence on the first, second, and third order TCF's is, of course, our primary task. Of these three quantities, the first order TCF is most sensitive to angular variation (refer to Tables 1, 2, and 3). Quantities such as velocity (Table 2), power flow angles (Table 2), coupling coefficients (Table 3), and second and third order TCF's (Table 1) do not vary quickly with angle.

This is not the case for $TCF^{(1)}$. Table 3 contains a summary of $\partial TCF^{1}/\partial\psi$. The large values of $\partial TCF^{(1)}/\partial\psi$ impose strict fabrication tolerances on the SAW cuts and mask alignment. Therefore it is essential to design a mask with reference registration marks to accurately determine the transducer orientation relative to the crystal edges. These reference markers are fabricated on all of the measured devices, so that propagation direction is accurately determined to within ±25 minutes. Fabrication accuracy to within 6 minutes is required to keep the total temperature variation due to $TCF^{(1)}$ within 45 ppm for $\partial TCF^{(1)}/\partial\psi = 0.3$ (PPM/°C)/degree over the temperature range of −50°C to 100°C. Table 4 contains summaries of $\partial TCF^{(1)}/\partial\phi$ and $\partial TCF^{(1)}/\partial\theta$. These values impose fabrication tolerances on the rotated quartz plate angles $\phi$ and $\theta$ of $\Delta\phi$ and $\Delta\theta$ less than 12 minutes to keep the total temperature variation due to $\partial TCF^{(1)}$ (15/40/40)$/\partial\phi$ within 45 ppm over the temperature range of −50°C to 100°C for example. This linear temperature variation may be compensated for by varying $\psi$ on any particular cut if all other cut parameters vary slowly with angle. To date all other cut parameters have been found to vary slowly with Phi, Theta and Psi.

TABLE 1. PROPAGATION CHARACTERISTICS OF SELECTED ORIENTATIONS

| Angles of Zero $TCF^{(1)}$ Degrees (S and T's Program) | | | $TCF^{(2)}/°C^{2}(X10^{-8})$ Finite Difference Program | $TCF^{(3)}/°C^{3}(X10^{-10})$ Finite Difference Program |
|---|---|---|---|---|
| Phi | Theta | Psi | | |
| 6 | 26 | 136.31 | −1.4 | |
| 6 | 27 | 135.93 | −1.3 | 0.67 |
| 6 | 28 | 135.59 | −1.3 | 0.57 |
| 7 | 26 | 135.99 | −1.5 | |
| 7 | 27 | 135.64 | −1.4 | |
| 7 | 28 | 135.27 | −1.3 | 0.65 |
| 8 | 26 | 135.74 | −1.4 | 0.65 |
| 8 | 27 | 135.36 | −1.4 | |
| 8 | 28 | 134.97 | −1.3 | |
| 1 | 26 | 137.78 | −1.2 | 0.68 |
| 1 | 27 | 137.48 | −1.2 | 0.65 |
| 1 | 28 | 137.17 | −1.1 | 0.67 |
| 0 | 26 | 138.07 | −1.2 | 0.67 |
| 0 | 27 | 137.78 | −1.1 | 0.68 |
| 0 | 28 | 137.49 | −1.1 | 0.62 |
| −1 | 26 | 138.37 | −1.2 | 0.60 |
| −1 | 27 | 138.09 | −1.2 | 0.62 |
| −1 | 28 | 137.80 | −1.1 | 0.73 |
| 14 | 39 | 40.195 | −1.0 | 0.64 |
| 14 | 40 | 40.415 | −1.0 | 0.66 |
| 14 | 41 | 40.64 | −1.0 | 0.75 |

TABLE 1. PROPAGATION CHARACTERISTICS OF SELECTED ORIENTATIONS (Cont)

| Angles of Zero TCF[1] Degrees (S and T's Program) | | | $TCF^{(2)}/°C^2(X10^{-8})$ Finite Difference | $TCF^{(3)}/°C^3(X10^{-10})$ Finite Difference |
|---|---|---|---|---|
| Phi | Theta | Psi | Program | Program |
| 15 | 39 | 39.79 | −1.0 | 0.63 |
| 15 | 40 | 40 | −1.0 | 0.74 |
| 15 | 41 | 40.23 | −1.0 | 0.73 |
| 16 | 39 | 39.4 | −1.0 | 0.68 |
| 16 | 40 | 39.605 | −1.0 | 0.66 |
| 16 | 41 | 39.825 | −1.1 | 0.60 |

TABLE 2. PROPAGATION CHARACTERISTICS OF SELECTED ORIENTATIONS

| Angles of Zero TCF[1], Degrees (S and T's Program) | | | Velocity | $K^2$ | Power Flow |
|---|---|---|---|---|---|
| Phi | Theta | Psi | (Msec) | $(X10^{-3})$ | Angle (Degree) |
| 6 | 26 | 136.31 | 3296.84 | 1.12 | −0.3 |
| 6 | 27 | 135.93 | 3293.60 | 1.12 | −0.2 |
| 6 | 28 | 135.59 | 3290.63 | 1.12 | −0.1 |
| 7 | 26 | 135.99 | 3303.33 | 1.12 | −0.5 |
| 7 | 27 | 135.64 | 3299.70 | 1.12 | −0.4 |
| 7 | 28 | 135.27 | 3296.33 | 1.12 | −0.3 |
| 8 | 26 | 135.74 | 3310.15 | 1.12 | −0.7 |
| 8 | 27 | 135.36 | 3306.11 | 1.12 | −0.6 |
| 8 | 28 | 134.97 | 3302.32 | 1.10 | −0.5 |
| 1 | 26 | 137.78 | 3268.80 | 1.10 | +0.7 |
| 1 | 27 | 137.48 | 3267.44 | 1.10 | +0.9 |
| 1 | 28 | 137.17 | 3266.36 | 1.10 | +1.0 |
| 0 | 26 | 138.07 | 3264.09 | 1.12 | +0.9 |
| 0 | 27 | 137.78 | 3263.09 | 1.10 | +1.1 |
| 0 | 28 | 137.49 | 3262.35 | 1.10 | +1.2 |
| −1 | 26 | 138.37 | 3259.65 | 1.10 | +1.1 |
| −1 | 27 | 138.09 | 3259.01 | 1.10 | −1.3 |
| −1 | 28 | 137.80 | 3258.64 | 1.08 | +1.5 |
| 14 | 39 | 40.195 | 3298.60 | 0.96 | −7.7 |
| 14 | 40 | 40.415 | 3306.67 | 0.96 | −8.1 |

TABLE 2. PROPAGATION CHARACTERISTICS OF SELECTED ORIENTATIONS (Cont)

| Angles of Zero $TCF^{(1)}$, Degrees (S and T's Program) | | | Velocity | $K^2$ | Power Flow |
|---|---|---|---|---|---|
| Phi | Theta | Psi | (Msec) | ($X10^{-3}$) | Angle (Degree) |
| 14 | 41 | 40.64 | 3315.19 | 0.94 | −8.6 |
| 15 | 39 | 39.79 | 3301.82 | 0.96 | −7.8 |
| 15 | 40 | 40.00 | 3310.14 | 0.94 | −8.3 |
| 15 | 41 | 40.23 | 3319.09 | 0.98 | −8.6 |
| 16 | 39 | 39.4 | 3305.38 | 0.96 | −8.0 |
| 16 | 40 | 39.605 | 3314.03 | 0.98 | −8.4 |

TABLE 3. $\partial TCF^{(1)}/\partial\psi$ FOR SELECTED CUTS

| Angles of Zero $TCF^{(1)}$ Degrees (S and T's Program) | | | $\partial TCF^{(1)}/\partial\psi$ |
|---|---|---|---|
| Phi | Theta | Psi | (PPM/C°)/Degree |
| 6 | 26 | 136.31 | +2.7 |
| 6 | 27 | 135.93 | +2.7 |
| 6 | 28 | 135.59 | +2.7 |
| 7 | 26 | 135.99 | +2.7 |
| 7 | 27 | 135.64 | +2.7 |
| 7 | 28 | 135.27 | +2.7 |
| 8 | 26 | 135.74 | +2.7 |
| 8 | 27 | 135.36 | +2.7 |
| 8 | 28 | 134.97 | +2.7 |
| 1 | 26 | 137.78 | +2.8 |
| 1 | 27 | 137.48 | +2.8 |
| 1 | 28 | 137.17 | +2.8 |
| 0 | 26 | 138.07 | +3.0 |
| 0 | 27 | 137.78 | +3.0 |
| 0 | 28 | 137.49 | +3.0 |
| −1 | 26 | 138.37 | +3.0 |
| −1 | 27 | 138.09 | +3.0 |
| −1 | 28 | 137.08 | +3.0 |
| 14 | 39 | 40.195 | −3.5 |
| 14 | 40 | 40.415 | −3.5 |
| 14 | 41 | 40.64 | −3.5 |
| 15 | 39 | 39.79 | −3.5 |

TABLE 3. $\partial TCF^{(1)}/\partial\psi$ FOR SELECTED CUTS (Cont)

| Angles of Zero $TCF^{(1)}$ Degrees (S and T's Program) | | | $\partial TCF^{(1)}/\partial\psi$ |
|---|---|---|---|
| Phi | Theta | Psi | (PPM/C°)/Degree |
| 15 | 40 | 40 | −3.5 |
| 15 | 41 | 40.23 | −3.5 |
| 16 | 39 | 39.4 | −3.7 |
| 16 | 40 | 39.605 | −3.7 |
| 16 | 41 | 39.825 | −3.7 |

TABLE 4. $\partial TCF^{(1)}/\partial\phi$ AND $\partial TCF^{(1)}/\partial\theta$ FOR SELECTED CUTS

| Angles of Zero $TCF^{(1)}$, Degrees (S and T's Program) | | | $\partial TCF^{(1)}/\partial\phi$ | $\partial TCF^{(1)}/\partial\theta$ |
|---|---|---|---|---|
| Phi | Theta | Psi | (PPM/C°)/Degree | (PPM/C°)/Degree |
| 7 | 27 | 135.64 | −0.7 | −0.5 |
| 0 | 27 | 137.76 | −0.8 | −0.8 |
| 15 | 40 | 40.00 | +1.5 | −0.7 |

## 3. MASK DESIGN

A mask was designed to take into account the sensitivity of $TCF^{(1)}$ due to small variations in the cut angles. The design incorporates rotated structures. Each device is offset with respect to its neighbor by 0.2°. Three individual devices are illustrated in Figure 1. The device specifications are as follows:

a. Transducer periodicity: 12.192 $\mu$m (center frequency ~260 MHz; varies with crystal orientation)

b. Delay time: 360$\lambda$ (~1.4 $\mu$s) (varies with crystal orientation)

c. Number of sets in output transducer: 15

d. Electrode pairs per set: 2.25

e. Electrode pairs in input transducer: 24

f. Aperture width: Input: 70 wavelengths
Output: 50 wavelengths

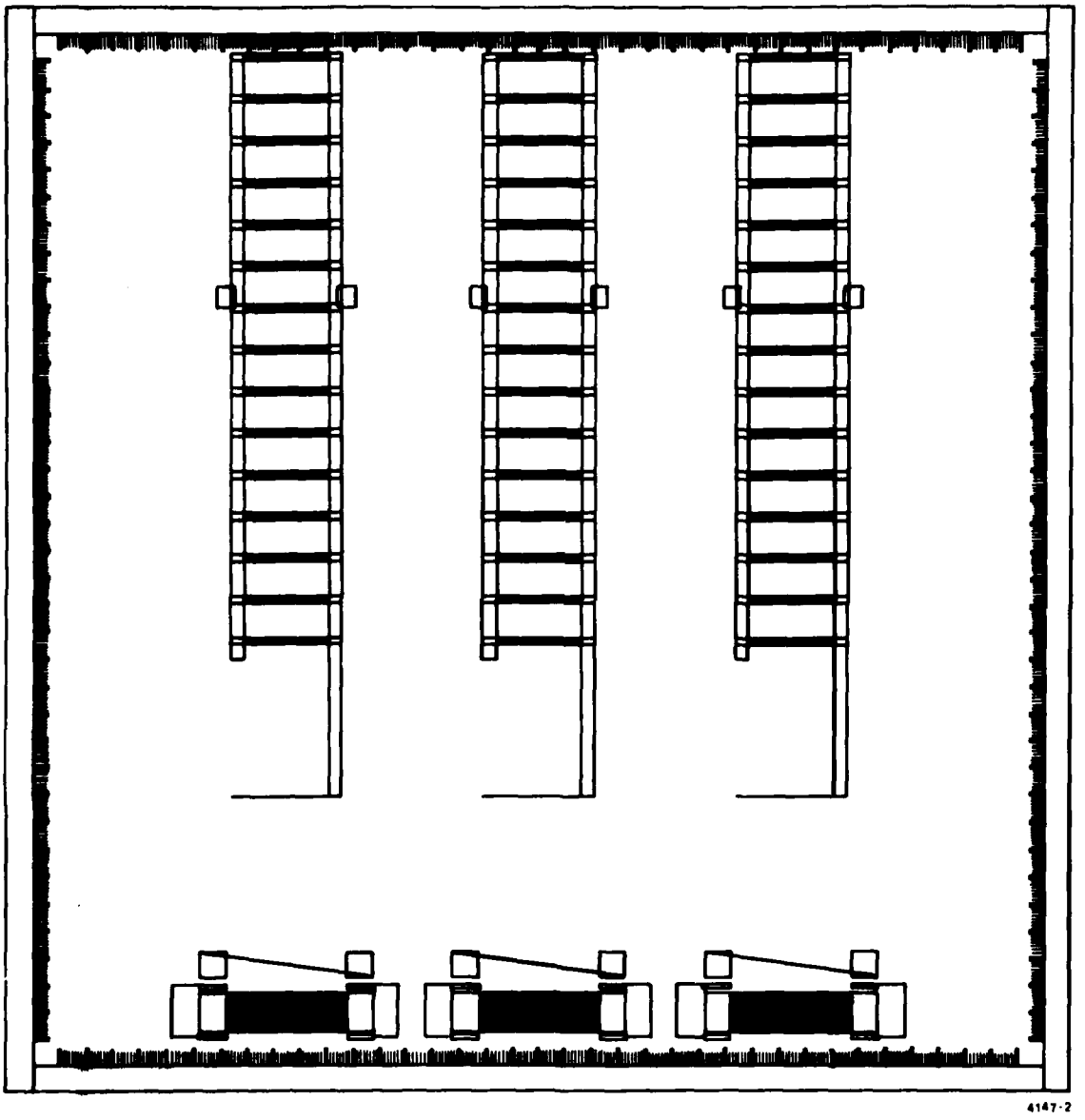


Figure 1. SAW Oscillator Device

Figure 2 is a photograph of a wafer fabricated using the above-mentioned design. Twelve oscillators propagating in different $\psi$ directions are fabricated on a single wafer. The principal advantage of this design is the ability to compensate for fabrication errors. From the experimental results plotted in Figure 3, we are able to observe significant frequency shifts due to small variations in PSI angle. These results confirm our theoretical calculations.

## 4. EXPERIMENTAL MEASUREMENT OF TCF

Wafers with orientations that provide low temperature coefficients of frequency were used to fabricate SAW oscillator devices. Considerable care has been taken to minimize fabrication tolerances. For angles $\phi$ and $\theta$, the estimated accuracy is within ±4 minutes; for angle $\psi$, the accuracy is within ±25 minutes.

The delay line oscillators described previously were used to measure the frequency stability at different temperatures. The experimental apparatus is shown in Figure 4. No coils were used to match the devices in order to eliminate inductance changes in the matching circuit over the temperature range tested.

The switches are designed to test ten oscillators in the same temperature chamber. The phase stability of the switches is essential to the measurements. The circuits are shown in Figure 5. The phase stability of the switches was found to be adequate for measuring the temperature stability of the device.

A digital thermacouple (Fluke 2160A-T) was taped to the bottom of the fixture to measure device temperature. The Fluke 2160A-T is accurate to within ±2°C over the temperature range of −75°C to +150°C. A thermometer was also used to measure the oven air temperature. Semi-rigid cable constituted all interconnections. This reduces loss, shields against feedthrough, and makes the apparatus less sensitive to the testing environment. ANZAC DS109 power splitters and AVETEK AWL500M amplifiers were used in the feedback loop. A Systron Donner (PLS 50-1) provided the DC power supply voltage. The mean supply voltage was maintained at 15.000 ± 0.001 volts during the measurements.

Frequency measurements were taken every 10°C, spanning the range from −55°C to +135°C. Stabilization of temperature and frequency was attained for each measurement before data was taken. This ensures that the device is in thermal equilibrium with its environment. The total experimental error is estimated to be less than ±10 PPM.

## 5. EXPERIMENTAL PROPAGATION CHARACTERISTICS

The propagation characteristics of selected devices were measured to verify the calculations. The experimental measured velocity is

$$v = f\lambda \qquad \lambda = 12.192\ \mu m$$

Table 5 lists the experimental velocities for the various cuts. The deviation (up to 0.2%) is in part caused by the slight deviation of crystal orientation due to the fabrication process, and in part caused by the uncertainty of center frequency due to the unknown phase shift in the feedback loop (±0.25 MHz).

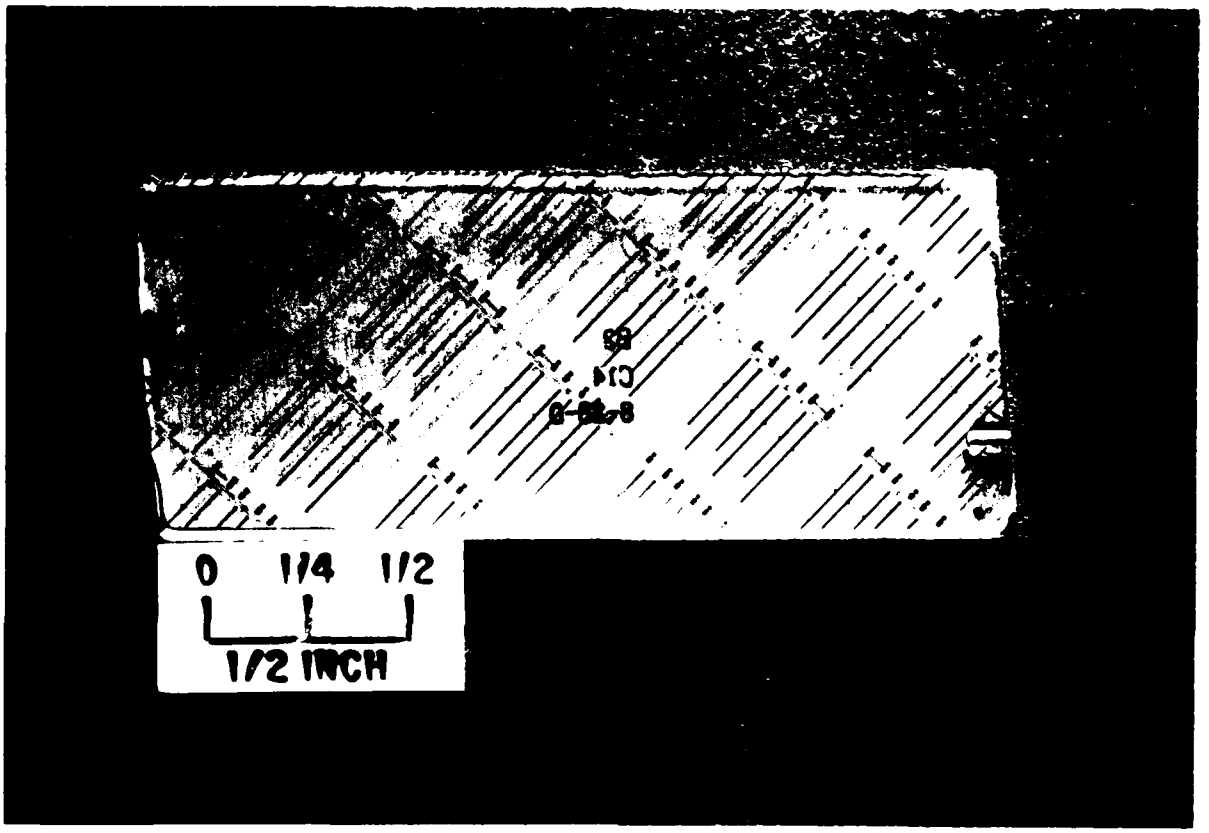


Figure 2. Photograph of a Fabricated Wafer With Propagation Directions of 8°27′/27°54′/133°54′ ± n(0.2°)

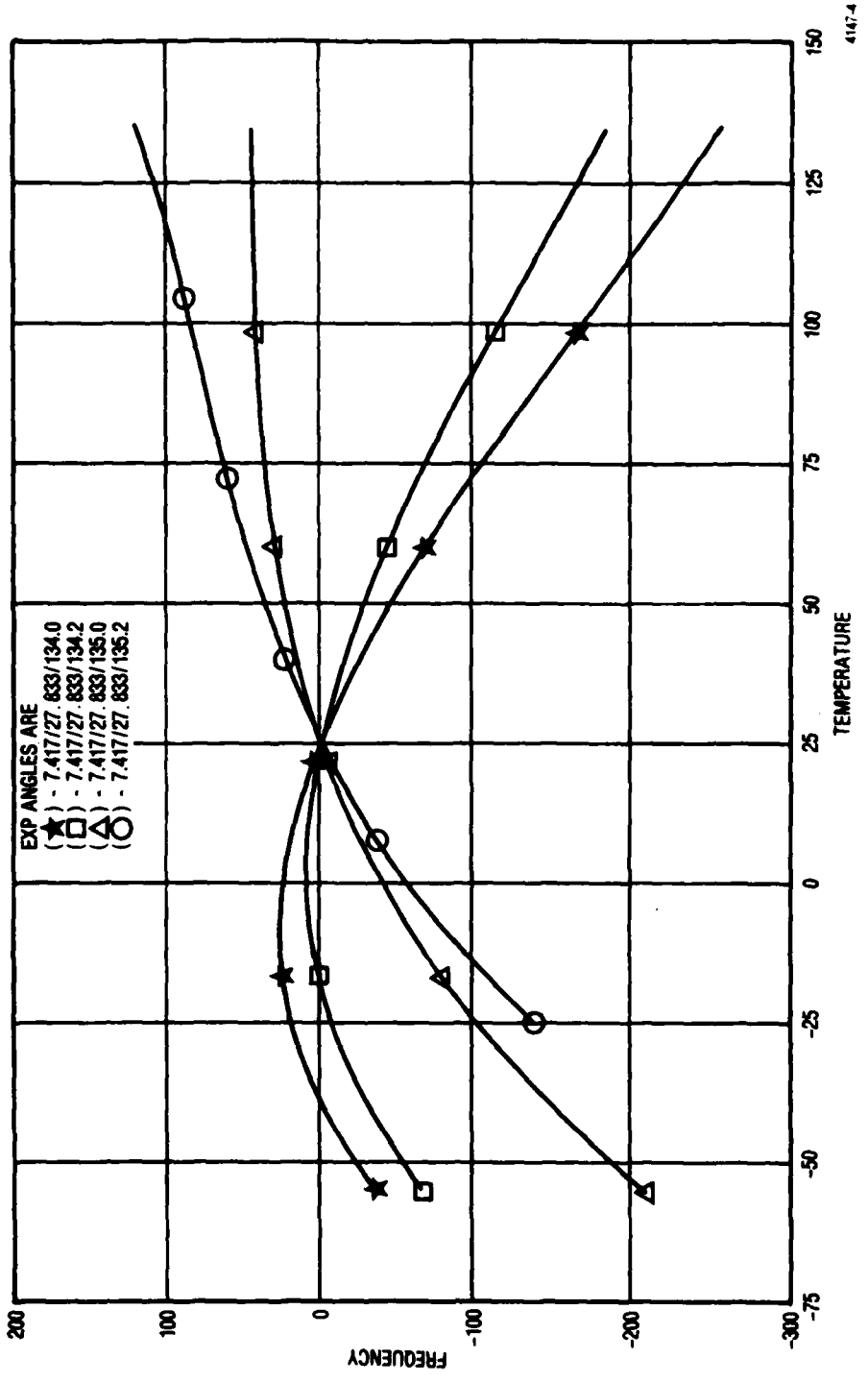


Figure 3. Frequency Temperature Curve With Different $\psi$ Angles

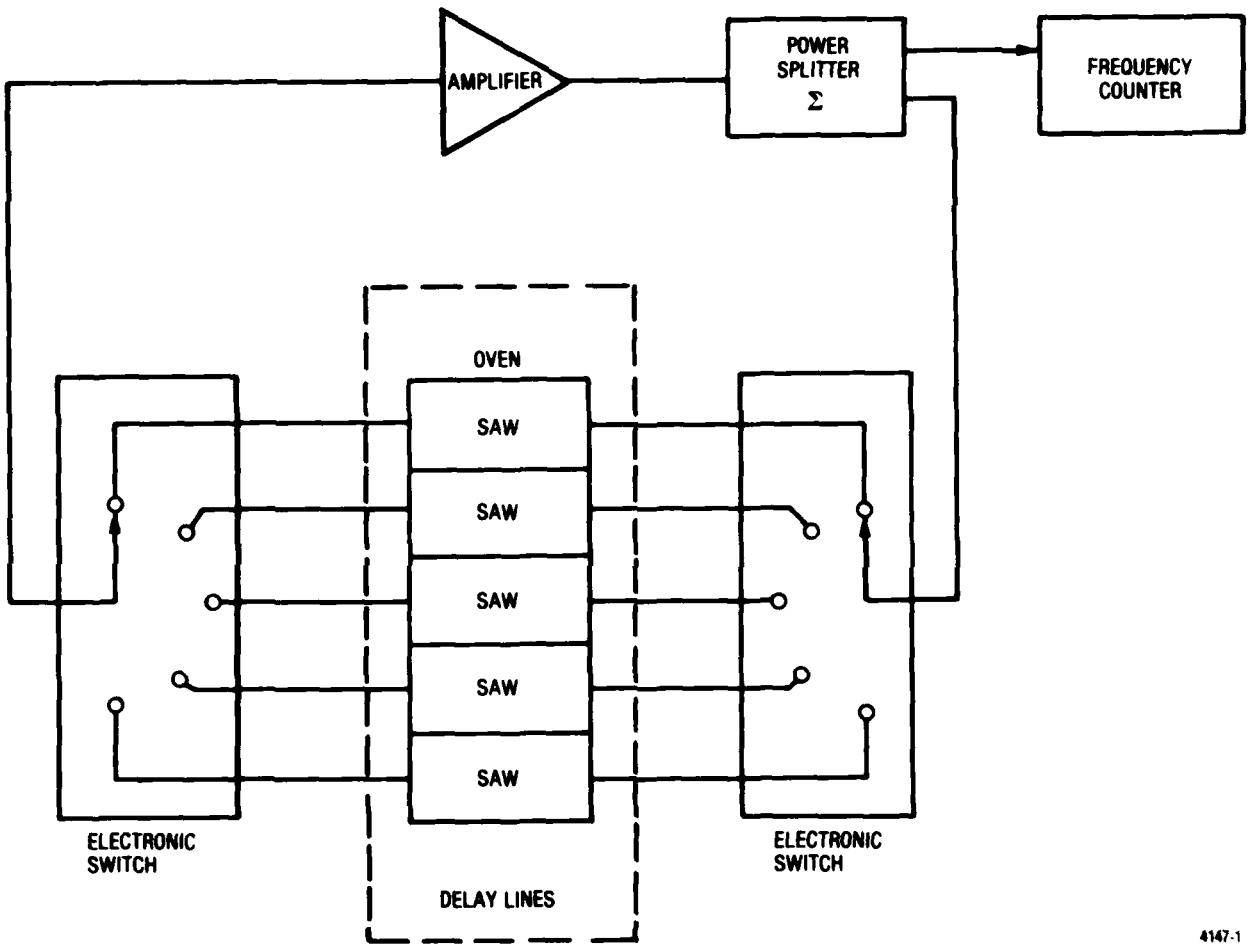


Figure 4. Measurement System

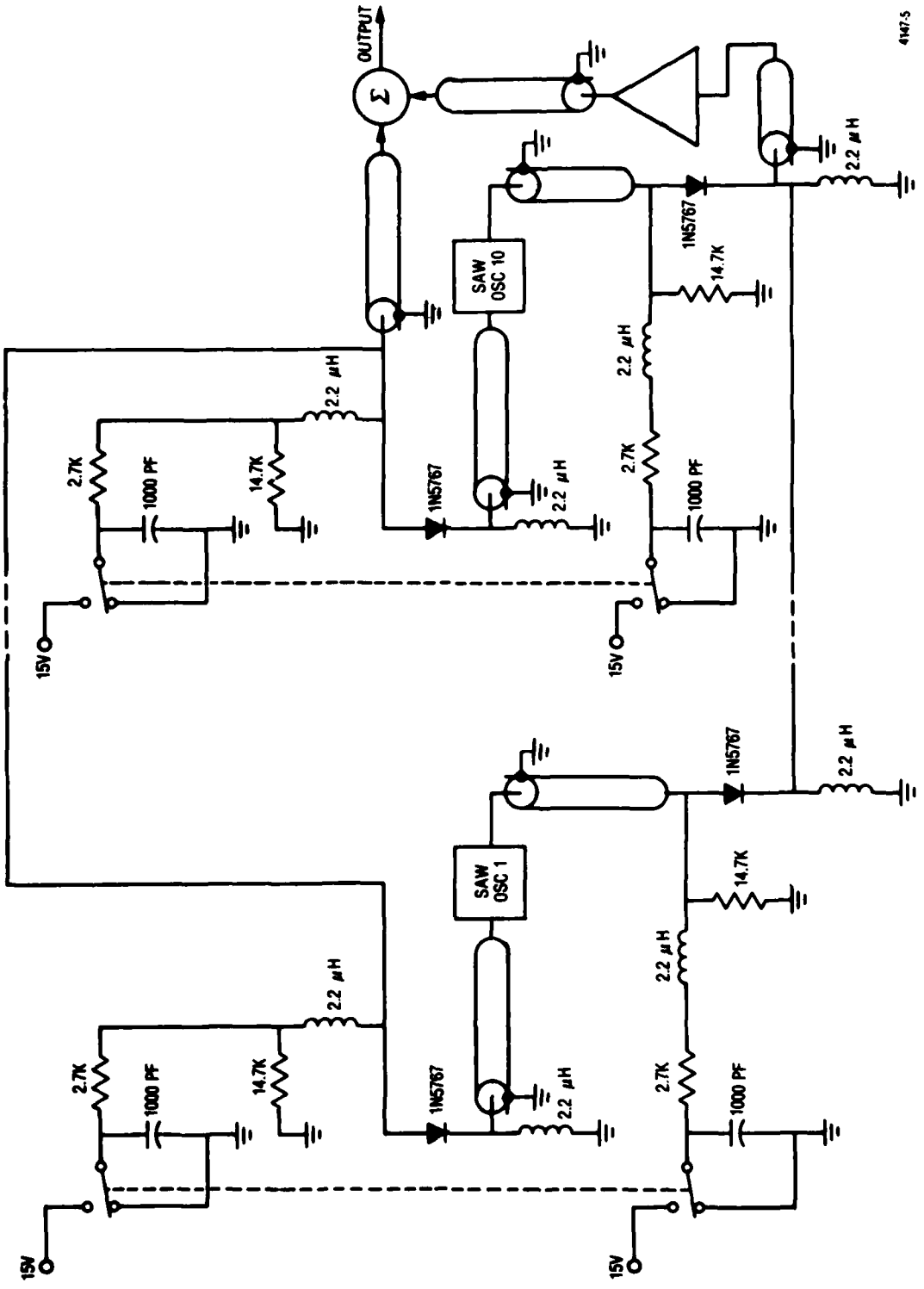


Figure 5. Test Circuits

The power flow angle of the doubly rotated cut quartz wafer has been measured by the laser probe technique. The measured result is in good agreement with calculations.

TABLE 5. EXPERIMENTAL VELOCITIES OF CUTS

| Phi | Theta | Psi | Measured Velocity | Calculated Velocity |
|---|---|---|---|---|
| −1.05 | 28.0667 | 136.534 | 3257.4 | 3260.9 |
| −0.9667 | 26.233 | 138.449 | 3256.8 | 3259.4 |
| −0.133 | 28.1 | 137.692 | 3259.0 | 3261.5 |
| −0.033 | 26.7 | 138.859 | 3262.1 | 3262.5 |
| 0.633 | 26.15 | 137.016 | 3267.6 | 3267.7 |
| 5.583 | 27.833 | 135.194 | 3289.7 | 3288.9 |
| 5.583 | 27.833 | 135.994 | 3290.7 | |
| 6.0 | 26.9667 | 135.812 | 3288.9 | 3293.7 |
| 6.067 | 25.933 | 133.099 | 3298.8 | 3299.4 |
| 7.41 | 27.83 | 134.2 | 3296.8 | 3299.1 |
| 8.033 | 26.9667 | 134.618 | 3304.1 | 3306.1 |
| 14.2833 | 39.1167 | 40.227 | 3294.8 | 3301.4 |
| 14.2833 | 39.1167 | 40.627 | 3296.8 | 3304.6 |
| 15.25 | 39.2 | 39.6187 | 3300.7 | 3303.4 |
| 15.3 | 40.6833 | 40.0308 | 3314.0 | 3317.3 |

The block diagram of the experimental set-up is shown in Figure 6.

In this procedure, the first order deflecting light due to the presence of the acoustic wave is measured by the photomultiplier. The light intensity is proportional to the acoustic power, while the angle of deflection is given by:

$$\text{Sin } \theta_n = \text{Sin } \theta_o + \frac{n\lambda}{\Lambda}$$

Where $\theta_n$ = angle of deflection of nth order

$\theta_o$ = angle of specular reflection

$\lambda$ = optical wavelength

$\Lambda$ = acoustic wavelength

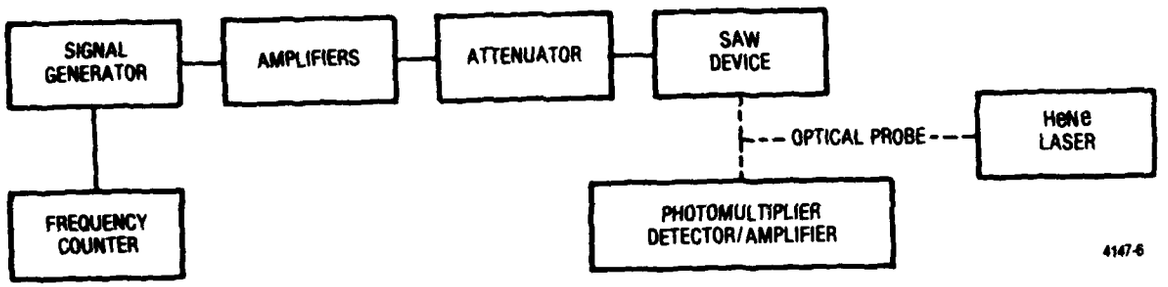


Figure 6. Experimental Set-Up For Laser Probe

The angular relation is demonstrated in Figure 7. The optical beam is provided by a He-Ne laser with spot size of $\simeq$100 $\mu$. The acoustic waves are generated by a 260 MHz transducer with $\Lambda$ equal to 12.192 $\mu$. During the measurement, the SAW device is translated up and down so that the optical beam is scanned across the acoustic path to detect the acoustic beam intensity distribution. The test equipment is shown in Figure 8.

Figures 9 and 10 show examples of plots of the relative acoustic beam intensities indicated by the deflected laser beam. These plots were taken in the near- and far-field regions, respectively. The exact distance between the near-field scan and the far-field scan is 8.131 mm. The center of the beams is estimated to be 0.05 mm in separation.

The measured power flow angle for this cut is

$$\theta_p = \tan^{-1} \frac{-0.05}{8.131} = -0.352°$$

The calculated power flow angle for this cut is

$$\theta_p' = -0.3°$$

The good agreement between the measurement and the calculated results indicates that the calculation is accurate. Acoustic dispersion and loss can also be calculated from this data.

## 6. EXPERIMENTAL MEASUREMENT OF FREQUENCY VERSUS TEMPERATURE

A few representative frequency-temperature measurements are presented in Figures 11 through 15. The stars represent experimental data points. The solid lines are linearly regressed curves used to define the measured first, second, and third order TCF's for these cuts, given in Table 6. Figures 11 through 15 are representative of cuts in region (YX wlt) 7/27/135. Cut (YX/wlt) 6.57/26.88/134.9 of Figure 11 has a small linear frequency term at room temperature and is well suited for use at both high and low temperatures. Its second order TCF is in good agreement with the computer calculations and is considerably smaller than that of ST-cut quartz (see Table 6). Cut (YX wlt) 5.58/27.83/135.1 of Figure 12 displays a larger total frequency variation over the range shown but is much more stable at higher temperatures. This illustrates how a simple change of crystal orientation can be used to temperature-compensate doubly rotated cut SAW devices for different mean operating temperatures. A slight rotation of $\psi$, as shown in Figure 3, could be used to set the first order TCF to zero while slightly altering the second order TCF of the device. This cut also represents a substantial improvement over the ST-cut (see Table 6). Figures 11 through 15 summarize some of our typical measurements to date. Results in this area are in excellent agreement with the theory. One of these cuts (8.033/26.967/134.6) has temperature stability of approximately 40 ppm from 0°C to 130°C; it is suitable for systems or weapons operating in elevated temperatures (see Figure 14).

On all cuts tested, the agreement between the experimental and calculated results has been excellent. These results establish a firm basis for performing the second iteration search for the optimum TCF orientations.

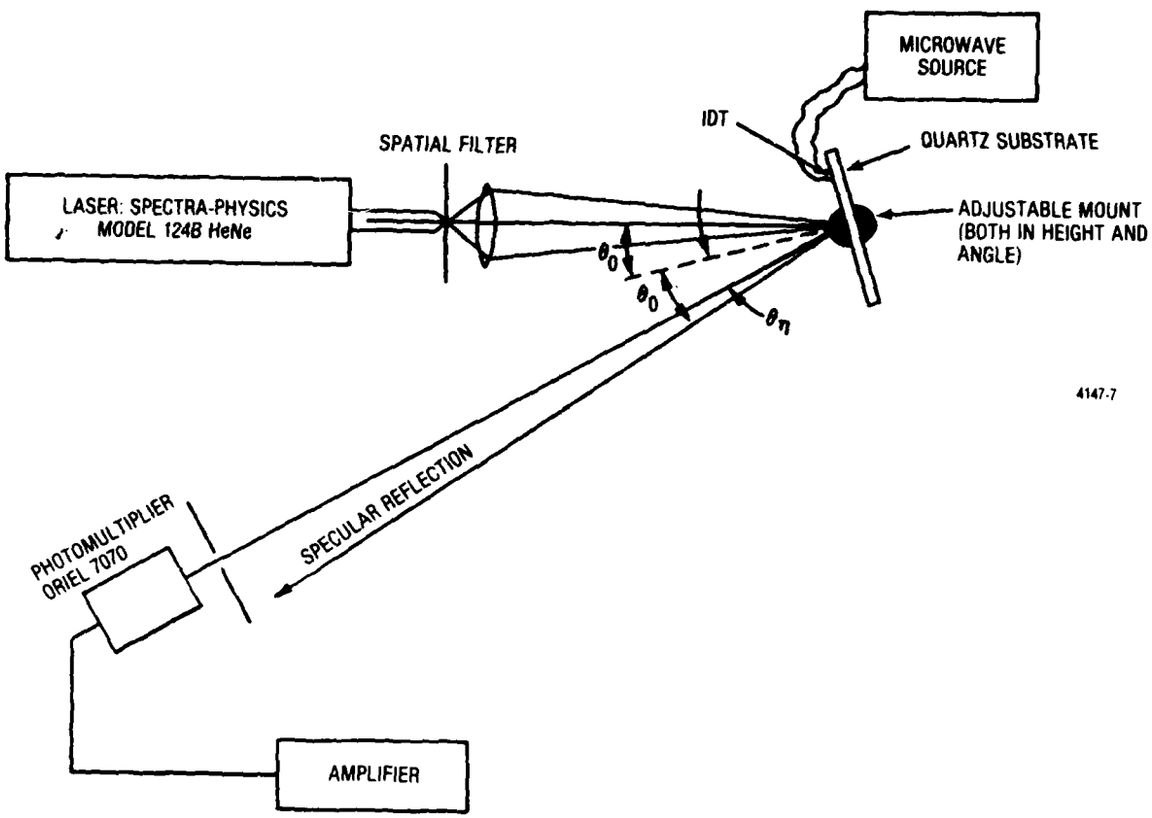


Figure 7. Angular Relation of Incidence and Reflected Beam

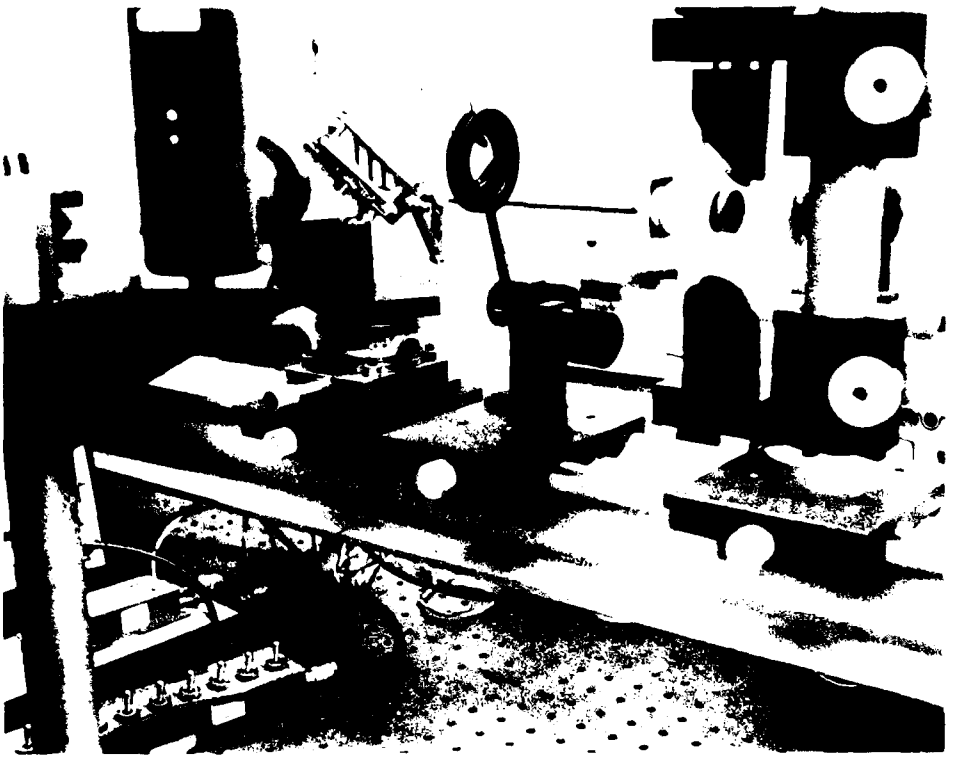

Figure 8. Test Set-up for Laser Probing of Acoustic Wave Beam-Steering Characteristics

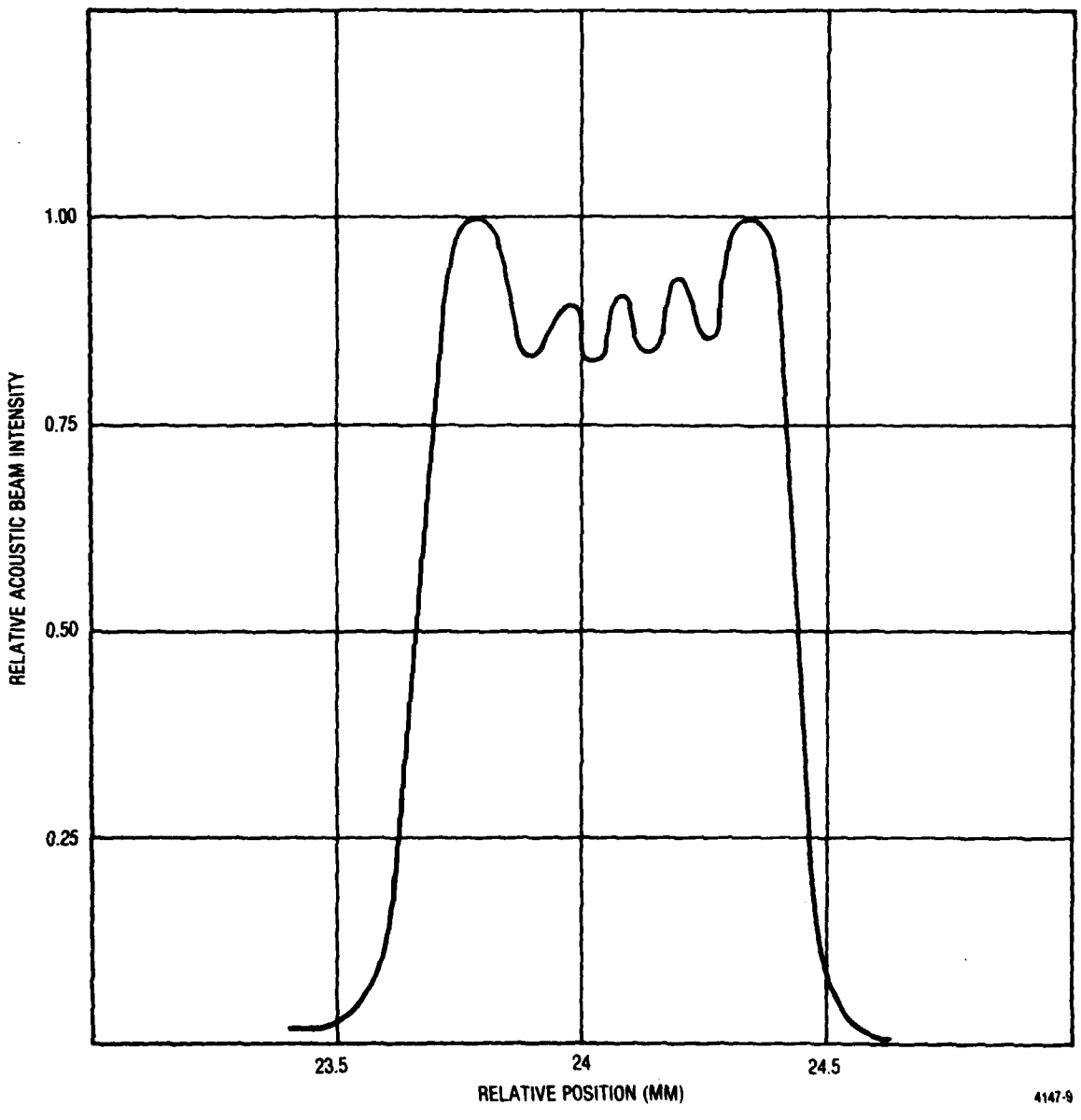


Figure 9. Intensity Distribution at Near Field

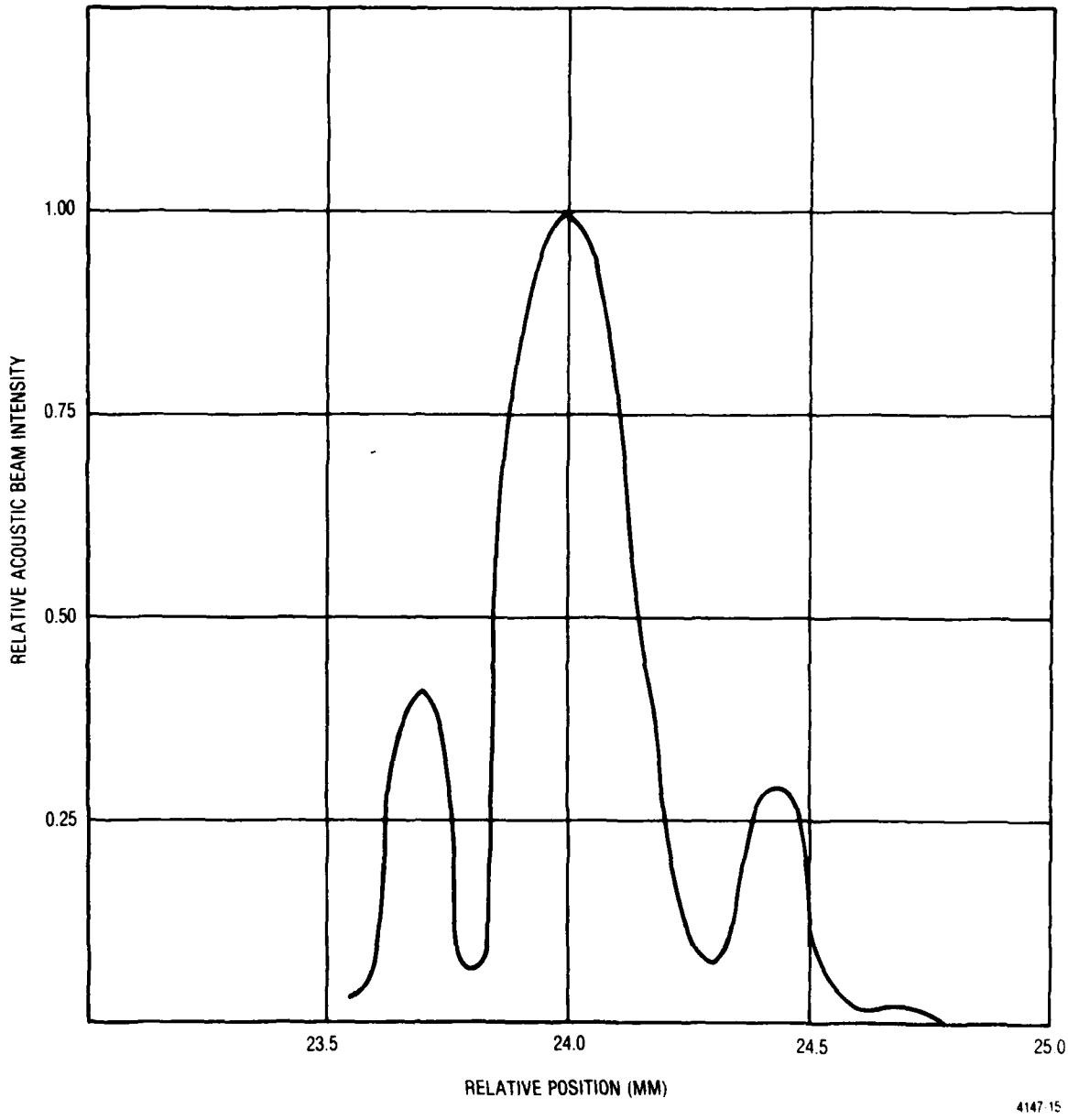


Figure 10. Intensity Distribution at Far Field

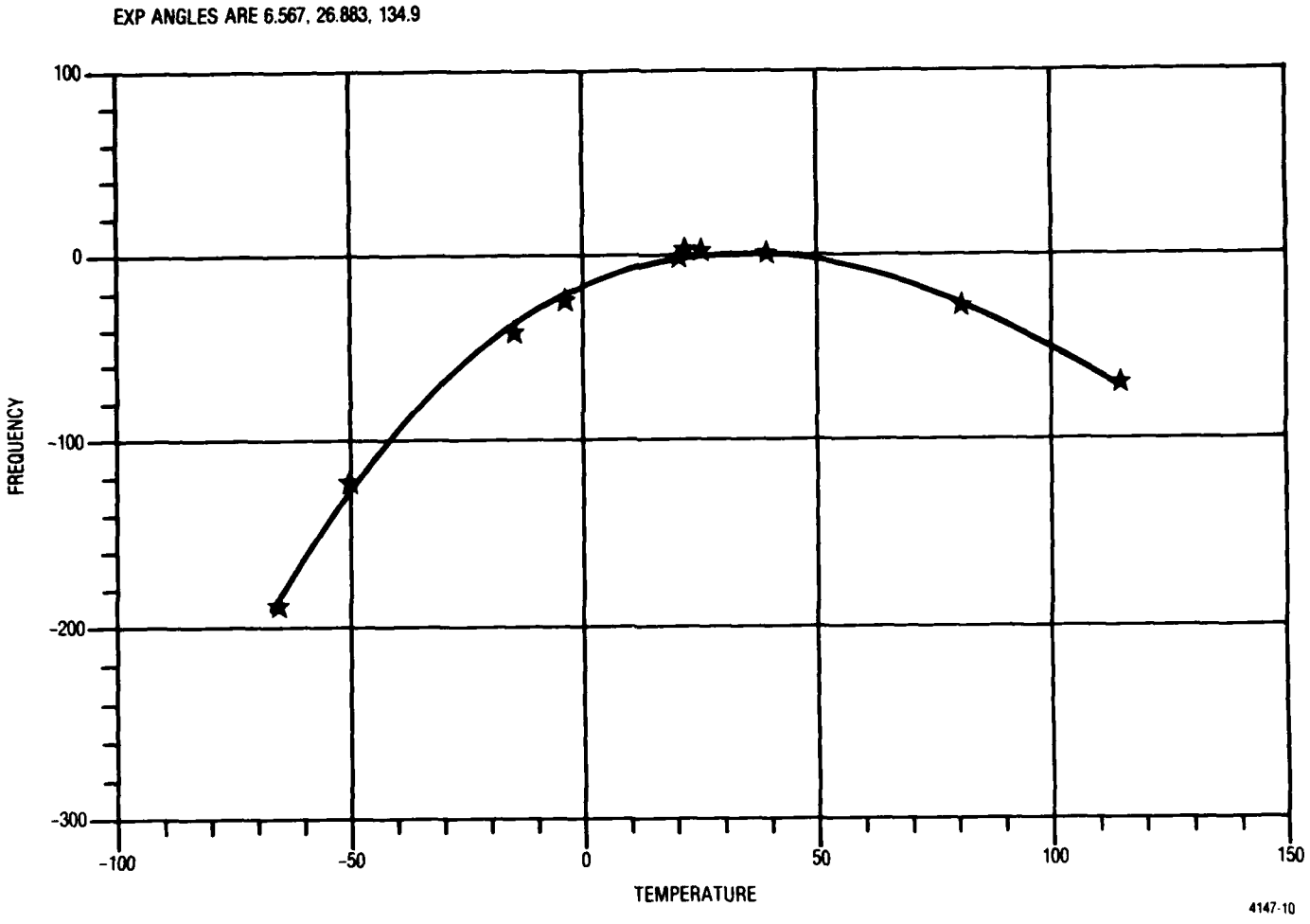


Figure 11. Experimental Frequency Response (Test No. 1)

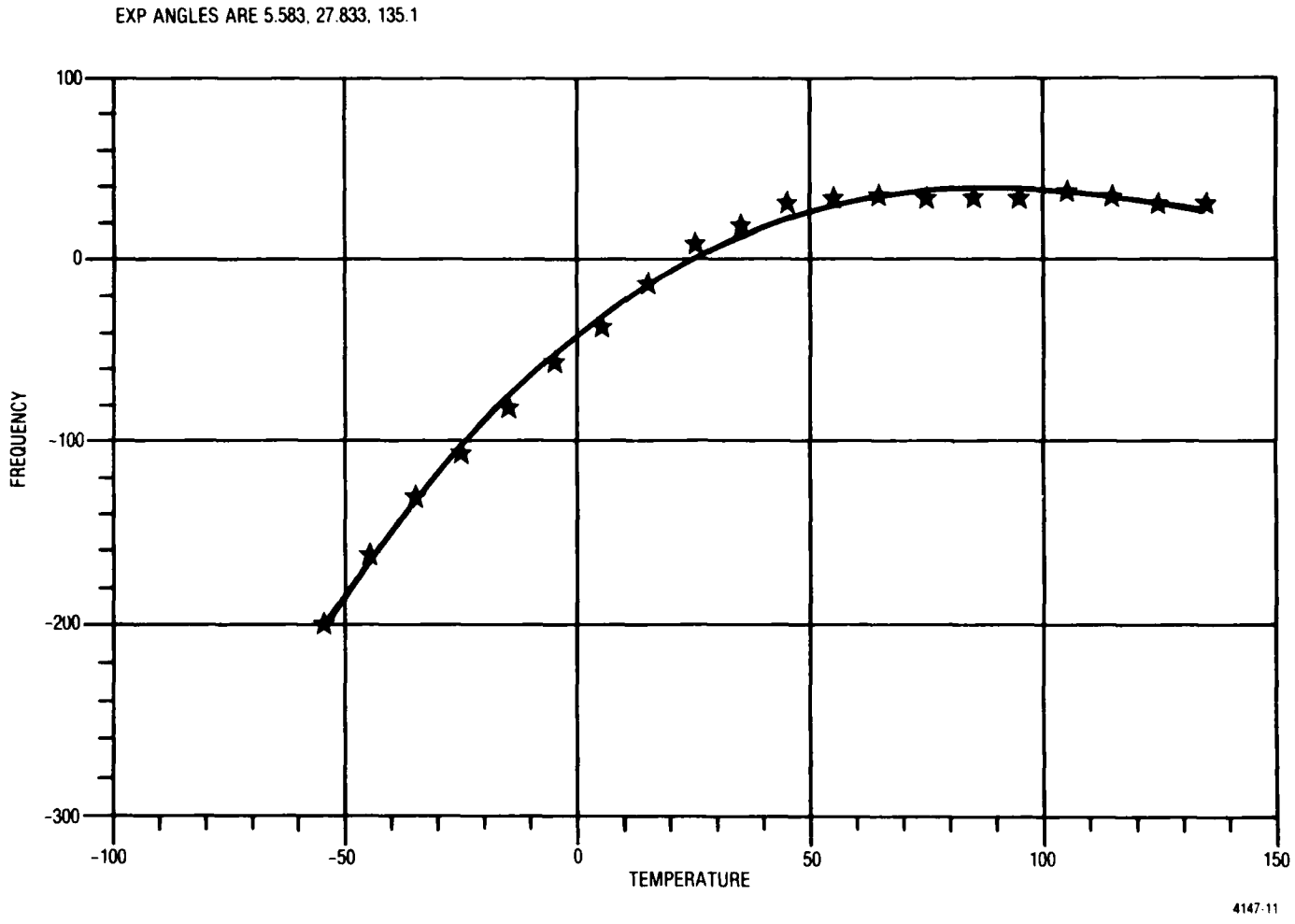


Figure 12. Experimental Frequency Response (Test No. 2)

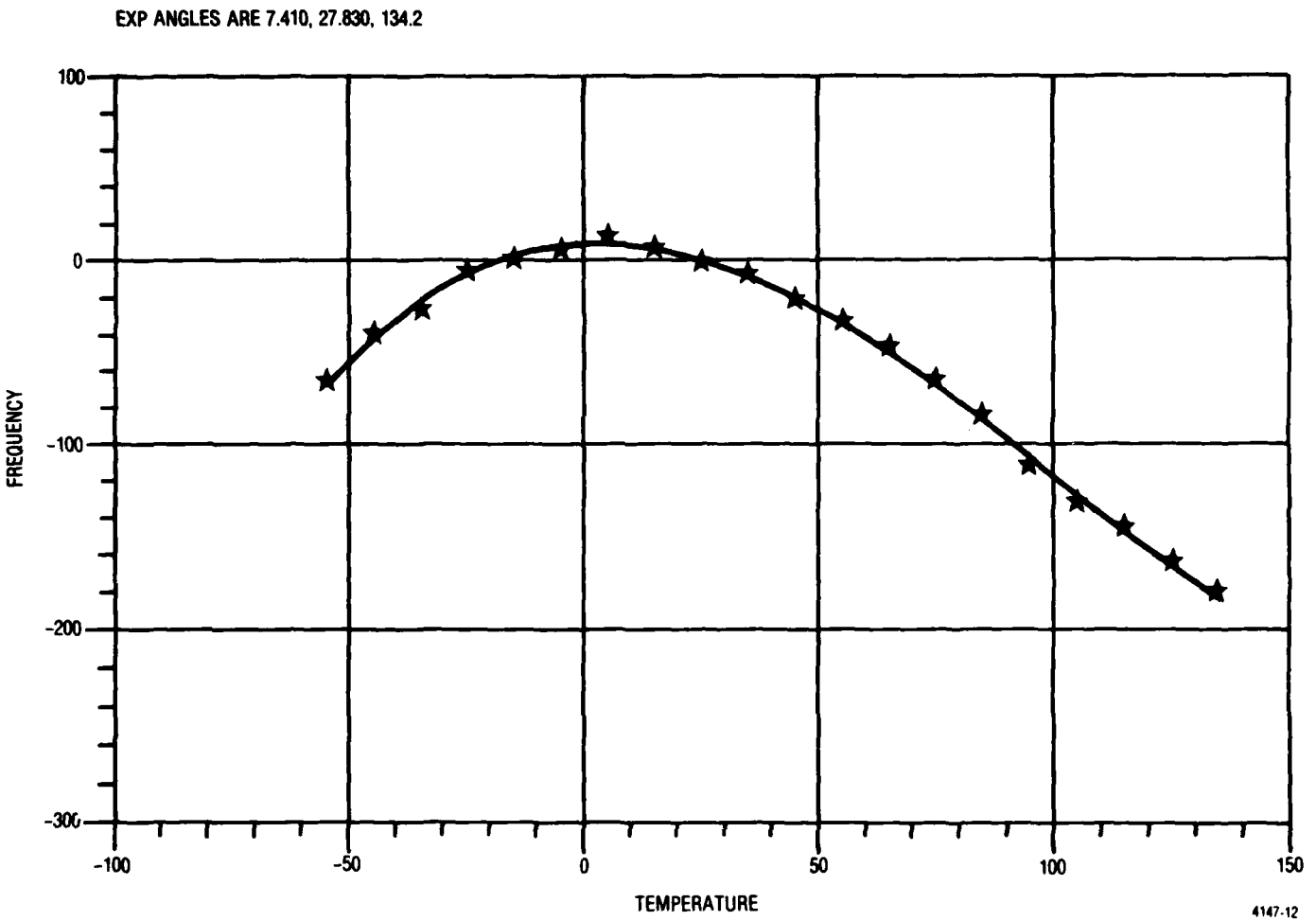


Figure 13. Experimental Frequency Response (Test No. 3)

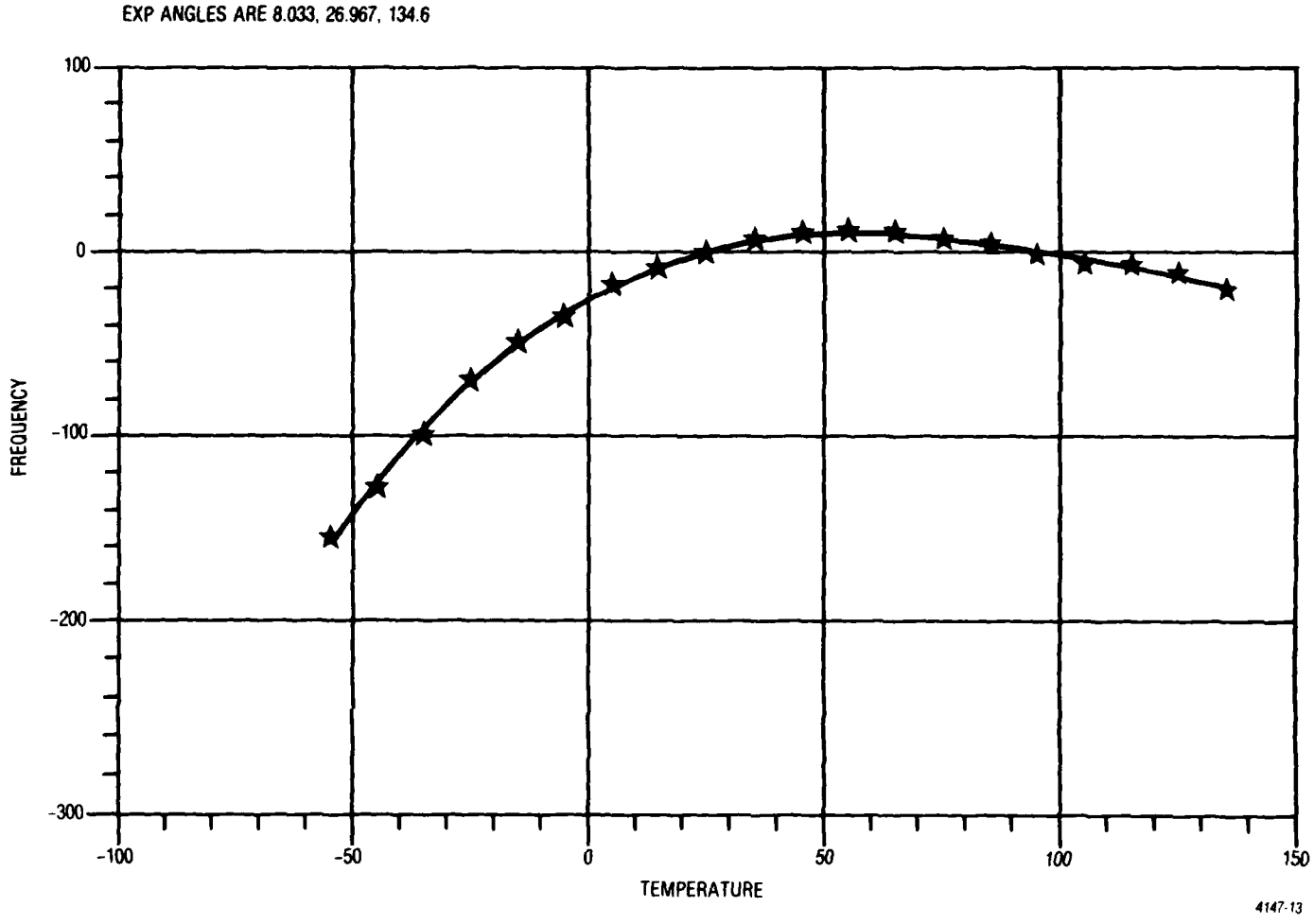


*Figure 14.* Experimental Frequency Response (Test No. 4)

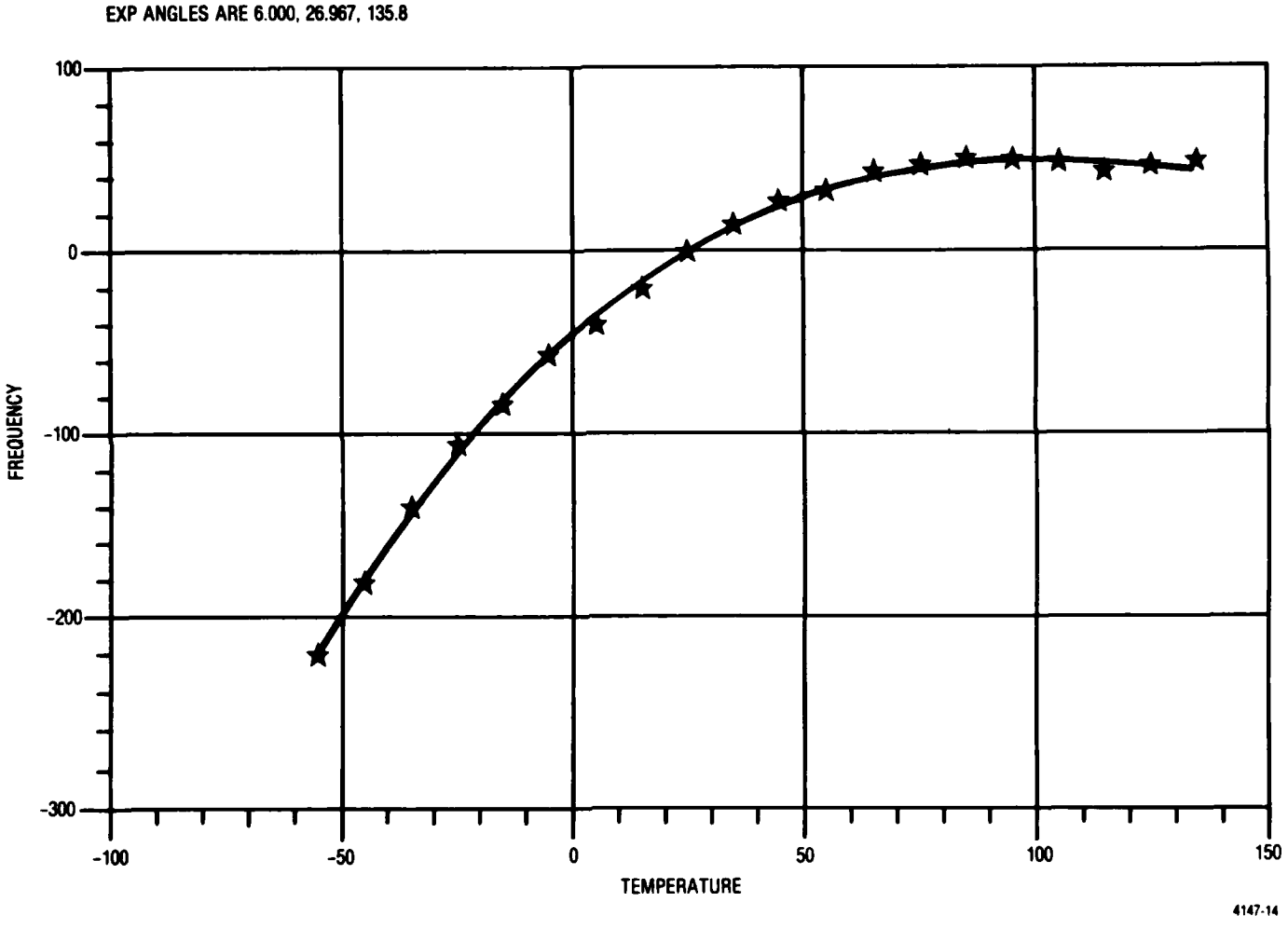


Figure 15. Experimental Frequency Response (Test No. 5)

TABLE 6. COMPARISON OF EXPERIMENTAL AND CALCULATED RESULTS

| Angles | | | Calculated | | | | Measured | | |
|---|---|---|---|---|---|---|---|---|---|
| Phi | Theta | Psi | $TCF^{(1)}$** | $TCF^{(1)}$*** | $TCF^{(2)}$*** | $TCF^{(3)}$*** | $TCF^{(1)}$ | $TCF^{(2)}$ | $TCF^{(3)}$ |
| 0 | 42.75 | 0* | $-0.07 \times 10^{-5}$ | $0.06 \times 10^{-5}$ | $-0.40 \times 10^{-7}$ | $0.11 \times 10^{-10}$ | $-0.1 \times 10^{-5}$ | $-0.37 \times 10^{-7}$ | $-0.17 \times 10^{-10}$ |
| 8.05 | 25.9 | 135.7 | −0.01 | 0.74 | −0.15 | 0.42 | 0.16 | −0.16 | 0.58 |
| 6.57 | 26.88 | 134.9 | −0.24 | 0.55 | −0.15 | 0.43 | 0.025 | −0.16 | 0.47 |
| 8.03 | 26.97 | 134.6 | −0.18 | 0.60 | −0.15 | 0.46 | 0.007 | −0.13 | 0.46 |
| 7.41 | 27.83 | 134.2 | −0.26 | 0.54 | −0.15 | 0.49 | −0.08 | −0.15 | 0.63 |
| 6.00 | 26.97 | 135.8 | −0.04 | 0.75 | −0.14 | 0.46 | 0.15 | −0.13 | 0.30 |
| 5.68 | 27.83 | 135.2 | −0.15 | 0.65 | −0.14 | 0.49 | 0.13 | −0.13 | 0.28 |

*Wafer obtained commercially, angular tolerance is unknown.

**Calculated using Sinha and Tiersten's program.

***Calculated using the finite difference approach.

# SECTION III

# CONCLUSION

It has been determined that $TCF^{(1)}$ is the most sensitive to angular variations; thus the large values of $\partial TCF1/\psi$ imposes strict fabrication tolerances on processing. It was necessary to incorporate a mask design using rotated structures to compensate for processing errors within the allowed fabrication tolerances.

Theoretical calculations of power flow angle, coupling coefficients, and second and third order TCF's indicate that they do not vary quickly with angle. Thus, by varying $\psi$ on any particular cut, linear temperature variations can be compensated for while all other cut parameters vary only slightly.

Experimental design and procedures followed during the measurements of the TCF's indicate that the experimental error is within 10 PPM. Table 6, which displays the comparison of theoretical and experimental results, illustrates the excellent agreement to date. Experimental results indicate that an improvement in $TCF^{(2)}$ by at least a factor of two over ST quartz can be obtained. A second iteration approach using a higher resolution is expected to improve the $TCF^{(2)}$ of the doubly rotated quartz over the ST cut by a factor of three to four. Determinations of experimental propagation characteristics using the laser probe technique demonstrated good agreement between measured and calculated values.

# APPENDIX

## TCF MAPS

This appendix contains TCF maps with Theta less than zero. The TCF maps with Theta greater than zero can be found in the first interim report. The two sets of maps span the entire set of singly and doubly rotated cuts on quartz. The circles denote values of the first-order SAW TCF. The crosses denote values of the second-order SAW TCF. The corresponding scales are found on the left and right hand sides of the graphs. Only data calculated on the 10° x 10° grid is plotted.

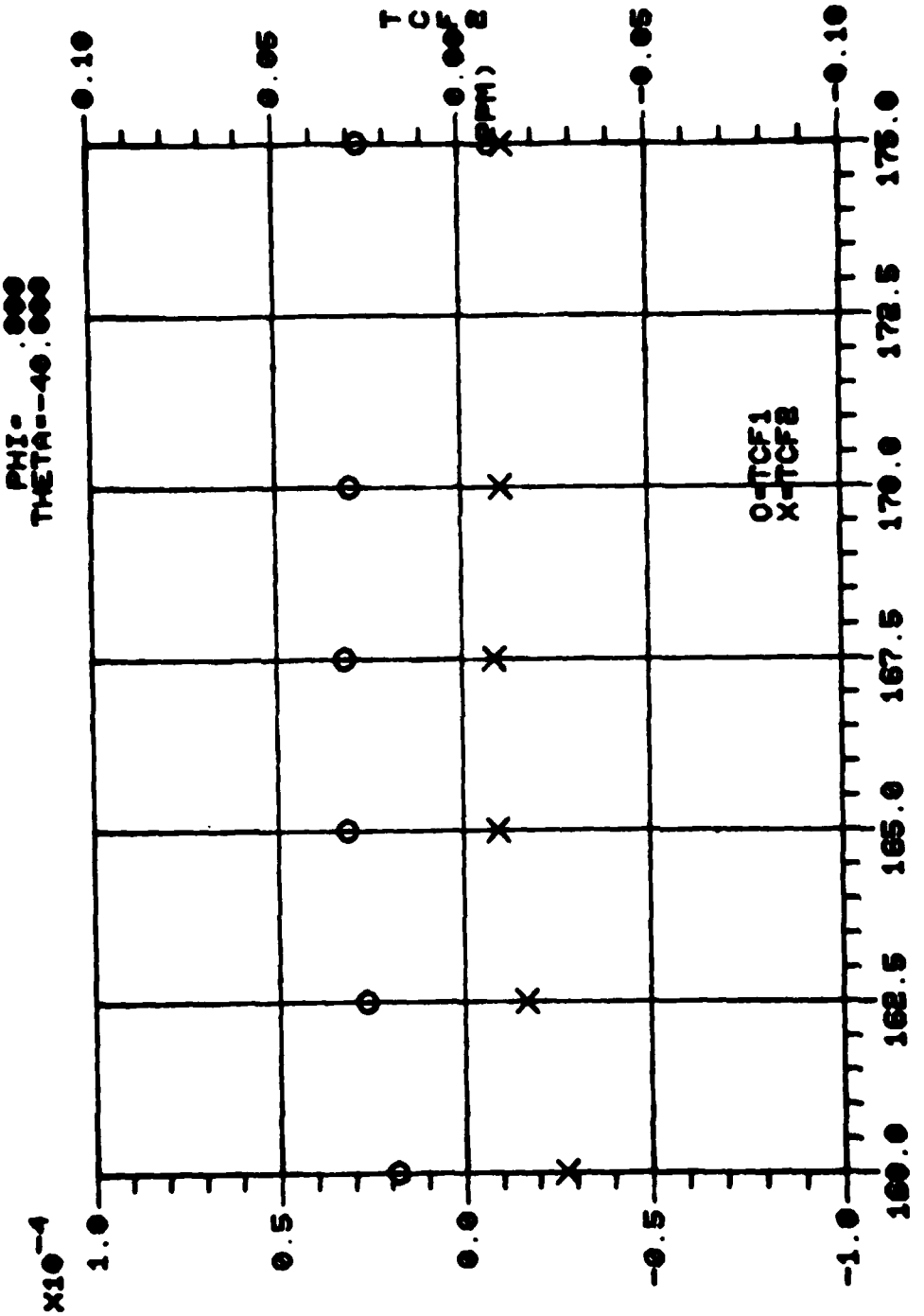
PHI=
THETA=-40.000
O=TCF1
X=TCF2
X10**-4
1.0
0.5
0.0
-0.5
-1.0
160.0
162.5
165.0
167.5
170.0
172.5
175.0
PSI

FIG 1

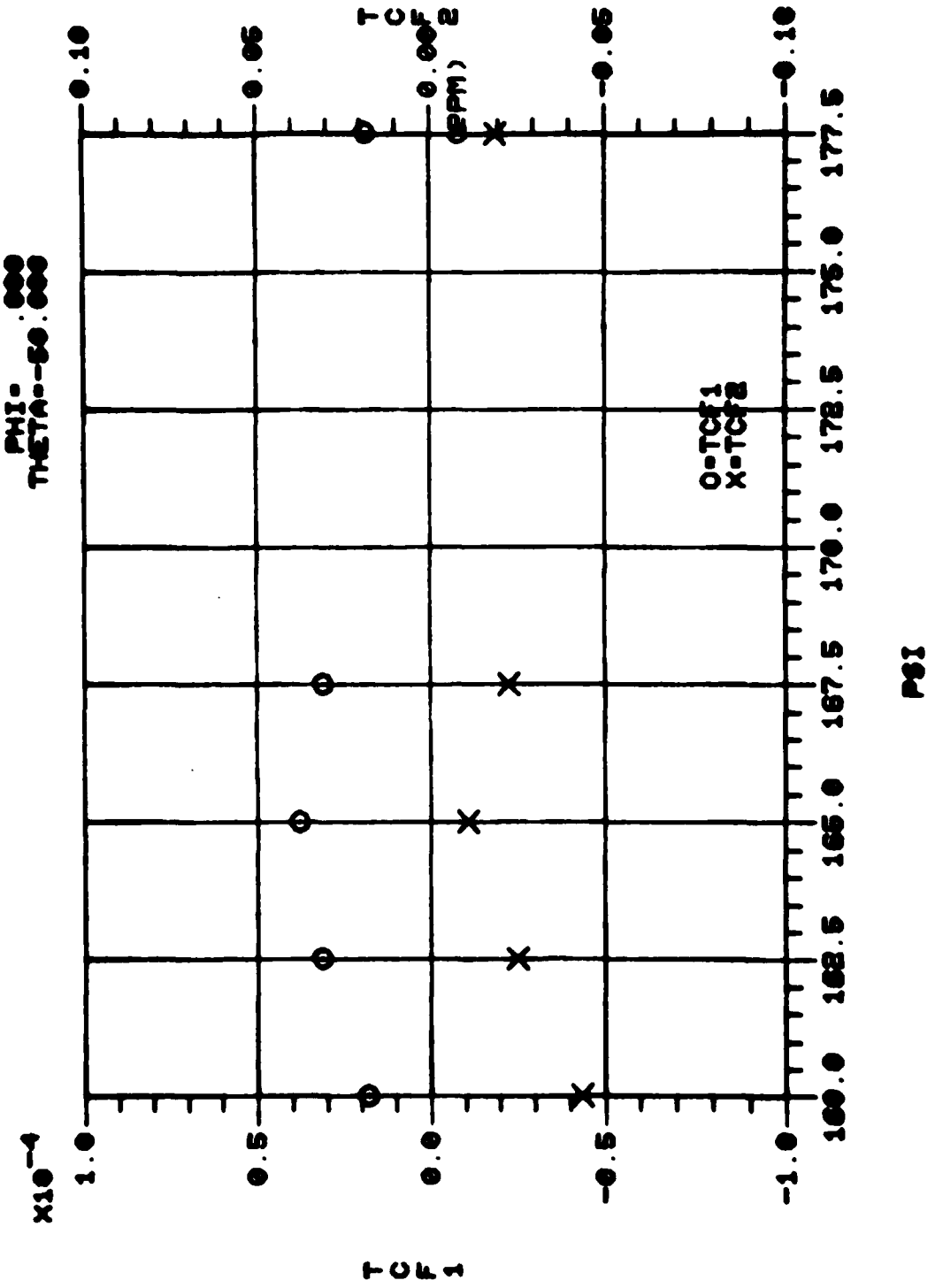
PHI=
THETA=-50.000
O-TCF1
X-TCF2
T C
(EPM)
0.10
0.05
0.00
-0.05
-0.10
X10**-4
1.0
0.5
0.0
-0.5
-1.0
160.0
162.5
165.0
167.5
170.0
172.5
175.0
177.5
PSI
TCF1

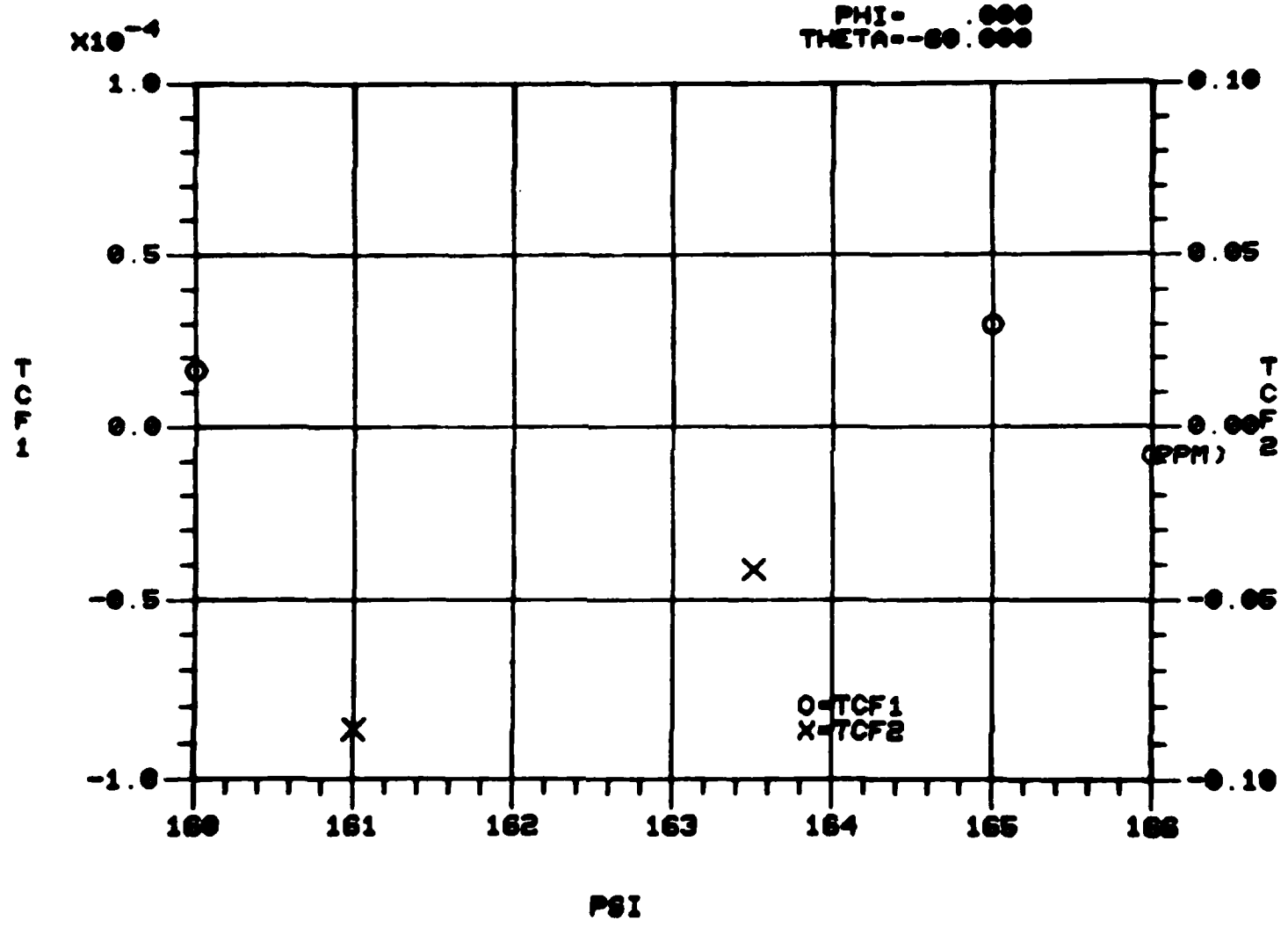
PHI=
THETA=-90.000
X10^-4
1.0
0.5
0.0
-0.5
-1.0
0.10
0.05
0.00
-0.05
-0.10
TCF1
TCF2
(PPM)
O=TCF1
X=TCF2
160
161
162
163
164
165
166
PSI

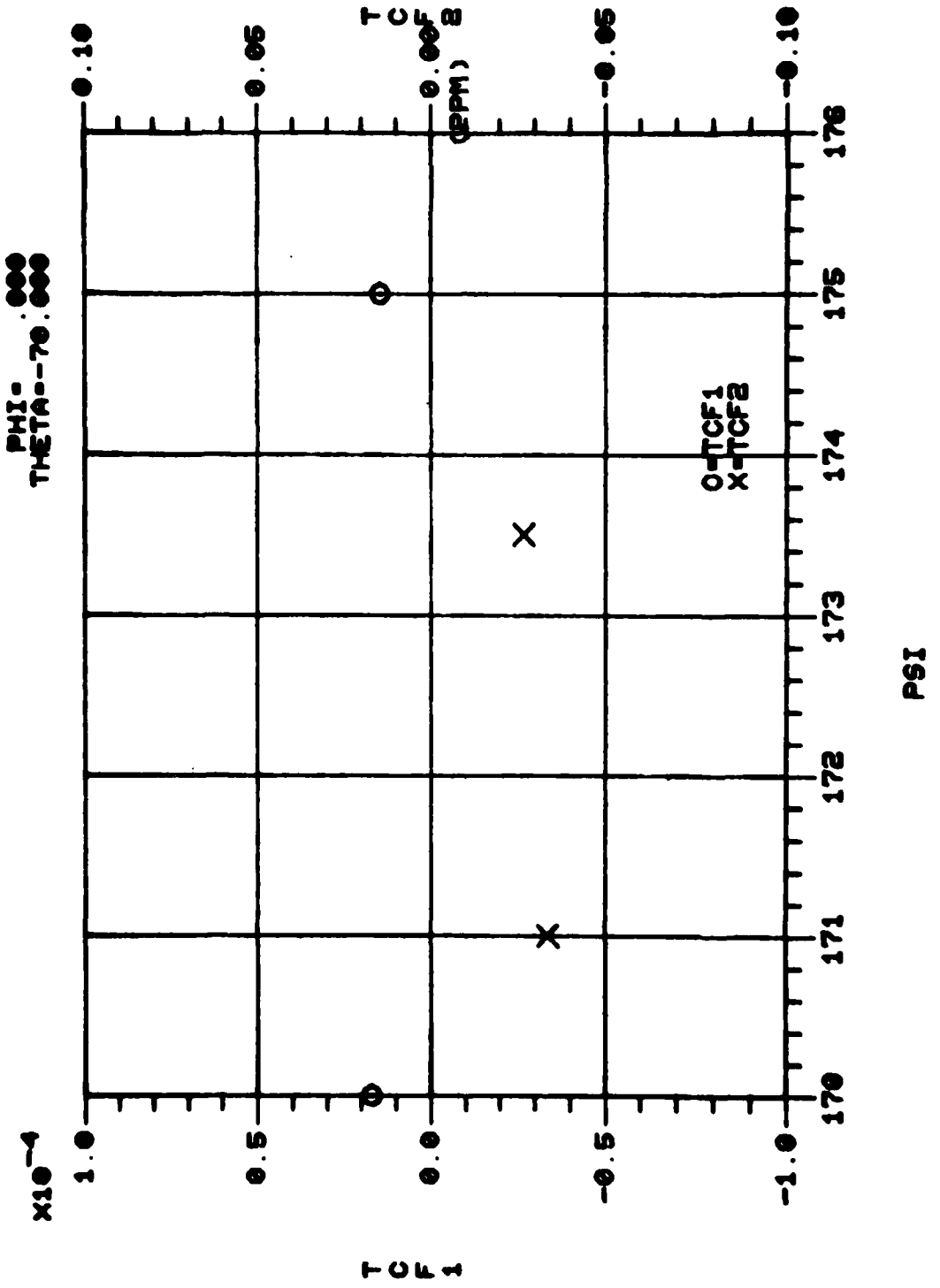
PHI=
THETA=-70.000
O=TCF1
X=TCF2
T C
(PPM)
0.10
0.05
0.00
-0.05
-0.10
170
171
172
173
174
175
176
PSI
X10^-4
1.0
0.5
0.0
-0.5
-1.0
TCF1

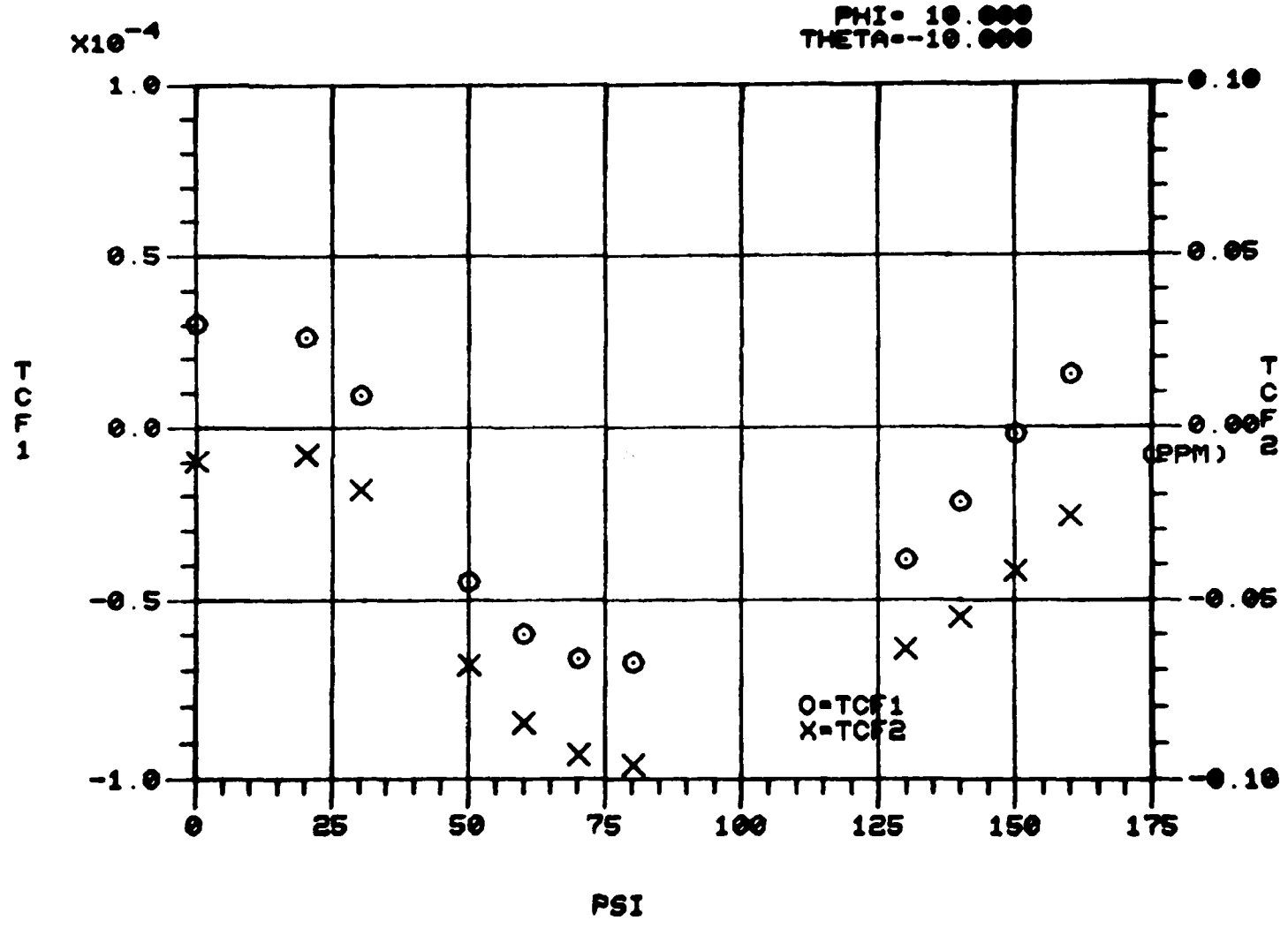
PHI= 10.000
THETA=-10.000
X10^-4
1.0
0.5
0.0
-0.5
-1.0
TCF1
0.10
0.05
0.00
-0.05
-0.10
TCF2
(PPM)
0=TCF1
X=TCF2
0
25
50
75
100
125
150
175
PSI

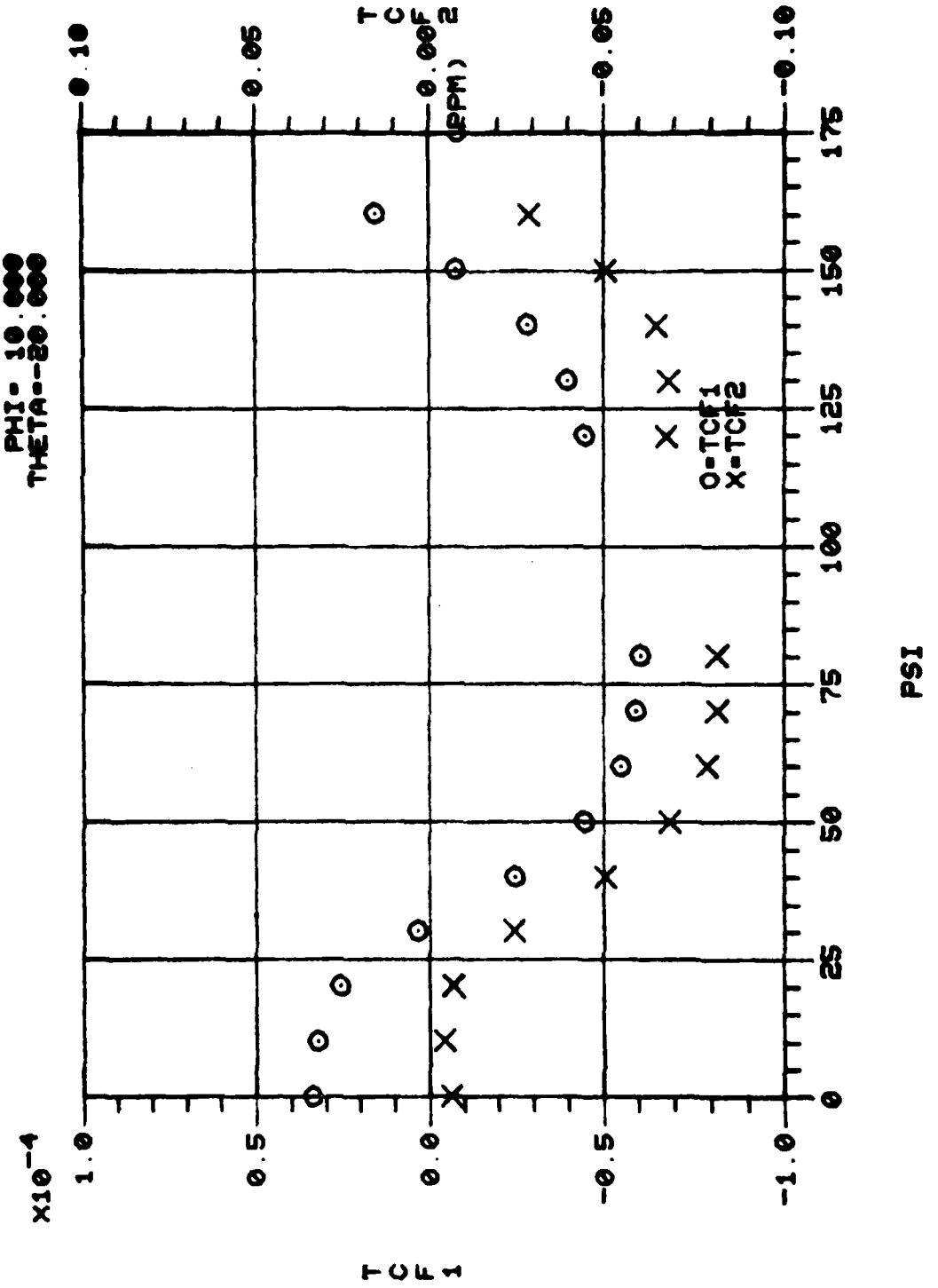
PHI= 10.000
THETA=-20.000
O-TCF1
X-TCF2
TCF1
PSI
TC (DPM) 2
X10^-4
0.10
0.05
0.00
-0.05
-0.10
1.0
0.5
0.0
-0.5
-1.0
0
25
50
75
100
125
150
175

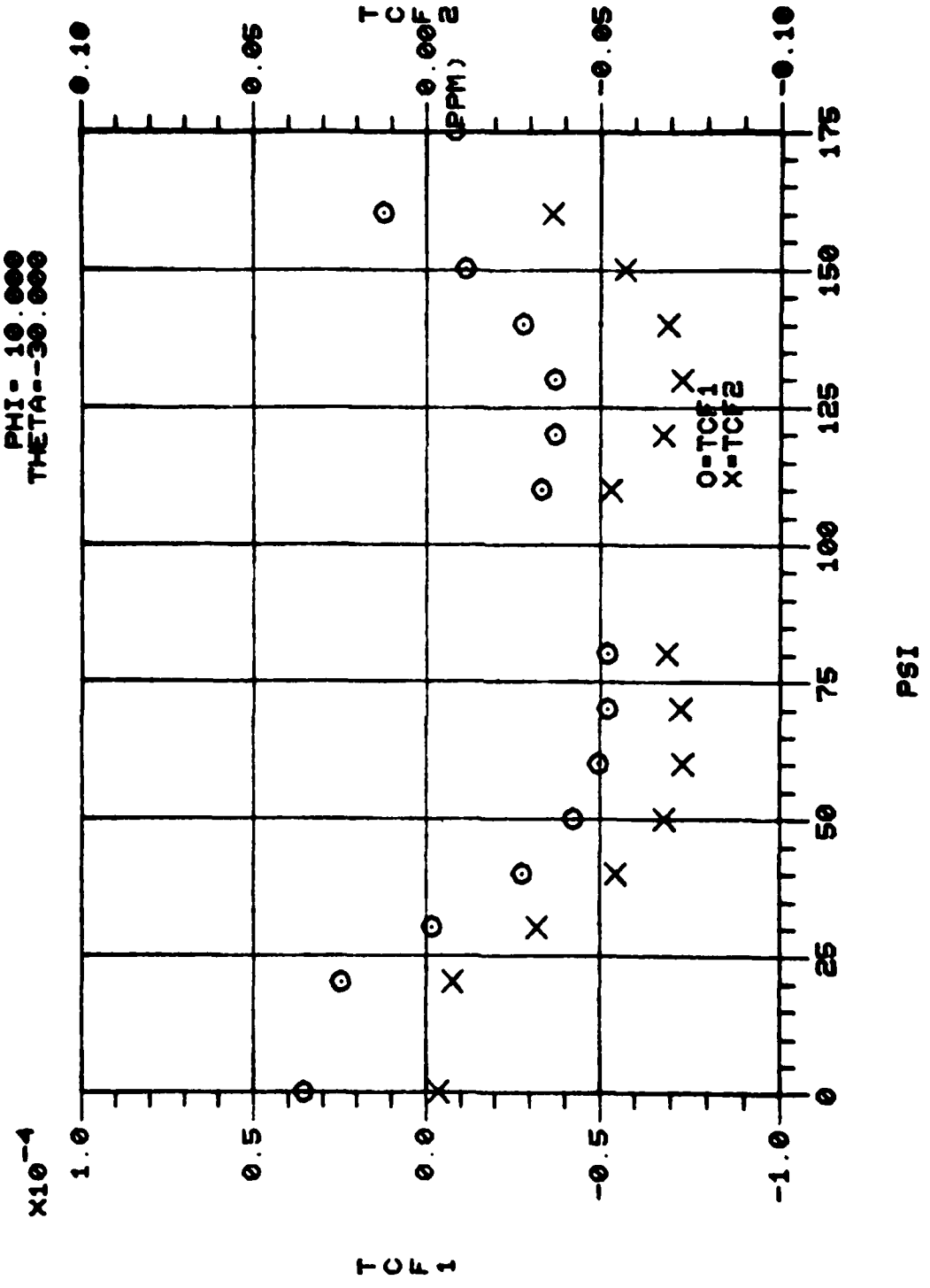
PHI= 10.000
THETA=-30.000
O-TCF1
X-TCF2
T C
0.00F
(PPM)
2
0.10
0.05
-0.05
-0.10
175
150
125
100
75
50
25
0
PSI
X10^-4
1.0
0.5
0.0
-0.5
-1.0
TCF1

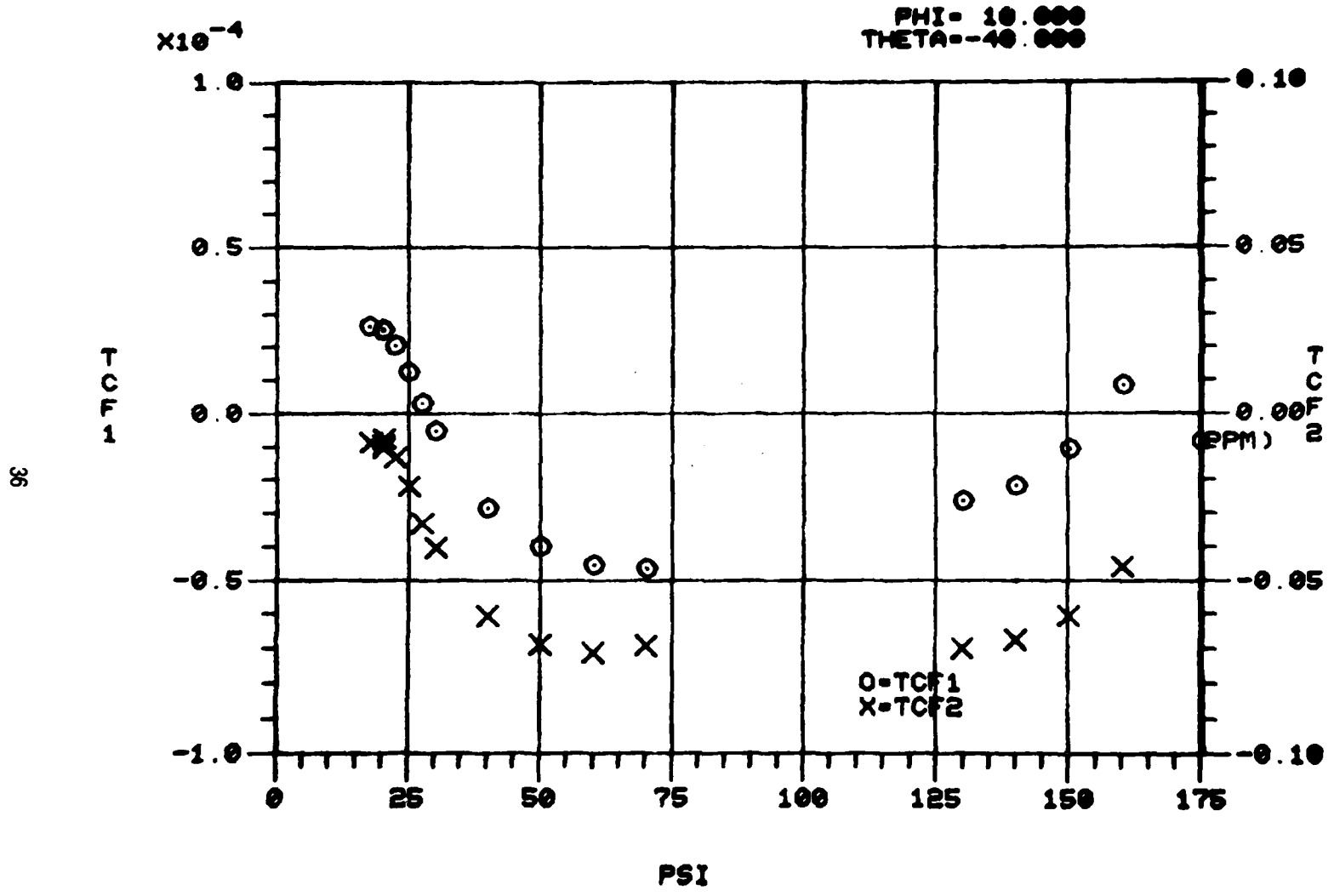
PHI= 10.000
THETA=-40.000
X10^-4
1.0
0.5
0.0
-0.5
-1.0
0.10
0.05
0.00
-0.05
-0.10
TCF1
TCF2
(PPM)
0
25
50
75
100
125
150
175
PSI
O=TCF1
X=TCF2

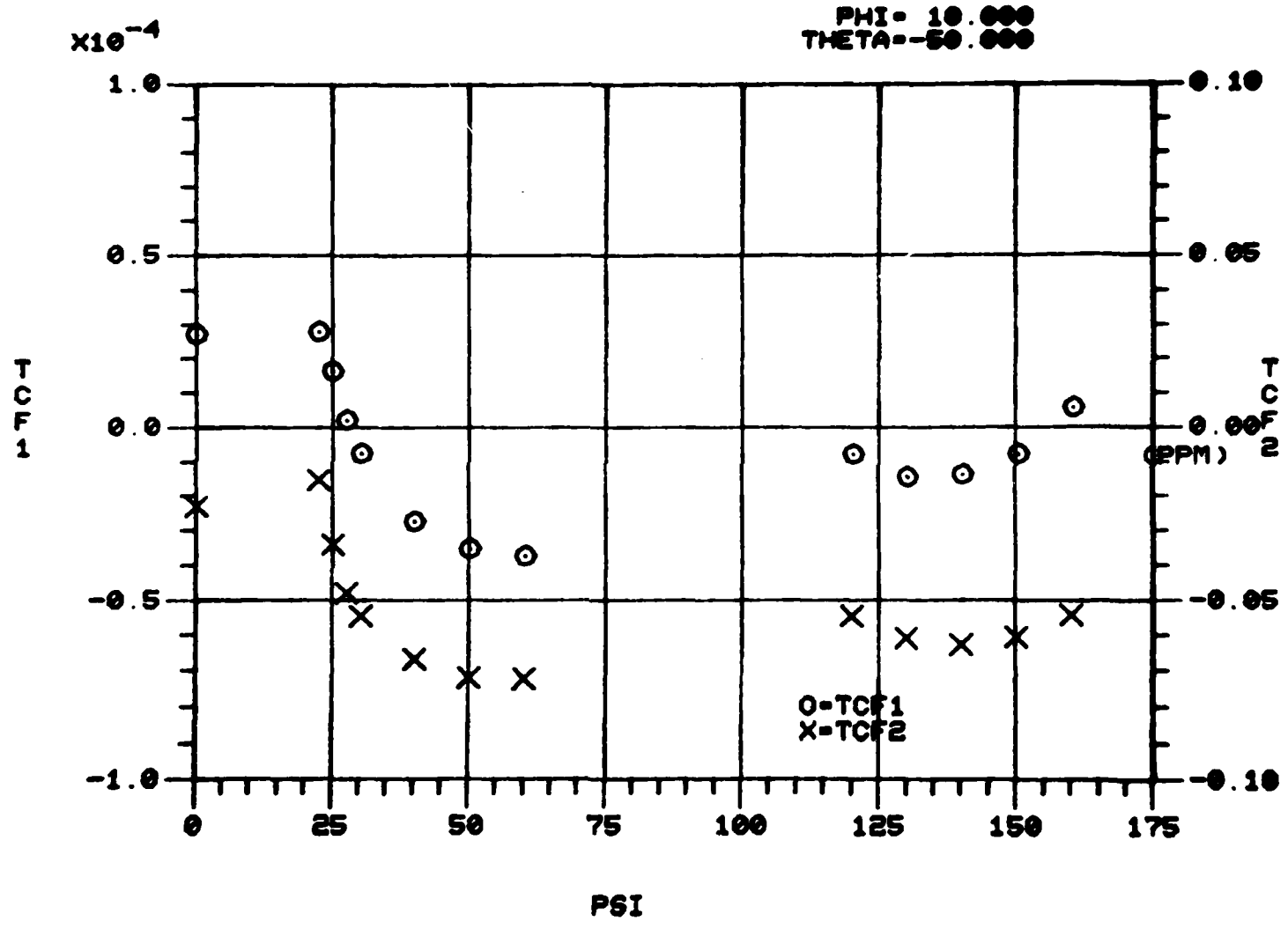
PHI= 10.000
THETA=-50.000
X10^-4
1.0
0.5
0.0
-0.5
-1.0
TCF1
0.10
0.05
0.00
-0.05
-0.10
TCF2
(PPM)
0
25
50
75
100
125
150
175
PSI
O-TCF1
X-TCF2

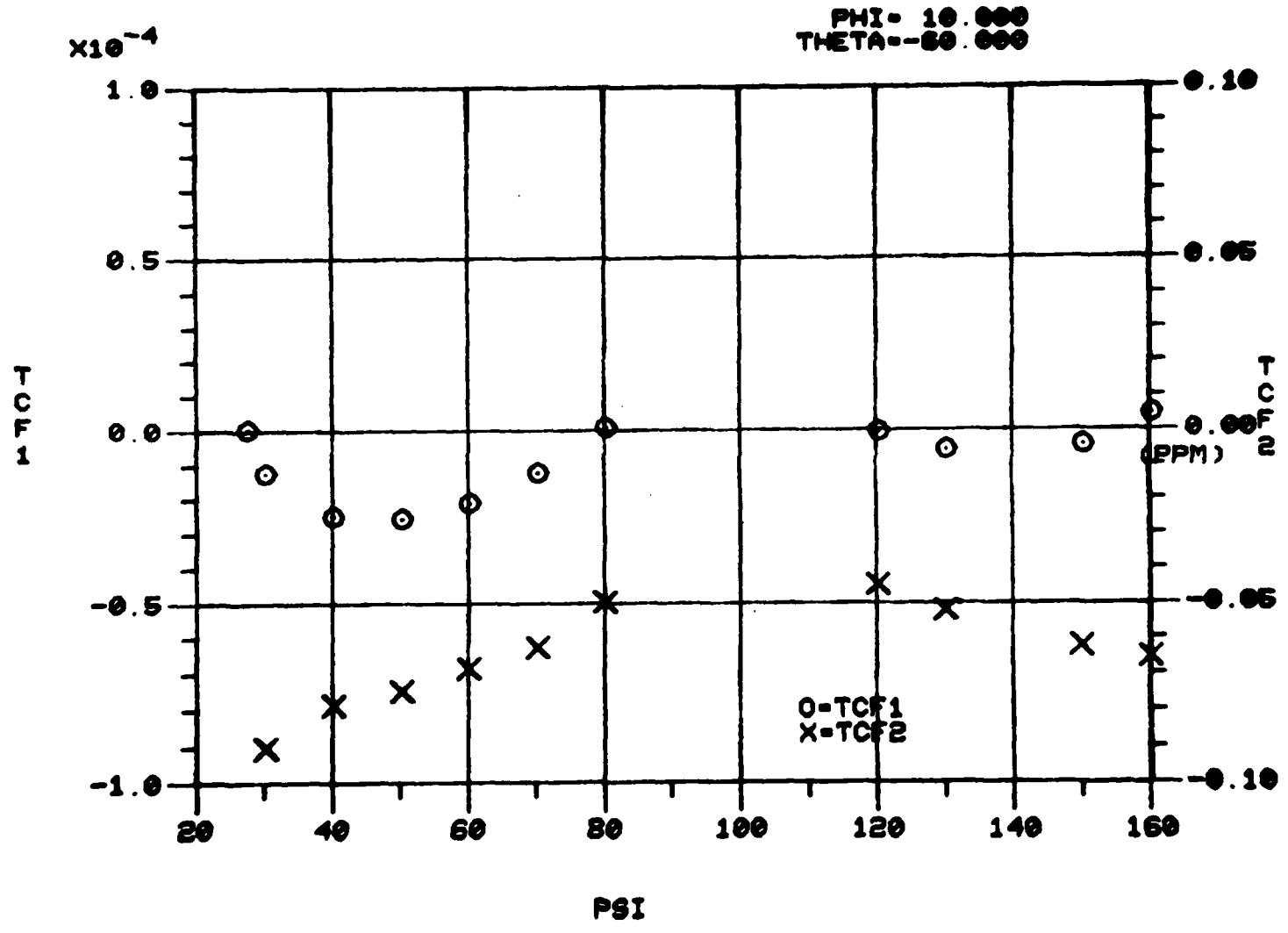
PHI= 10.000
THETA=-60.000
X10^-4
1.0
0.5
0.0
-0.5
-1.0
TCF1
0.10
0.05
0.00
-0.05
-0.10
TCF2
(PPM)
O=TCF1
X=TCF2
20
40
60
80
100
120
140
160
PSI

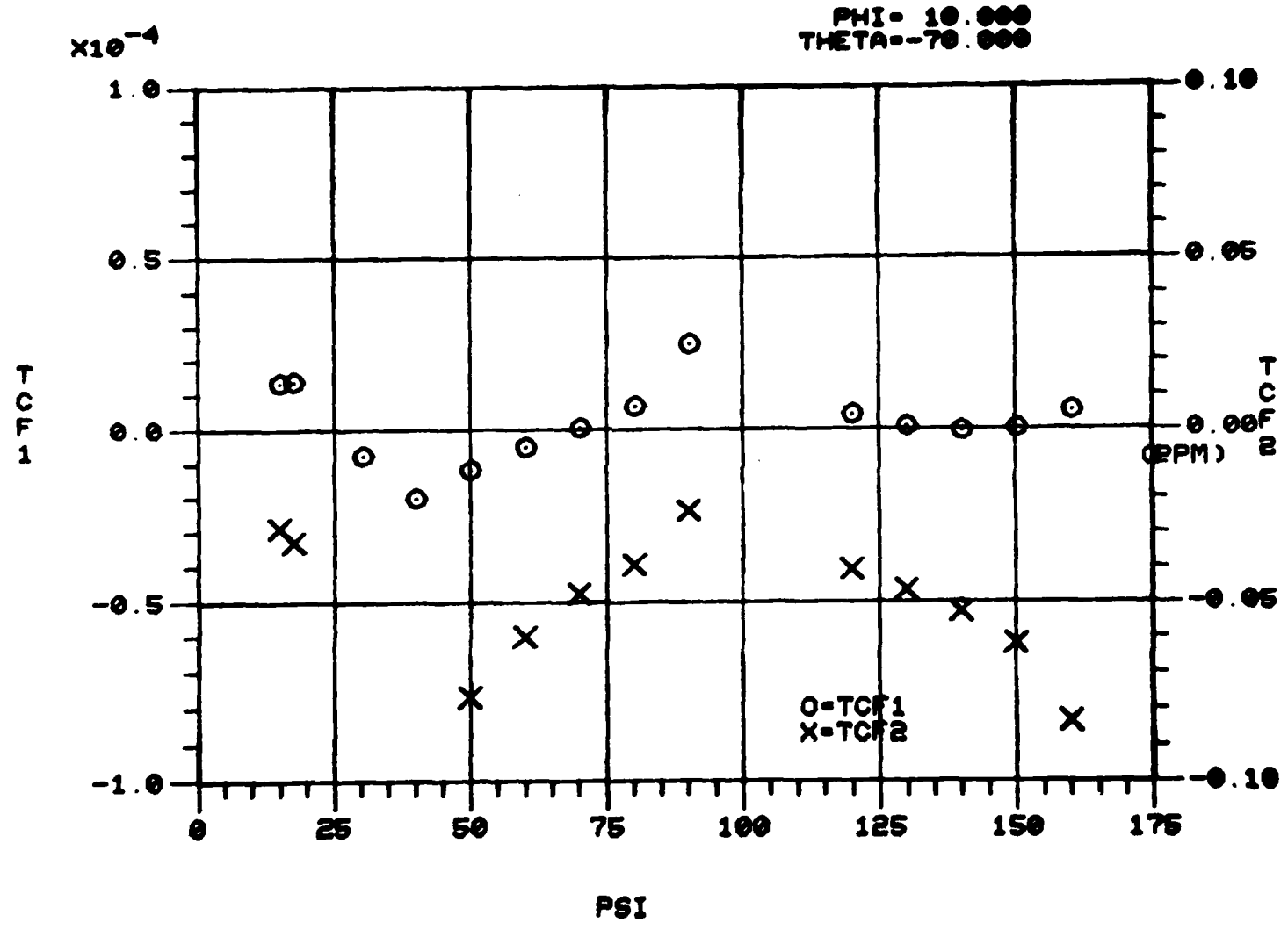
PHI= 10.000
THETA=-70.000
X10⁻⁴
1.0
0.5
0.0
-0.5
-1.0
0.10
0.05
0.00
-0.05
-0.10
TCF1
TCF2
(PPM)
0
25
50
75
100
125
150
175
PSI
O=TCF1
X=TCF2

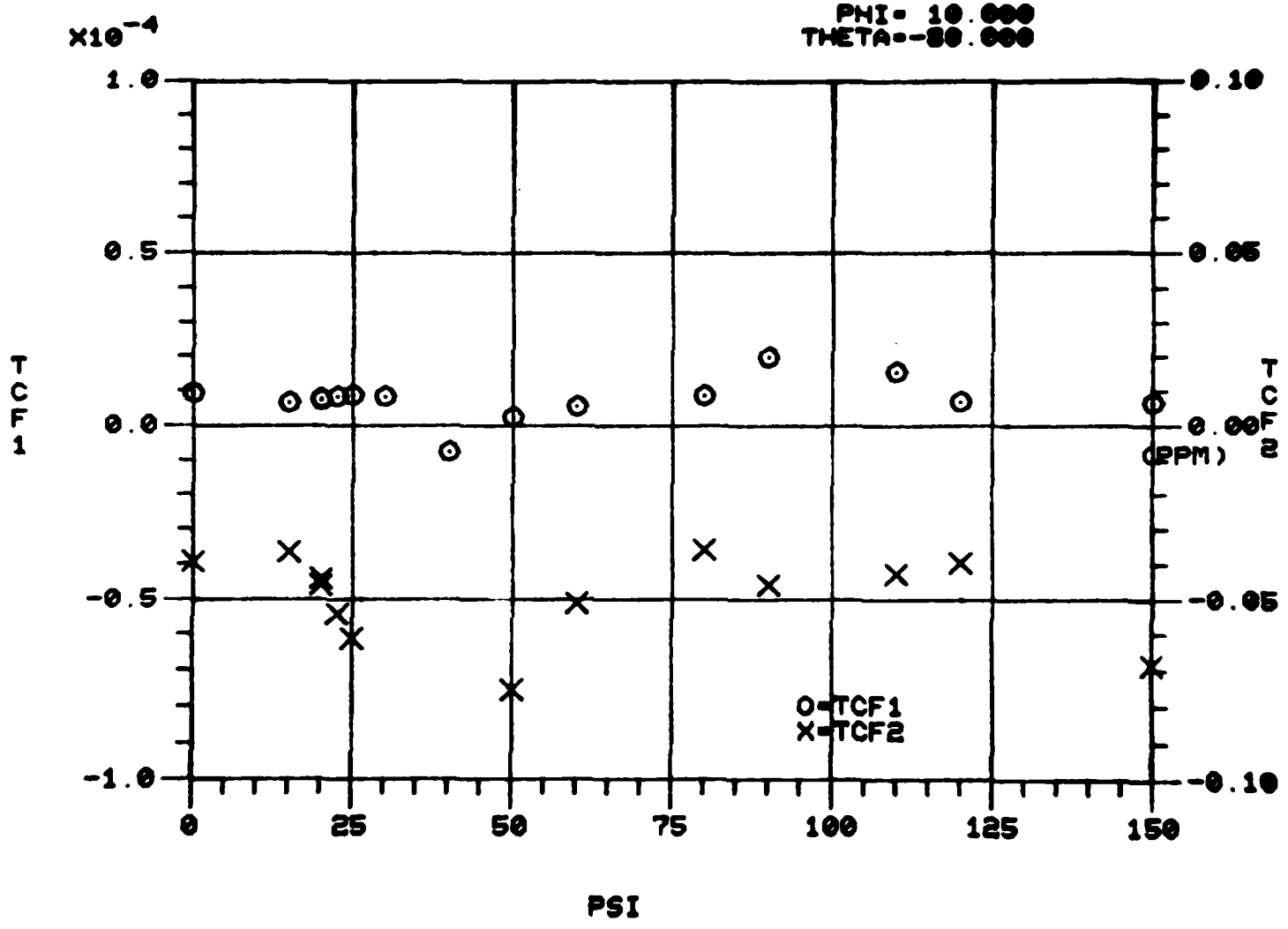
PHI= 10.000
THETA=-80.000
X10^-4
1.0
0.5
0.0
-0.5
-1.0
0.10
0.05
0.00
-0.05
-0.10
TCF1
TCF2
(PPM)
O=TCF1
X=TCF2
0
25
50
75
100
125
150
PSI

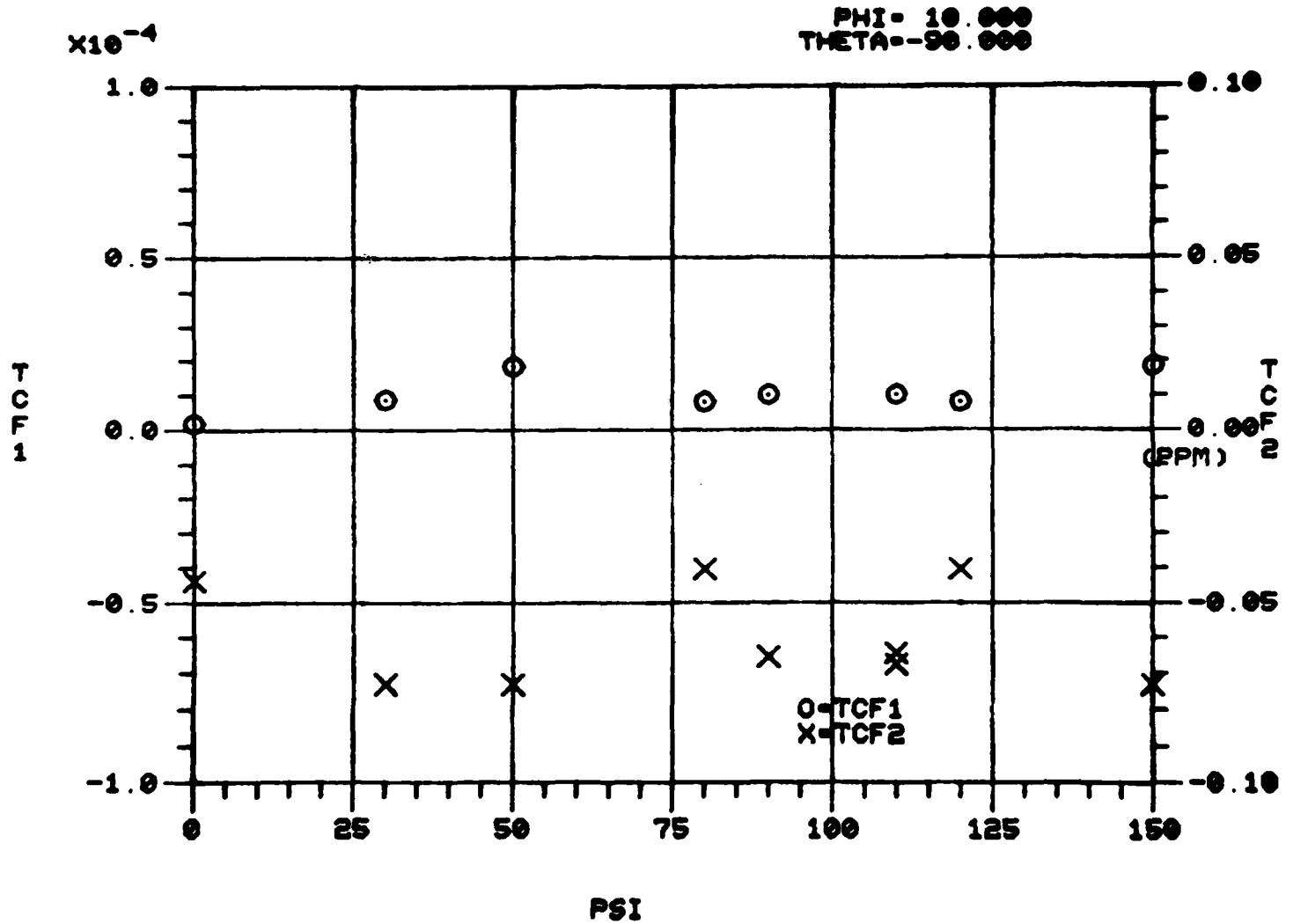
PHI= 10.000
THETA=-90.000
X10-4
1.0
0.5
0.0
-0.5
-1.0
0.10
0.05
0.00
-0.05
-0.10
TCF1
TCF2
(PPM)
O=TCF1
X=TCF2
0
25
50
75
100
125
150
PSI

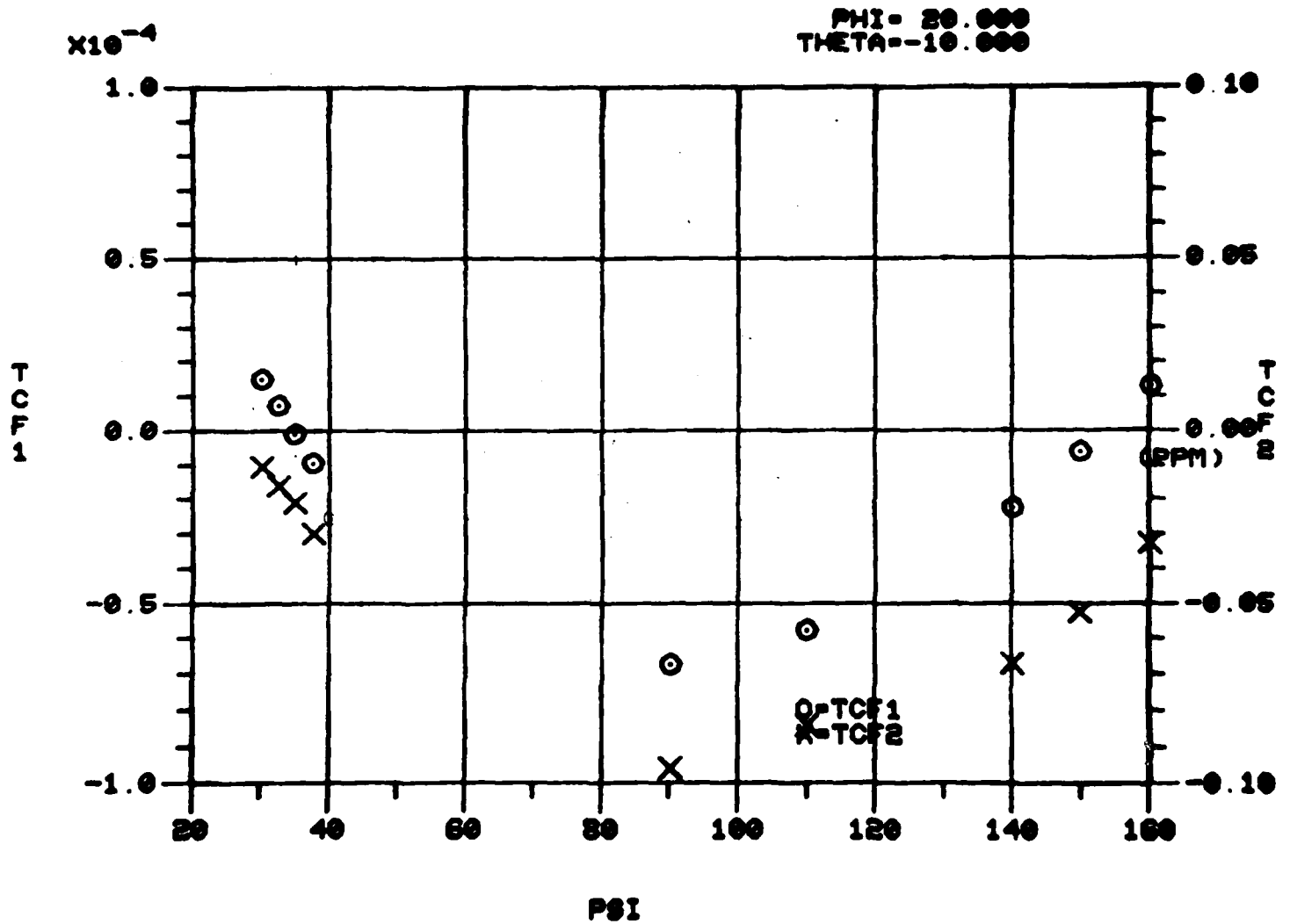
PHI= 20.000
THETA=-10.000
X10^-4
1.0
0.5
0.0
-0.5
-1.0
TCF1
0.10
0.05
0.00
-0.05
-0.10
TCF2
(PPM)
20
40
60
80
100
120
140
160
PSI
O=TCF1
X=TCF2

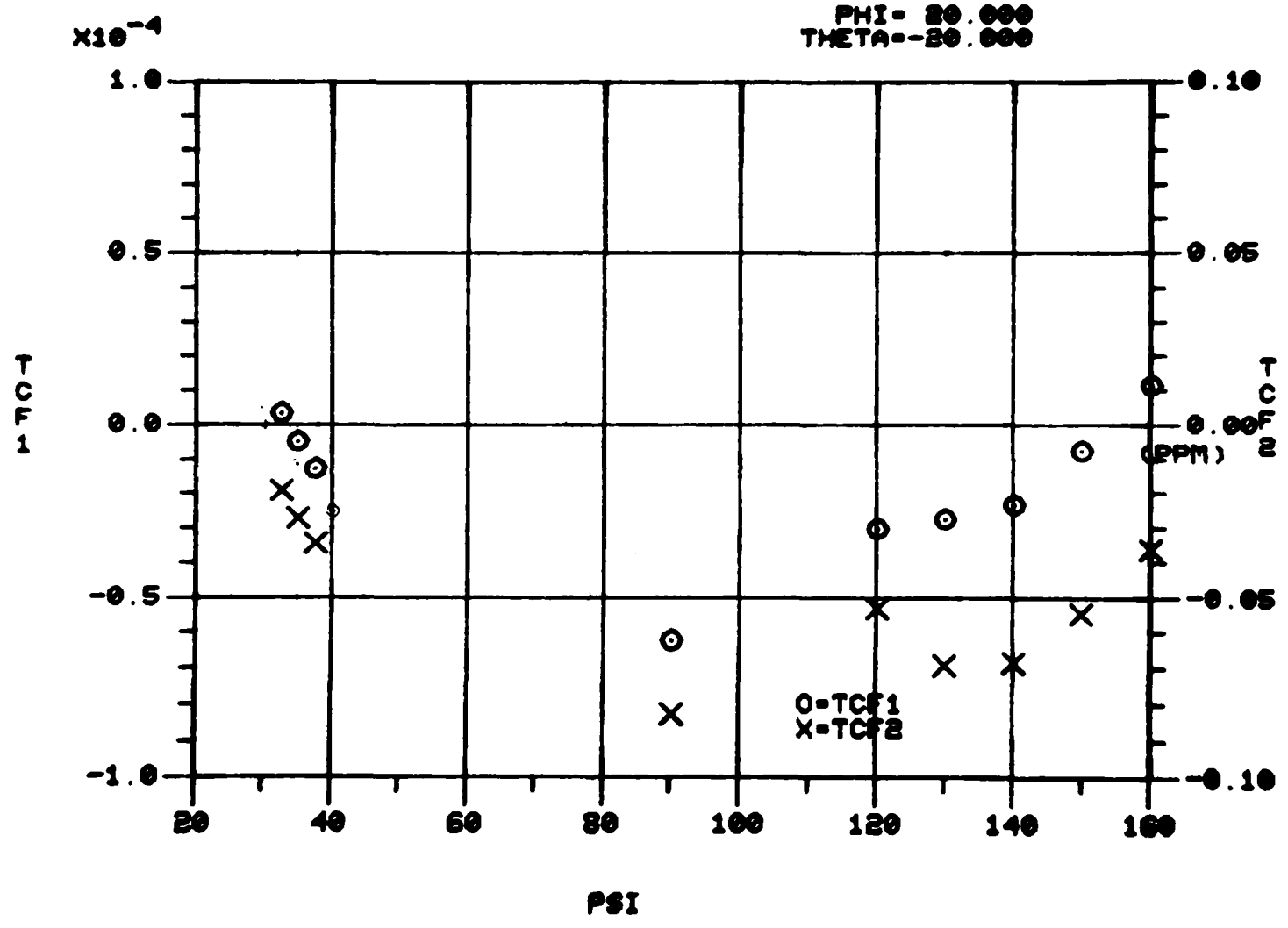
PHI= 20.000
THETA=-20.000
X10-4
1.0
0.5
0.0
-0.5
-1.0
0.10
0.05
0.00
-0.05
-0.10
TCF1
TCF2
(PPM)
O=TCF1
X=TCF2
20
40
60
80
100
120
140
160
PSI

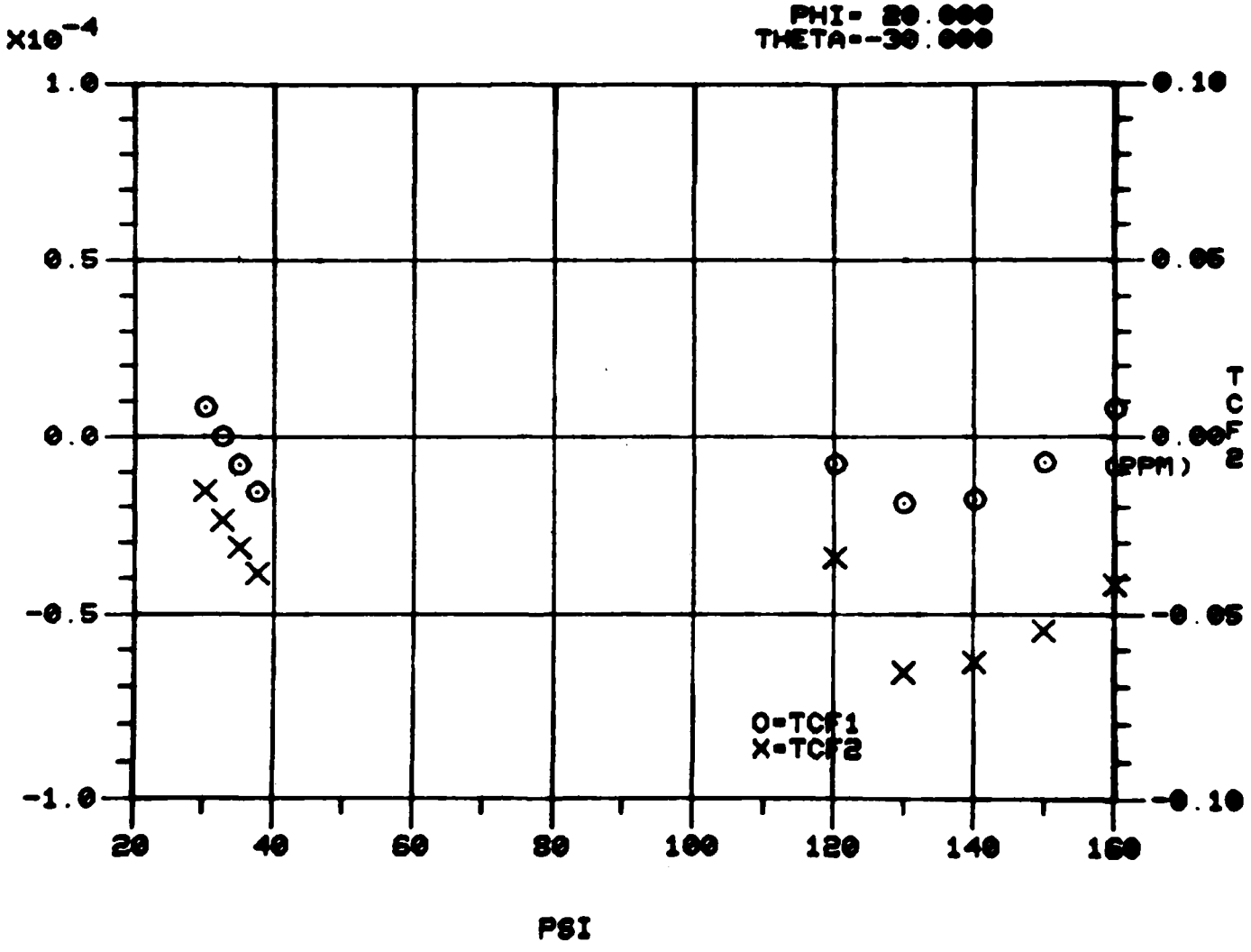
PHI= 20.000
THETA=-30.000
X10-4
1.0
0.5
0.0
-0.5
-1.0
0.10
0.05
0.00
-0.05
-0.10
TCF1
TCF2
(PPM)
20
40
60
80
100
120
140
160
PSI
O=TCF1
X=TCF2

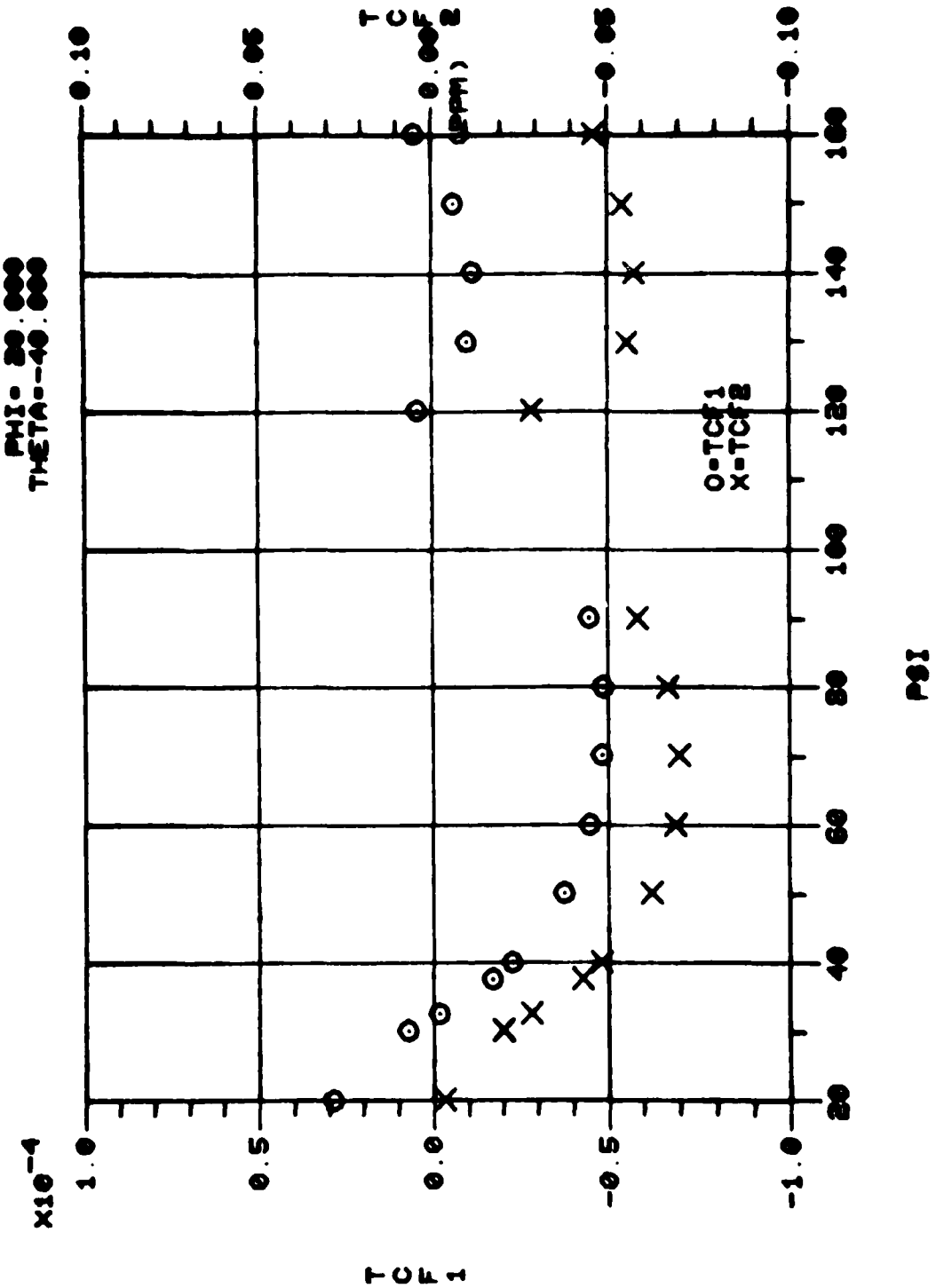
PHI= 20.000
THETA=-40.000
O-TCF1
X-TCF2
PSI
TCF

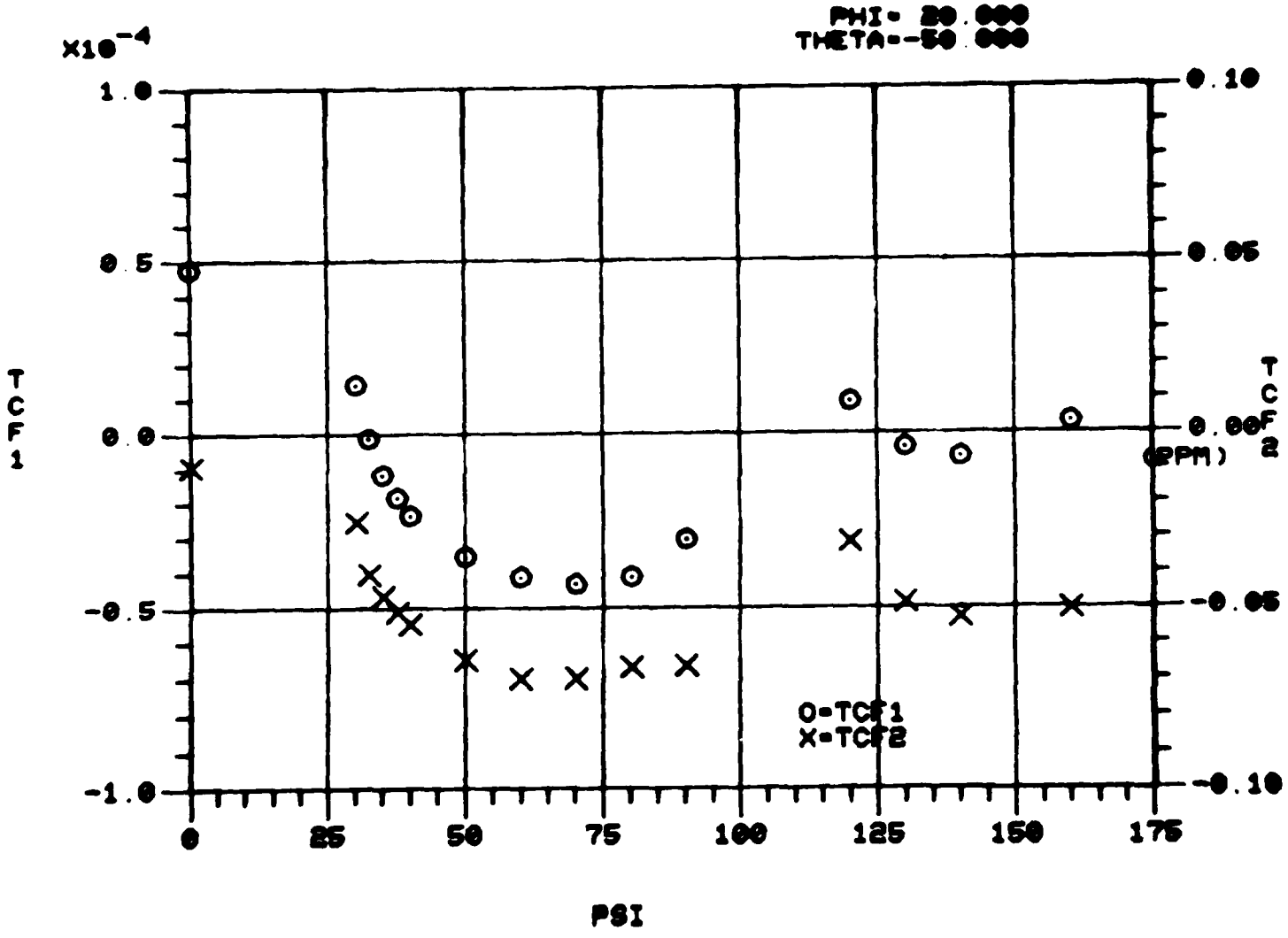
PHI= 20.000
THETA=-50.000
X10^-4
1.0
0.5
0.0
-0.5
-1.0
TCF1
0.10
0.05
0.00
-0.05
-0.10
TCF2
(PPM)
0=TCF1
X=TCF2
0
25
50
75
100
125
150
175
PSI

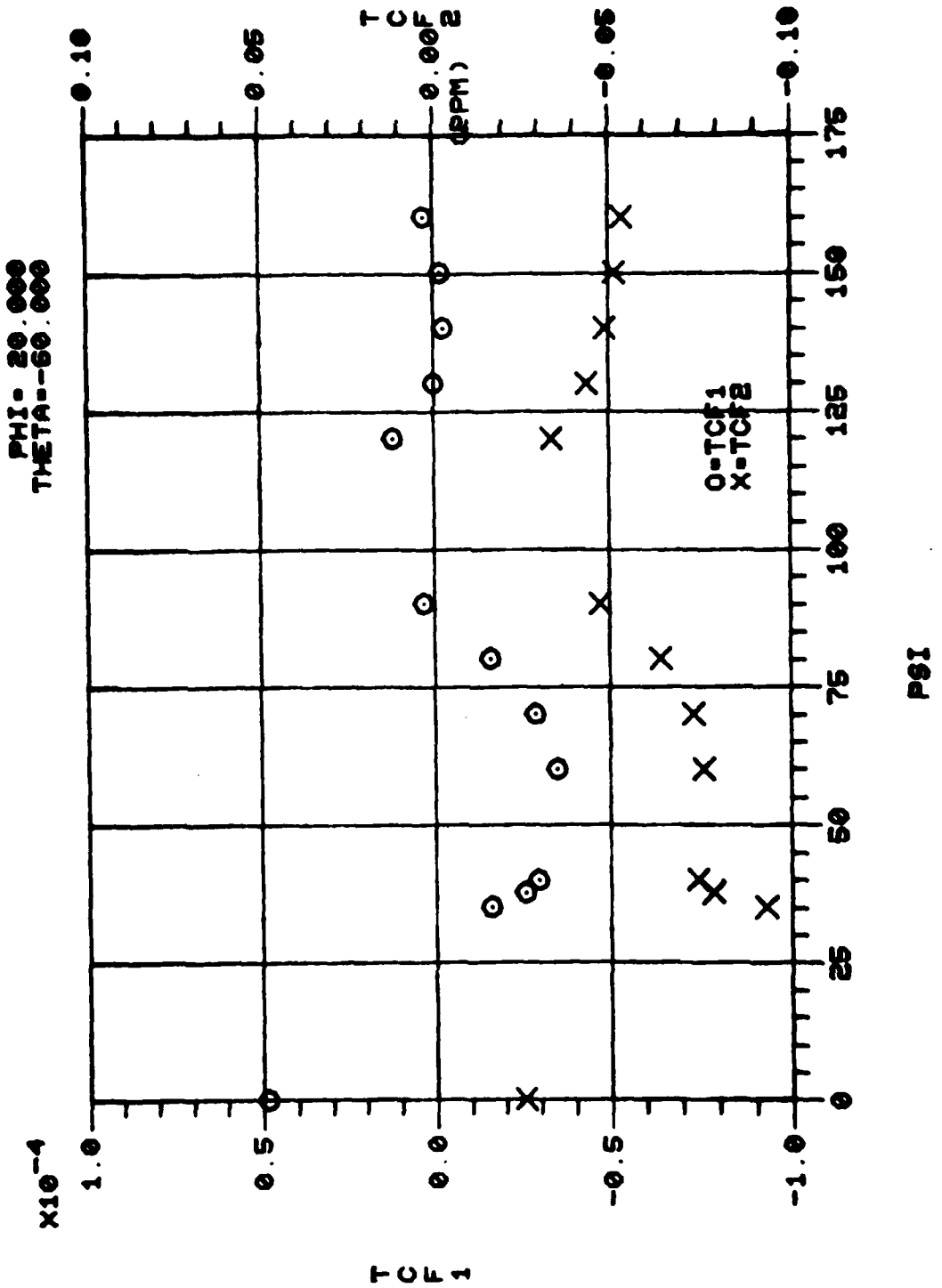
T C
0.00F
(PPM)
2
0.10
0.05
-0.05
-0.10
PHI= 20.000
THETA=-60.000
O-TCF1
X-TCF2
175
150
125
100
75
50
25
0
PSI
X10⁻⁴
1.0
0.5
0.0
-0.5
-1.0
TCF 1

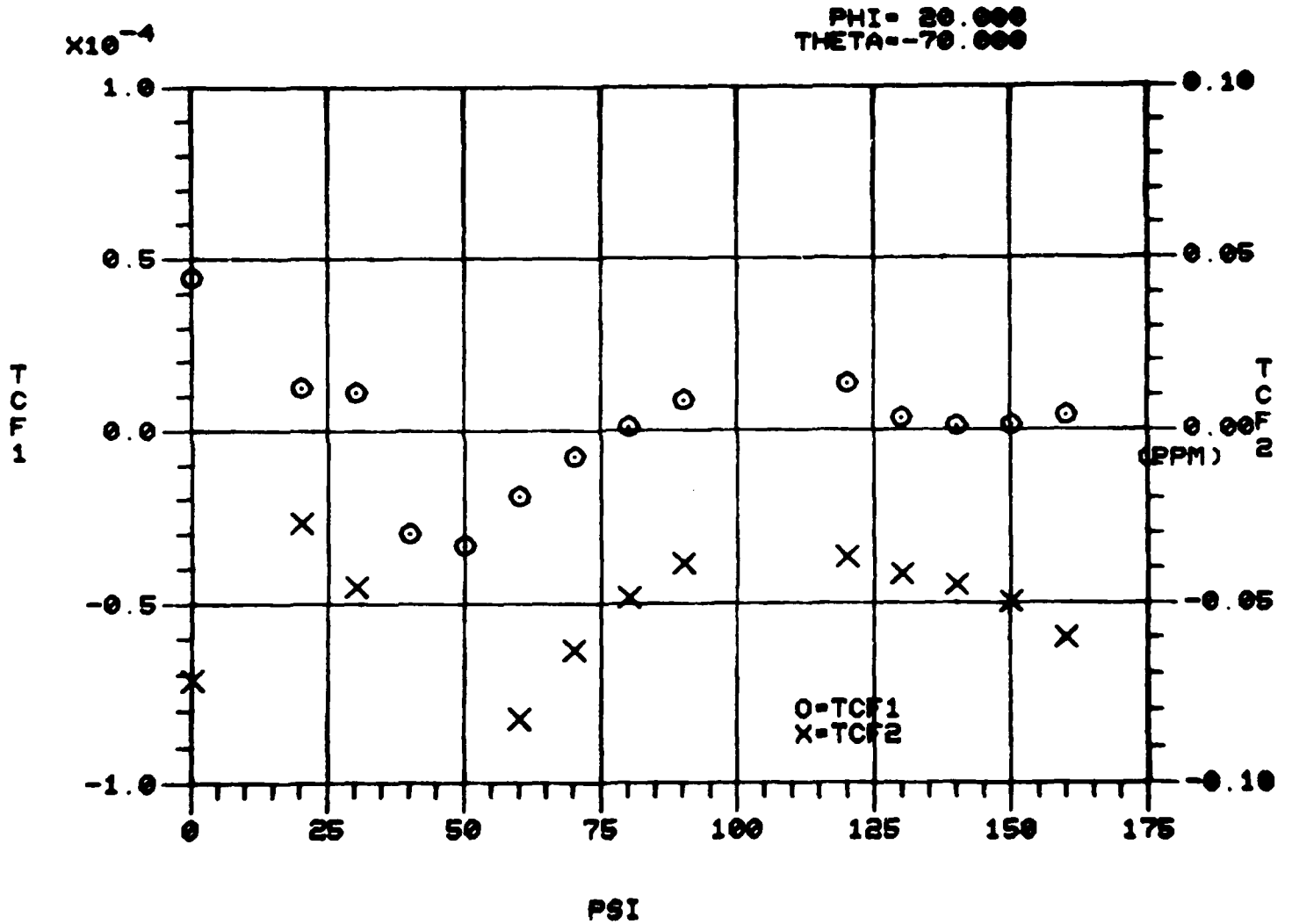
PHI= 20.000
THETA=-70.000
X10^-4
1.0
0.5
0.0
-0.5
-1.0
TCF1
0.10
0.05
0.00
-0.05
-0.10
TCF2
(PPM)
0
25
50
75
100
125
150
175
PSI
O=TCF1
X=TCF2

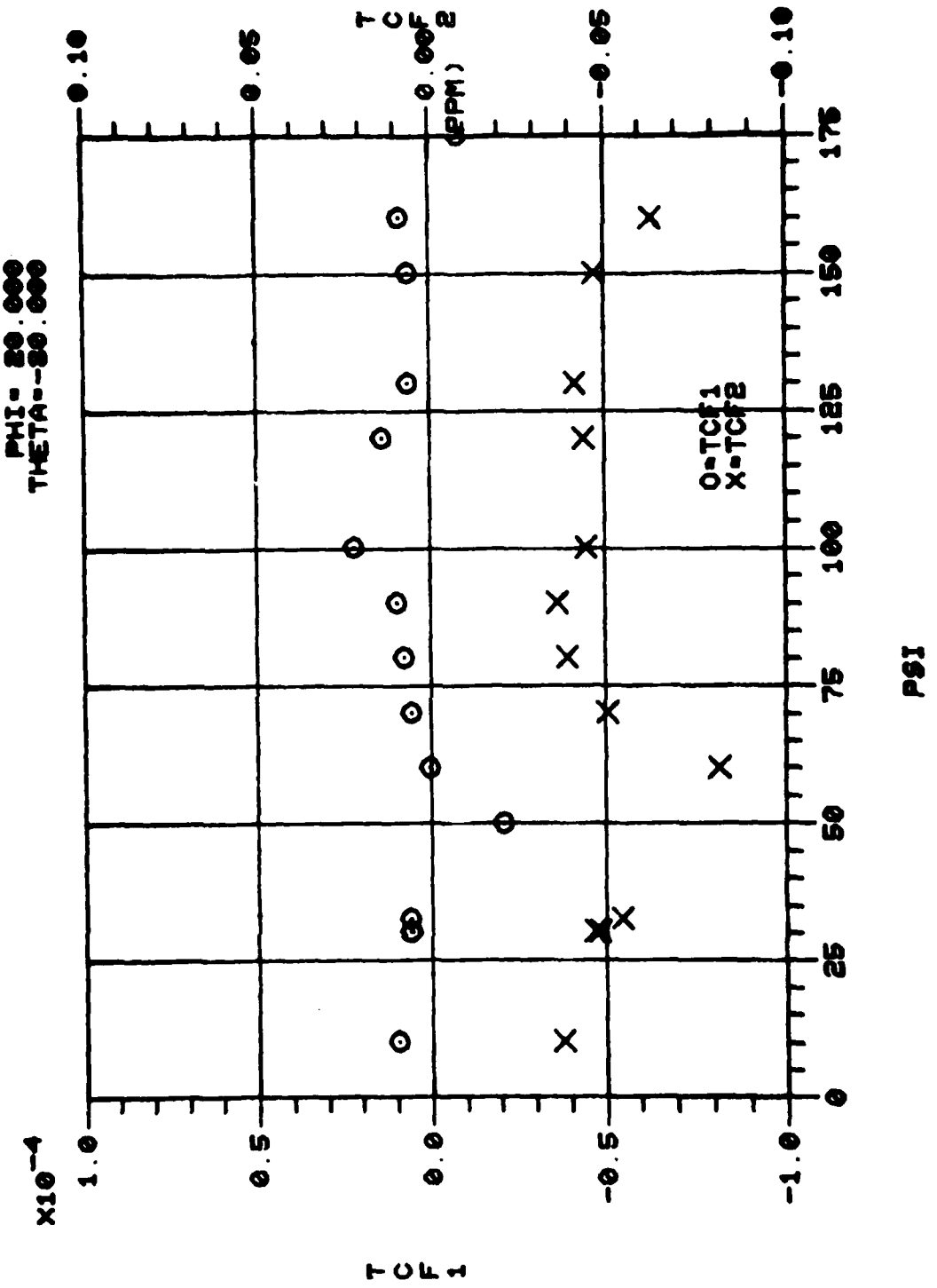
PHI= 20.000
THETA=-30.000
O-TCF1
X-TCF2
T C
(PPM)
2
0.10
0.05
0.00
-0.05
-0.10
175
150
125
100
75
50
25
0
1.0
0.5
0.0
-0.5
-1.0
X10-4
PSI
TCF1

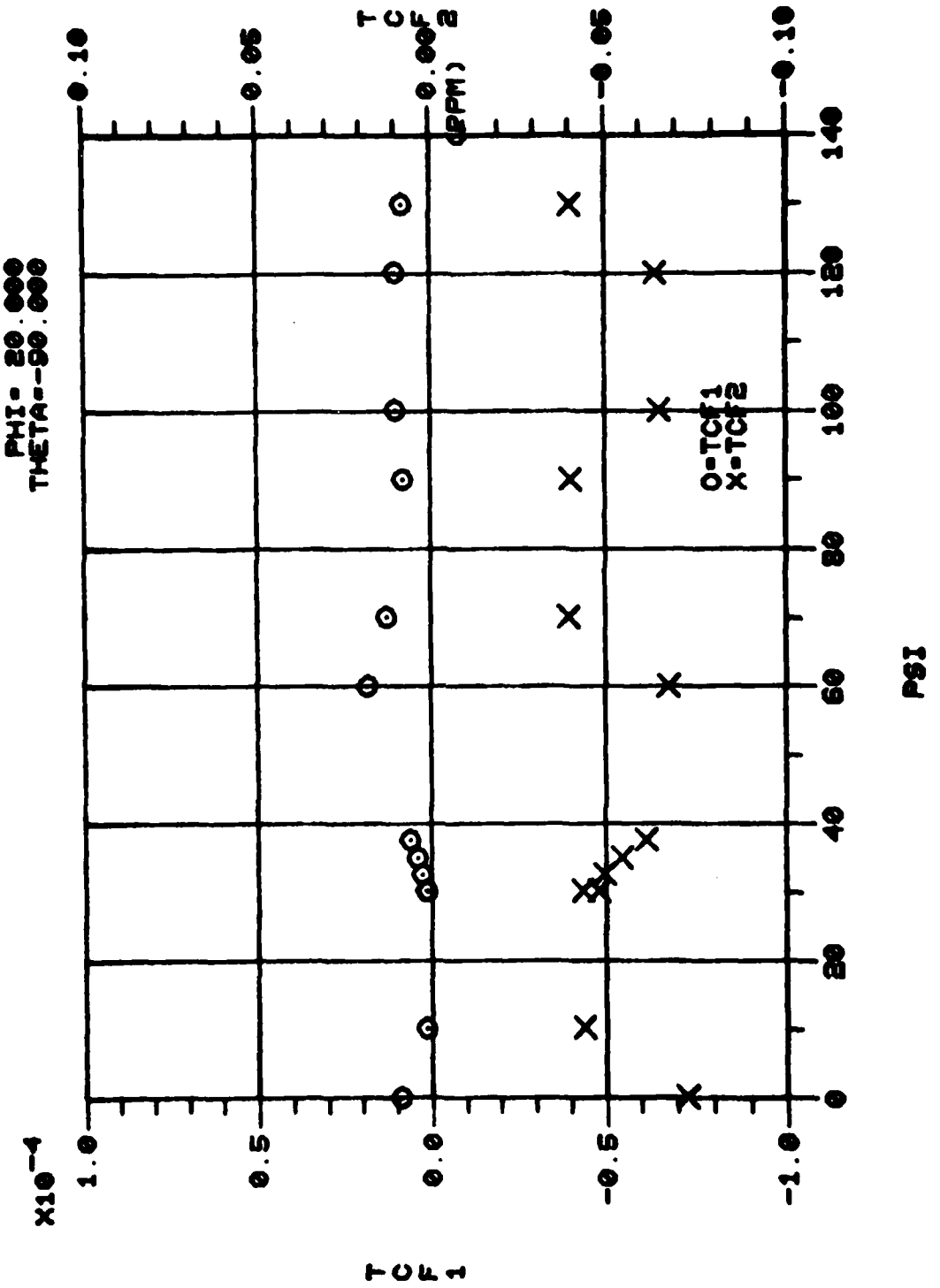
PHI= 20.000
THETA=-90.000
O-TCF1
X-TCF2
T C
(PPM)
2
0.10
0.05
0.00
-0.05
-0.10
140
120
100
80
60
40
20
0
PSI
X10**-4
1.0
0.5
0.0
-0.5
-1.0
TCF1

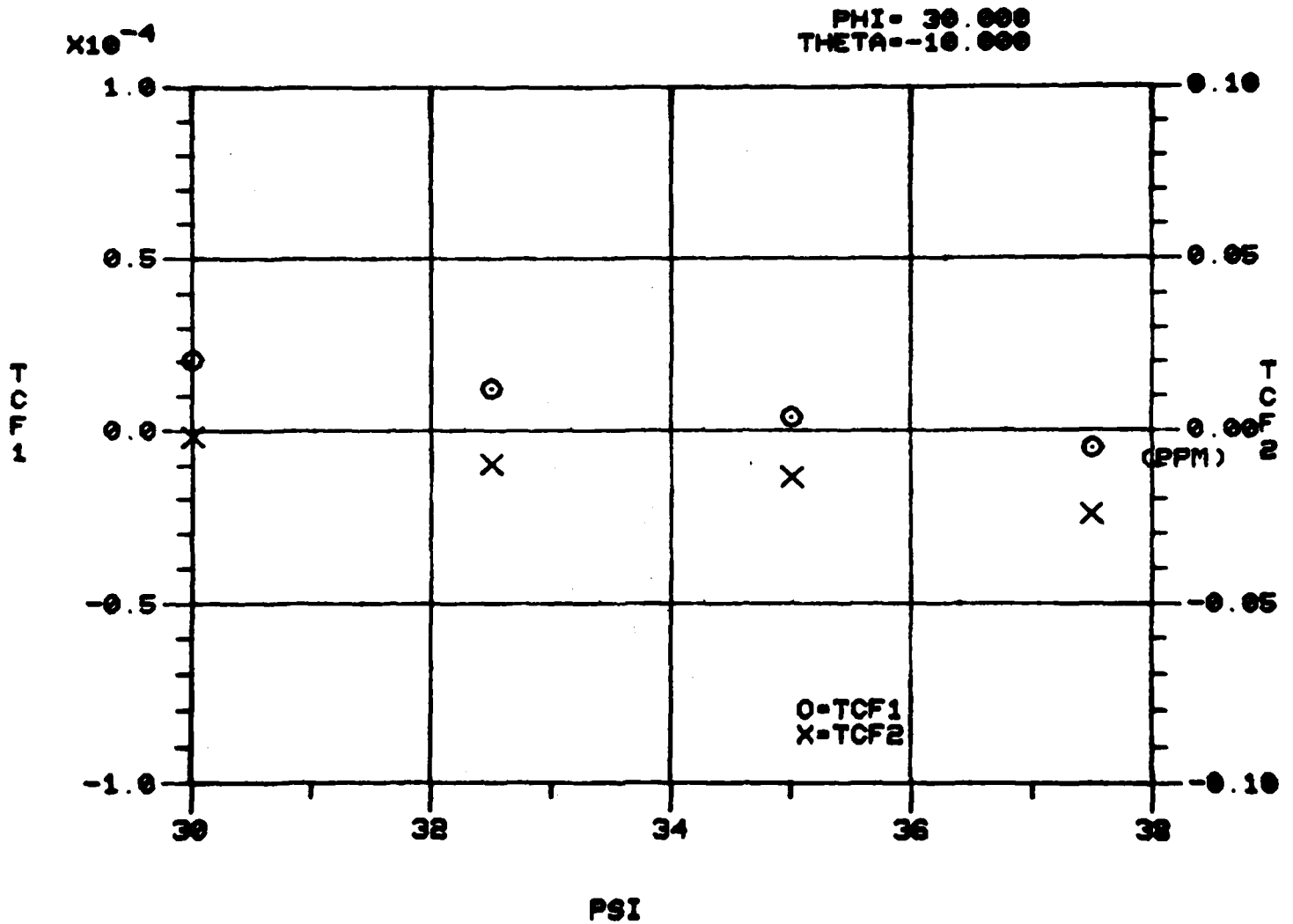
PHI= 30.000
THETA=-10.000
X10^-4
1.0
0.5
0.0
-0.5
-1.0
0.10
0.05
0.00
-0.05
-0.10
TCF1
TCF2
(PPM)
O=TCF1
X=TCF2
30
32
34
36
38
PSI

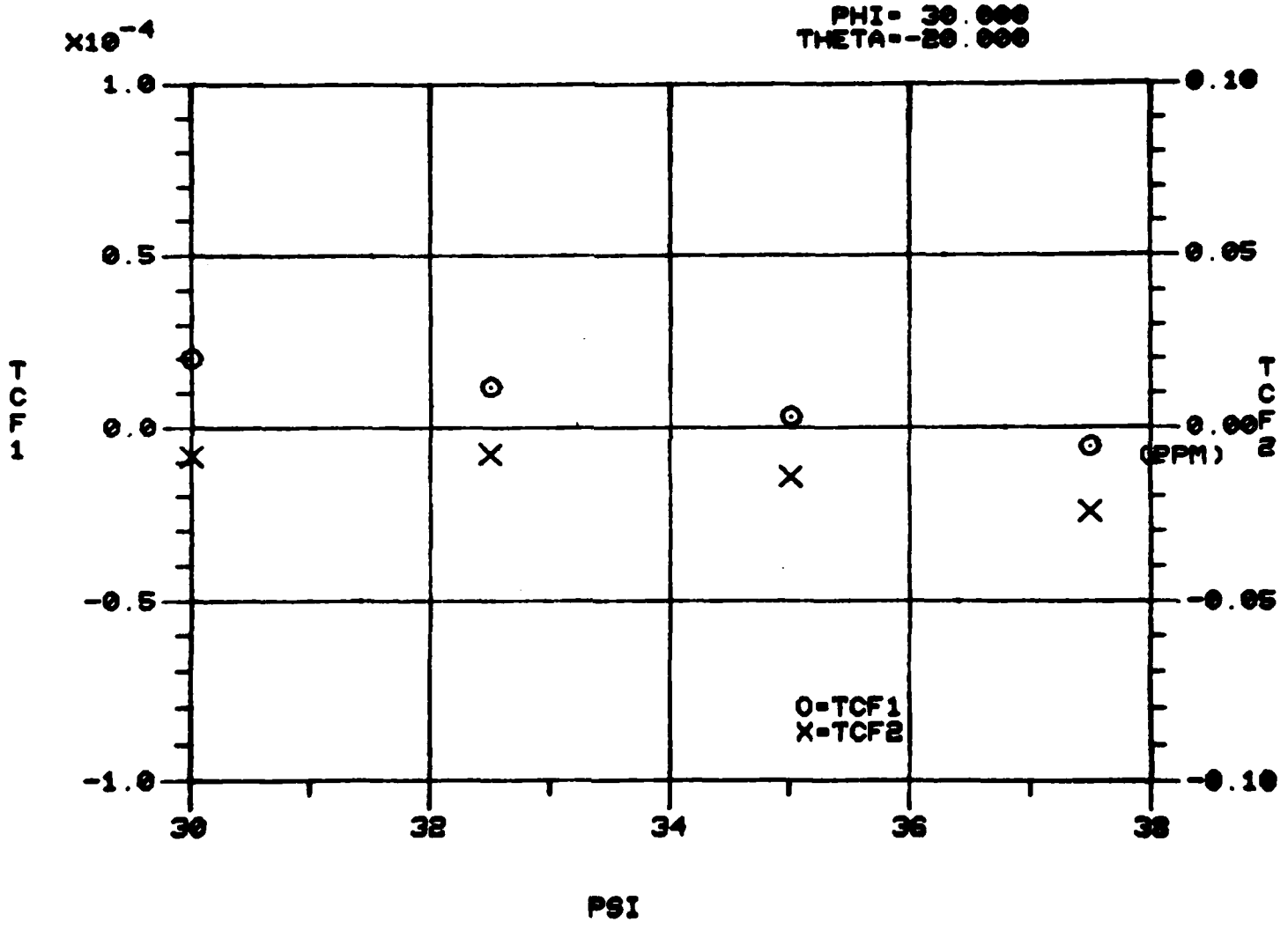
PHI= 30.000
THETA=-20.000
X10^-4
1.0
0.5
0.0
-0.5
-1.0
0.10
0.05
0.00
-0.05
-0.10
TCF1
TCF2
(PPM)
O=TCF1
X=TCF2
30
32
34
36
38
PSI

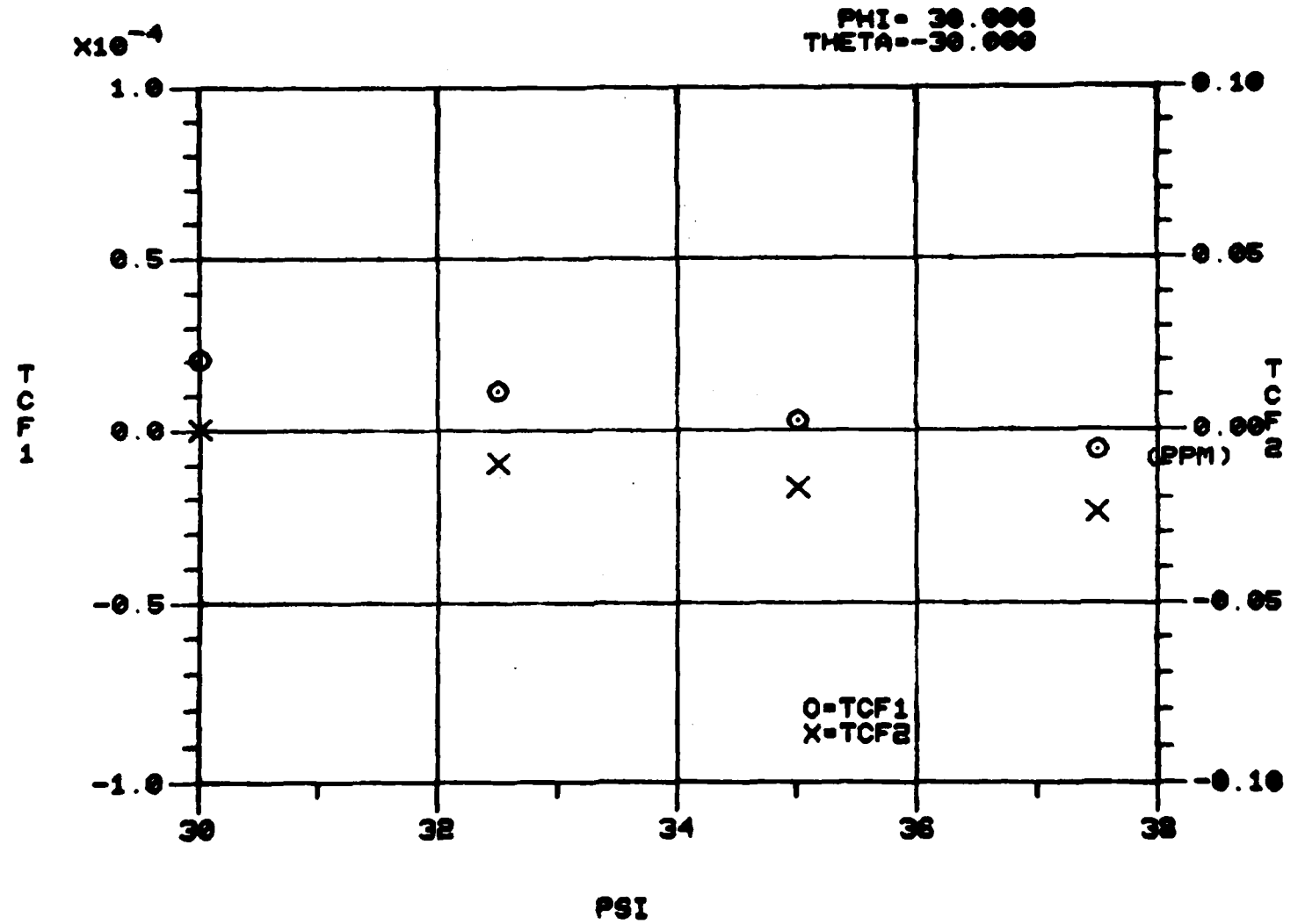
PHI= 30.000
THETA=-30.000
X10^-4
1.0
0.5
0.0
-0.5
-1.0
0.10
0.05
0.00
-0.05
-0.10
TCF1
TCF2
(PPM)
O=TCF1
X=TCF2
30
32
34
36
38
PSI

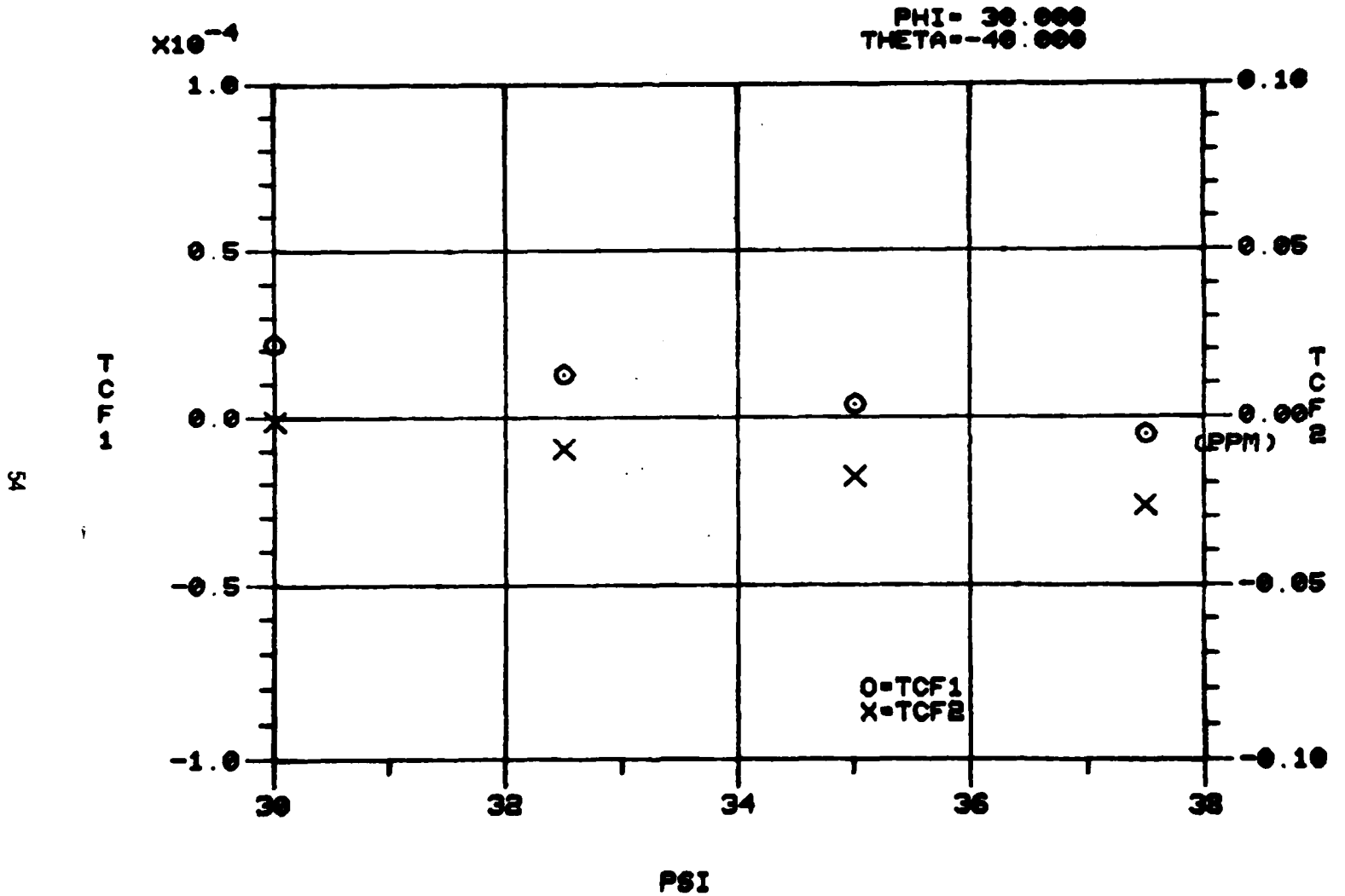
PHI= 30.000
THETA=-40.000
X10^-4
1.0
0.5
0.0
-0.5
-1.0
0.10
0.05
0.00
-0.05
-0.10
TCF1
TCF2
(PPM)
O=TCF1
X=TCF2
30
32
34
36
38
PSI

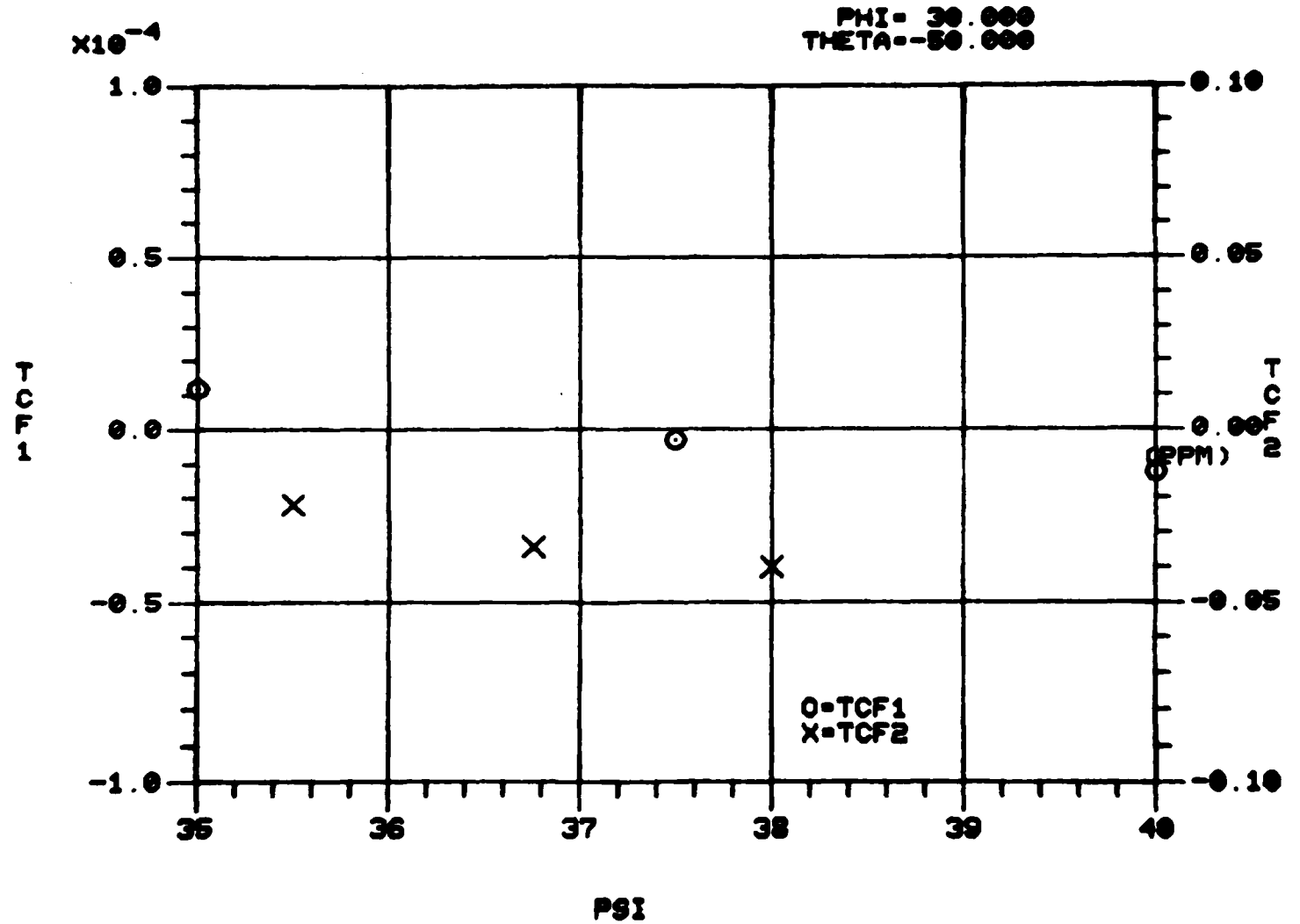
PHI= 30.000
THETA=-50.000
X10^-4
1.0
0.5
0.0
-0.5
-1.0
0.10
0.05
0.00
-0.05
-0.10
TCF1
TCF2
(PPM)
35
36
37
38
39
40
PSI
O=TCF1
X=TCF2

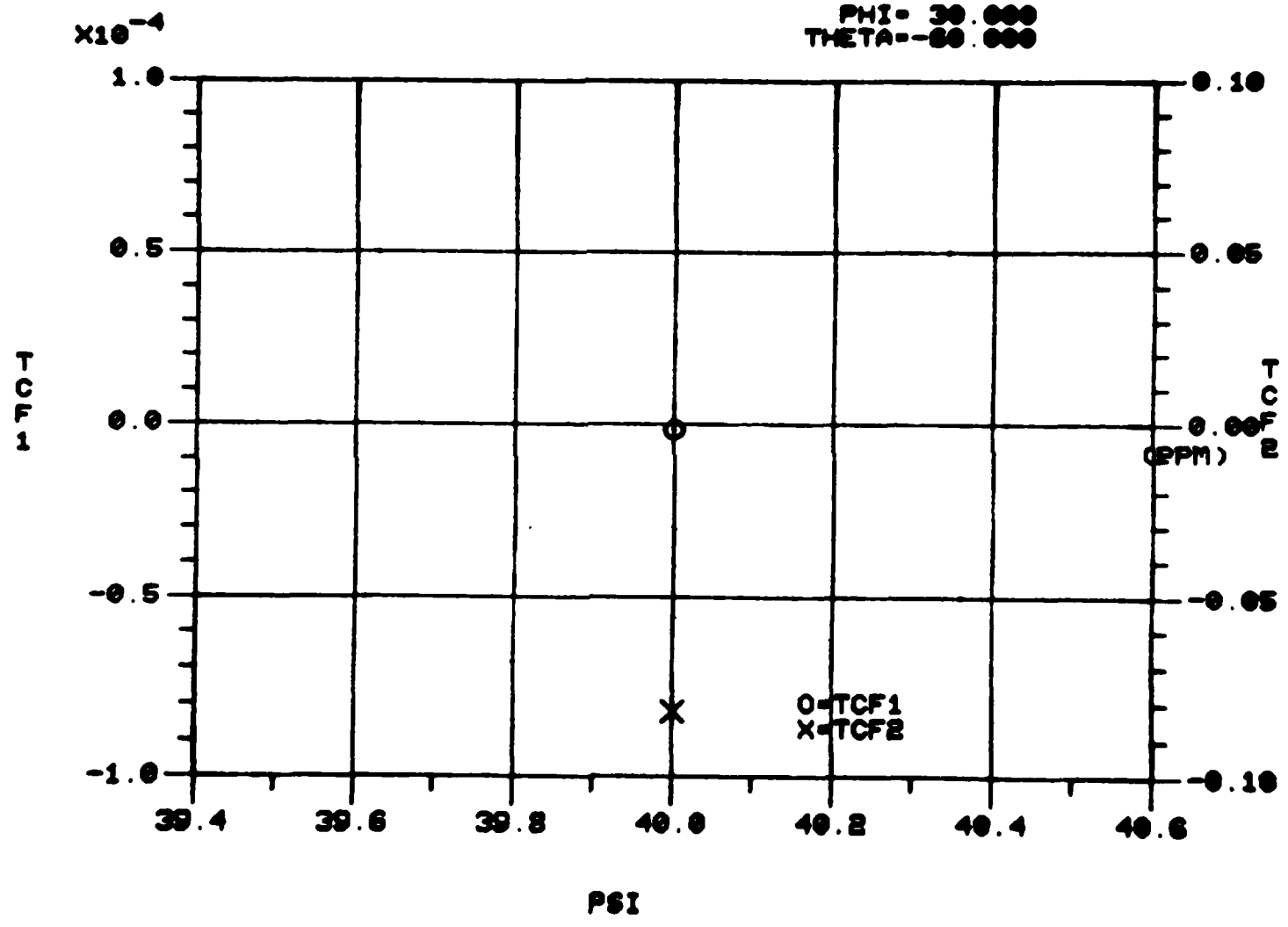
PHI= 30.000
THETA=-60.000
X10^-4
1.0
0.5
0.0
-0.5
-1.0
0.10
0.05
0.00
-0.05
-0.10
TCF1
TCF2
(PPM)
O=TCF1
X=TCF2
39.4
39.6
39.8
40.0
40.2
40.4
40.6
PSI

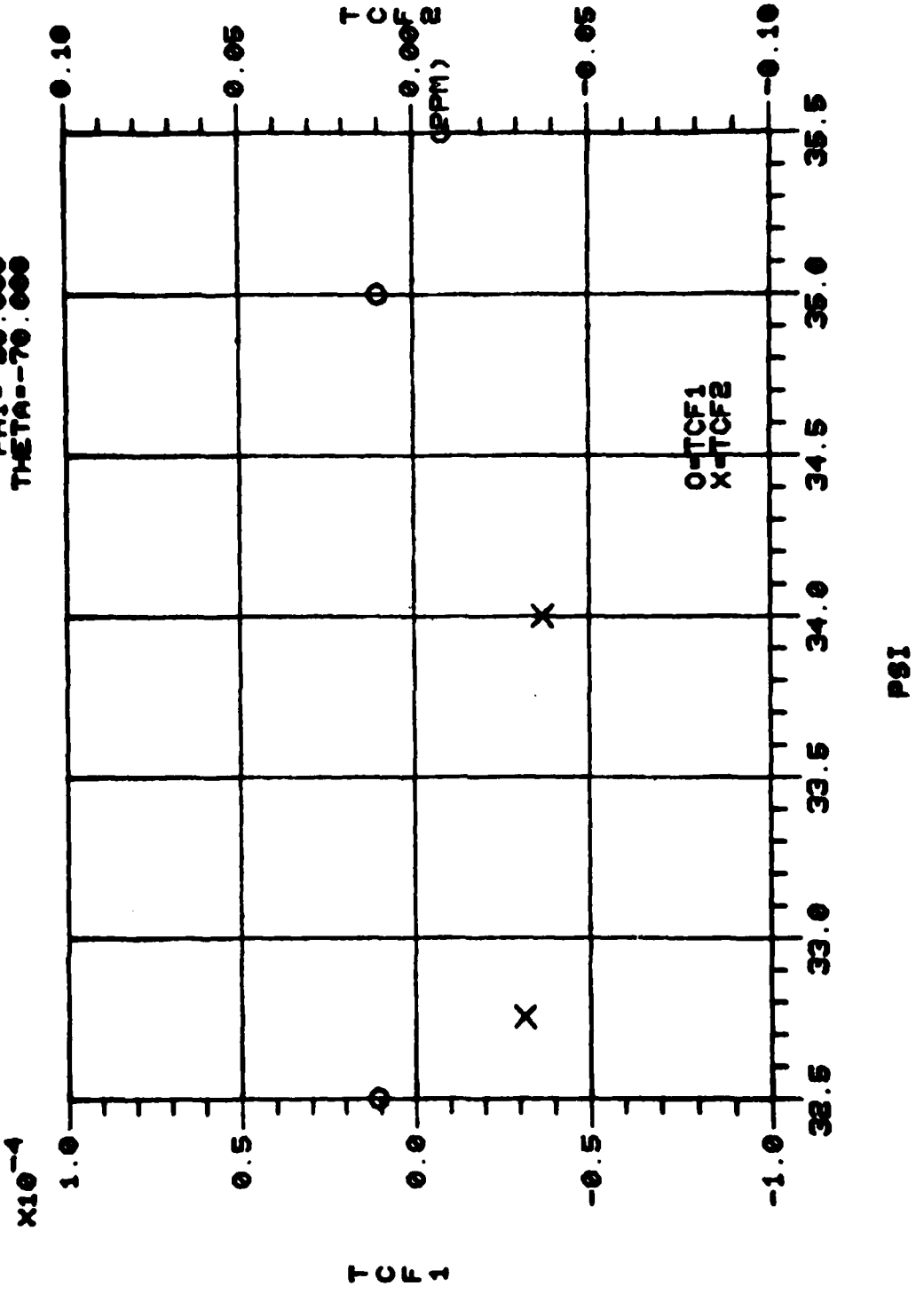
PHI= 30.000
THETA=-70.000
O=TCF1
X=TCF2
T C
0.00F
(PPM) 2
0.10
0.05
-0.05
-0.10
35.5
35.0
34.5
34.0
33.5
33.0
32.5
X10⁻⁴
1.0
0.5
0.0
-0.5
-1.0
PSI
TCF1

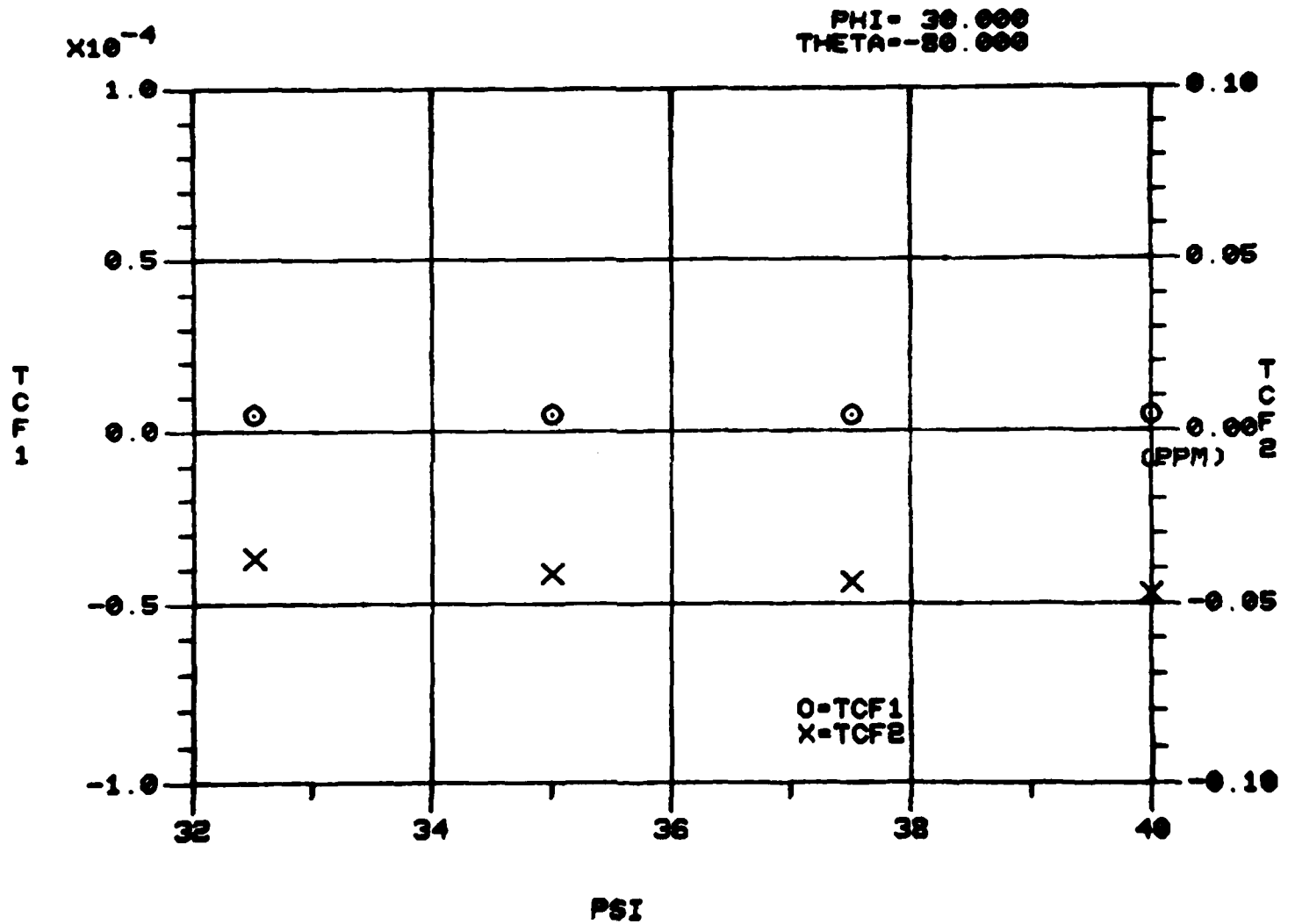
PHI= 30.000
THETA=-80.000
X10^-4
1.0
0.5
0.0
-0.5
-1.0
TCF1
0.10
0.05
0.00
-0.05
-0.10
TCF2
(PPM)
O=TCF1
X=TCF2
32
34
36
38
40
PSI

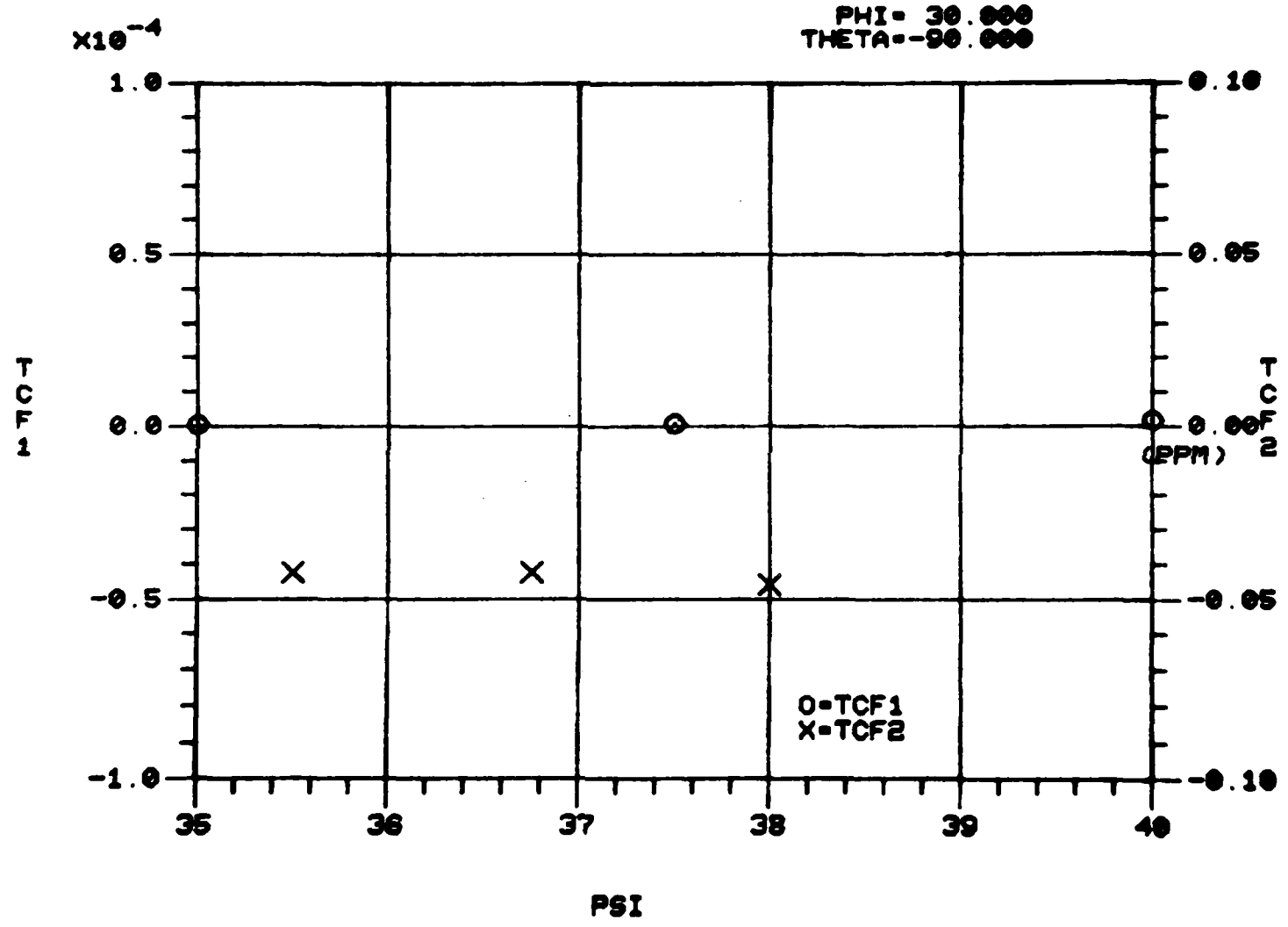
PHI= 30.000
THETA=-90.000
X10^-4
1.0
0.5
0.0
-0.5
-1.0
0.10
0.05
0.00
-0.05
-0.10
TCF1
TCF2
(PPM)
35
36
37
38
39
40
PSI
O=TCF1
X=TCF2

## ELECTRONICS TECHNOLOGY AND DEVICES LABORATORY
## MANDATORY CONTRACT DISTRIBUTION LIST

101 Defense Technical Information Center
ATTN: DTIC-TCA
Cameron Station (Bldg 5)
012 Alexandria, VA 22314

203 GIDEP Engineering & Support Dept
TE Section
PO Box 398
001 NORCO, CA 91760

205 Director
Naval Research Laboratory
ATTN: CODE 2627
001 Washington, DC 20375

301 Rome Air Development Center
ATTN: Documents Library (TILD)
001 Griffiss AFB, NY 13441

437 Deputy for Science & Technology
Office, Asst Sec Army (R&D)
001 Washington, DC 20310

438 HQDA (DAMA-ARZ-D/Dr. F.D. Verderame)
001 Washington, DC 20310

482 Director
US Army Materiel Systems Analysis Actv
ATTN: DRXSY-MP
001 Aberdeen Proving Ground, MD 21005

563 Commander, DARCOM
ATTN: DRCDE
5001 Eisenhower Avenue
001 Alexandria, VA 22333

564 Cdr, US Army Signals Warfare Lab
ATTN: DELSW-OS
Vint Hill Farms Station
001 Warrenton, VA 22186

705 Advisory Group on Electron Devices
201 Varick Street, 9th Floor
002 New York, NY 10014

579 Cdr, PM Concept Analysis Centers
ATTN: DRCPM-CAC
Arlington Hall Station
001 Arlington, VA 22212

602 Cdr, Night Vision & Electro-Optics
ERADCOM
ATTN: DELNV-D
001 Fort Belvoir, VA 22060

603 Cdr, Atmospheric Sciences Lab
ERADCOM
ATTN: DELAS-SY-S
001 White Sands Missile Range, NM 88002

607 Cdr, Harry Diamond Laboratories
ATTN: DELHD-CO, TD (In Turn)
2800 Powder Mill Road
001 Adelphi, MD 20783

609 Cdr, ERADCOM
ATTN: DRDEL-CG, CD, CS (In Turn)
2800 Powder Mill Road
001 Adelphi, MD 20783

612 Cdr, ERADCOM
ATTN: DRDEL-CT
2800 Powder Mill Road
001 Adelphi, MD 20783

680 Commander
US Army Electronics R&D Command
000 Fort Monmouth, NJ 07703
1 DELET-MQ
1 DELEW-D
1 DELET-DD
1 DELSD-L (Tech Library)
2 DELSD-L-S (STINFO)
34 Originating Office
1 DELET-MF

681 Commander
US Army Communications R&D Command
ATTN: USMC-LNO
001 Fort Monmouth, NJ 07703

# ELECTRONICS TECHNOLOGY AND DEVICES LABORATORY
## SUPPLEMENTAL CONTRACT DISTRIBUTION LIST
## (ELECTIVE)

103 Code R123, Tech Library
DCA Defense Comm Engrg Ctr
1800 Wiehle Ave
001 Reston, VA 22090

104 Defense Communications Agency
Technical Library Center
Code 205 (P. A. Tolovi)
001 Washington, DC 20305

206 Commander
Naval Eiectronics Laboratory Center
ATTN: Library
001 San Diego, CA 92152

207 Cdr, Naval Surface Weapons Center
White Oak Laboratory
ATTN: Library Code WX-21
001 Silver Spring, MD 20910

314 Hq, Air Force Systems Command
ATTN: DLCA
Andrews Air Force Base
001 Washington, DC 20331

403 Cdr, MICOM
Redstone Scientific Info Center
ATTN: Chief, Document Section
001 Redstone Arsenal, AL 35809

406 Commandant
US Army Aviation Center
ATTN: ATZQ-D-MA
001 Fort Rucker, AL 36362

407 Director, Ballistic Missile Defense
Advanced Technology Center
ATTN: ATC-R, PO Box 1500
001 Huntsville, AL 35807

418 Commander
HQ, Fort Huachuca
ATTN: Technical Reference Div
001 Fort Huachuca, AZ 85613

475 Cdr, Harry Diamond Laboratories
ATTN Library
2800 Powder Mill Road
001 Adelphi, MD 20783

477 Director
US Army Ballistic Research Labs
ATTN: DRXBR-LB
001 Aberdeen Proving Ground, MD 21005

*481 Harry Diamond Laboratories
ATTN: DELHD-RCB (Dr. J. Nemarich)
2800 Powder Mill road
001 Adelphi, MD 20783

482 Director
US Army Materiel Systems Analysis Actv
ATTN: DRXSY-T, MP (In Turn)
001 Aberdeen Proving Ground, MD 21005

507 Cdr, AVRADCOM
ATTN: DRSAV-E
PO Box 209
001 St. Louis, MO 63166

511 Commander, Picatinny Arsenal
ATTN: SARPA-FR-5, -ND-A-4,
-TS-S (In Turn)
001 Dover, NJ 07801

515 Project Manager, REMBASS
ATTN: DRCPM-RBS
001 Fort Monmouth, NJ 07703

517 Commander
US Army Satellite Communications Agcy
ATTN: DRCPM-SC-3
001 Fort Monmouth, NJ 07703

518 TRI-TAC Office
ATTN: TT-SE
001 Fort Monmouth, NJ 07703

*For Millimeter & Microwave Devices Only

## ELECTRONICS TECHNOLOGY AND DEVICES LABORATORY
## SUPPLEMENTAL CONTRACT DISTRIBUTION LIST (CONT)
## (ELECTIVE)

519 Cdr, US Army Avionics Lab
AVRADCOM
ATTN: DAVAA-D
001 Fort Monmouth, NJ 07703

520 Project Manager, FIREFINDER
ATTN: DRCPM-FF
001 Fort Monmouth, NJ 07703

521 Commander
Project Manager, SOTAS
ATTN: DRCPM-STA
001 Fort Monmouth, NJ 07703

531 Cdr, US Army Research Office
ATTN: DRXRO-PH (Dr. Lontz)
DRXRO-IP (In Turn)
PO Box 12211
001 Research Triangle Park, NC 27709

556 HQ, TCATA
Technical Information Center
ATTN: Mrs. Ruth Reynolds
001 Fort Hood, TX 76544

568 Commander
US Army Mobility Eqp Res & Dev Cmd
ATTN: DRDME-R
001 Fort Belvoir, VA 22060

604 Chief
Ofc of Missile Electronic Warfare
Electronic Warfare Lab, ERADCOM
001 White Sands Missile Range, NM 88002

606 Chief
Intel Materiel Dev & Support Ofc
Electronic Warfare Lab, ERADCOM
001 Fort Meade, MD 20755

608 Commander
ARRADCOM
DRDAR-TSB-S
001 Aberdeen Proving Ground, MD 21005

614 Cdr, ERADCOM
ATTN: DRDEL-LL, -SB, -AP (In Turn)
2800 Powder Mill Road
001 Adelphi, MD 27083

617 Cdr, ERADCOM
ATTN: DRDEL-AQ
2800 Powder Mill Road
001 Adelphi, MD 20783

619 Cdr, ERADCOM
ATTN: DRDEL-PA, -ILS, -ED (In Turn)
2800 Powder Mill Road
001 Adelphi, MD 20783

701 MTI — Lincoln Laboratory
ATTN: Library (RM A-082)
PO Box 73
002 Lexington, MA 02173

703 NASA Scientific & Tech Info Facility
Baltimore/Washington Intl Airport
001 PO Box 8757, MD 21240

704 National Bureau of Standards
Bldg 225, RM A-331
ATTN: Mr. Leedy
001 Washington, DC 20231

707 TACTEC
Batelle Memorial Institute
505 King Avenue
001 Columbus, OH 43201

## ELECTRONICS TECHNOLOGY AND DEVICES LABORATORY
## SUPPLEMENTAL CONTRACT DISTRIBUTION LIST (CONT)
## (ELECTIVE)

Coordinated Science Laboratory
University of Illinois
Urbana, Illinois 61801
ATTN: Dr. Bill J. Hunsinger (1)

Dr. J.S. Bryant
OCRD
ATTN: DARD-ARP
Washington, DC 20310 (1)

Dr. R. LaRosa
Hazeltine Corporation
Greenlawn, New York 11740 (1)

General Electric Co.
Electronics Lab
Electronics Park
Syracuse, NY 13201
ATTN: Mr. S. Wanuga (1)

Air Force Cambridge Labs
ATTN: CRDR (Dr. P. Carr & Dr. A.J. Slobodnik)
Bedford, MA 01730 (2)

Mr. R. Weglein
Hughes Research Laboratories
3011 Malibu Canyon Road
Malibu, California 90265 (1)

Mr. H. Bush CORC
RADC
Griffiss Air Force Base
New York 13440 (1)

Dr. Tom Bristol
Hughes Aircraft Company
Ground Systems Group
Bldg 600/MS D235
1901 W. Malvern
Fullerton, CA 92634 (2)

Commander, AFAL
ATTN: Mr. W.J. Edwards, TEA
Wright-Patterson AFB, Ohio 45433 (1)

Anderson Laboratories, Inc.
1280 Blue Hills Ave
ATTN: Dr. A.A. Comparini
Bloomfield, Conn. 06002 (1)

Mr. Henry Friedman
RADC/OCTE
Griffiss AFB, NY 13440 (1)

Autonetics, Division of North American Rockwell
P.O. Box 4173
3370 Miraloma Avenue
Anaheim, CA 92802
ATTN: Dr. G.R. Pulliam (1)

General Dynamics, Electronics Division
P.O. Box 81127
San Diego, CA 92138
ATTN: Mr. R. Badewitz (1)

Texas Instruments, Inc.
P.O. Box 5936
13500 N. Central Expressway
Dallas, Texas 75222
ATTN: Dr. L.T. Clairborne (2)

Raytheon Company
Research Division
28 Seyon Street
Waltham, Massachusetts 02154
ATTN: Dr. M.B. Schulz (1)

Sperry Rand Research Center
100 North Road
Sudbury, Massachusetts 01776
ATTN: Dr. H. Van De Vaart (1)

Microwave Laboratory
W.W. Hansen Laboratories of Physics
Stanford University
Stanford, CA 94305
ATTN: Dr. H.J. Shaw (2)

## ELECTRONICS TECHNOLOGY AND DEVICES LABORATORY
## SUPPLEMENTAL CONTRACT DISTRIBUTION LIST (CONT)
## (ELECTIVE)

Polytechnic Institute of Brooklyn
Route No. 110
Farmingdale, NY 11735
ATTN: Dr. A.A. Oliner (1)

Westinghouse Electric Corp.
Research & Development Center
Beulah Road
Pittsburgh, PA 15235
ATTN: Dr. J. DeKlerk (1)

Stanford Research Institute
Menlo Park, CA 94025
ATTN: Dr. A. Bahr (1)

International Business Machines Corp.
Research Division
P.O. Box 218
Yorktown Heights, NY 10598
ATTN: Dr. F. Bill (1)

TRW
Defense and Space Sys Group
One Space Park
Redondo Beach, CA 90278
ATTN: Dr. R.S. Kagiwada (1)

Tektronix Inc.
P.O. Box 500
Beaverton, OR 97077
ATTN: Dr. R. Li (1)

Dr. Fred S. Hickernell
Integrated Circuit Facility
Motorola Government Electronics Division
8201 East McDowell Road
Scottsdale, AZ 85257 (1)

Prof. H.F. Tiersten
Jonsson Engineering Center
Rensselaer Polytechnic Institute
Troy, NY 12181 (1)

McGill University
ATTN: G.W. Farnell
Montreal 110, Canada (1)

Advanced Technology Center, Inc.
Subsidiary of LTV Aerospace Corp.
P.O. Box 6144
Dallas, Texas 75222
ATTN: Mr. A.E. Sobey (1)

United Aircraft Research Labs
ATTN: Dr. Thomas W. Grudkowski
East Hartford, Conn. 06108 (1)

Science Center
Rockwell International
Thousand Oaks, CA 91360
ATTN: Dr. T.C. Lim (1)

University of Southern CA
Electronic Science Lab
School of Engineering
University Park, Los Angeles
California 900
ATTN: Dr. K. Lakin, SSC 303 (1)

SAWTEK, Inc.
P.O. Box 7756
2451 Shader Road
Orlando, Florida 32854
ATTN: Mr. S. Miller (1)

Prof. P.C.Y. Lee
School of Engineering
Princeton University
Princeton, NJ 08540 (1)

Mr. John A. Kusters
Hewlett-Packard
5301 Stevens Creek Boulevard
Santa Clara, CA 95050 (1)

Dr. Tom Young
Sandia Laboratories
P.O. Box 5800
Albuquerque, NM 87185 (1)

Dr. William J. Tanski
Sperry Research Center
100 North Road
Sudbury, MA 01776 (1)

## ELECTRONICS TECHNOLOGY AND DEVICES LABORATORY
## SUPPLEMENTAL CONTRACT DISTRIBUTION LIST (CONT)
## (ELECTIVE)

Dr. B.A. Auld
E.L. Ginzton Laboratory
Stanford University
Stanford, CA 94305 (1)

Mr. Marvin E. Frerking
MS 137-138
Collins Radio Company
855 35th Street, NE
Cedar Rapids, IA 52406 (1)

Dr. William R. Shreve
HP Laboratories
1501 Page Mill Road
Palo Alto, CA 94304 (1)

Dr. Thomas M. Reeder
MS 50-362
Tektronix, Inc.
P.O. Box 500
Beaverton, OR 97077 (1)

Dr. Robert L. Rosenberg
Bell Laboratories
Crawfords Corner Road
Holmdel, NJ 07733 (1)

Dr. B.K. Sinha
Schlumberger-Doll Research Center
P.O. Box 307
Ridgefield, CT 06877 (1)

Dr. Robert S. Wagers
Texas Instruments, Inc.
13500 N. Central Expwy.
P.O. Box 225936, MS 134
Dallas, TX 75265 (1)

Dr. Richard C. Williamson
Lincoln Laboratory
P.O. Box 73
Lexington, MA 02173 (1)

## SUPPLEMENT TO DISTRIBUTION LIST

D. Chrissotimos, Code 763
National Aeronautics and Space
Administration
Goddard Space Flight Center
Greenbelt, MD 20771 (1)

Naval Research Laboratories
Code 5237
Washington, DC 20375
ATTN: Dr. D. Webb (1)

HQ ESD (DRI)
L.G. Hanscom AFB
Bedford, MA 01731 (1)

Commander
US Army Missile Command
ATTN: DRSMI-RE (Mr. Pittman)
Redstone Arsenal, AL 35809 (1)

Army Materials and Mechanics Research
Center (AMMRC)
Watertown, MA 02172
ATTN: DMXMR-EO (1)

Commander, Picatinny Arsenal
ATTN: SARPA-FR-S
Bldg. 350
Dover, NJ 07801 (2)

A. Kahan
RADC/ESE
Hanscom AFB
Bedford, MA 01731 (1)

Dr. Robert O'Connell
Department of EE
Univ. of Missouri - Columbia
Columbia, MO 65201 (1)

Prof. John F. Vetelino
Dept of EE
Univ. of Maine - Orono
Orono, ME 04469 (1)

END

DATE
FILMED

6-81

DTIC